PHD THESIS

FATIGUE LIFE PREDICTION OF OVERHEAD CONDUCTORS AND THEIR WIRES: EXPERIMENTAL AND NUMERICAL INVESTIGATIONS

IAN DE MEDEIROS MATOS

February 2024

UNIVERSIDADE DE BRASÍLIA

FACULDADE DE TECNOLOGIA

DEPARTAMENTO DE ENGENHARIA MECÂNICA

UNIVERSIDADE DE BRASÍLIA
FACULDADE DE TECNOLOGIA
DEPARTAMENTO DE ENGENHARIA MECÂNICA

FATIGUE LIFE PREDICTION OF OVERHEAD CONDUCTORS AND THEIR WIRES: EXPERIMENTAL AND NUMERICAL INVESTIGATIONS

IAN DE MEDEIROS MATOS

ADVISOR: FÁBIO COMES DE CASTRO

PHD THESIS IN MECHANICAL SCIENCES

FEBRUARY – 2024.

UNIVERSIDADE DE BRASÍLIA
FACULDADE DE TECNOLOGIA
DEPARTAMENTO DE ENGENHARIA MECÂNICA

FATIGUE LIFE PREDICTION OF OVERHEAD CONDUCTORS AND THEIR WIRES: EXPERIMENTAL AND NUMERICAL INVESTIGATIONS

IAN DE MEDEIROS MATOS

A THESIS SUBMITTED TO THE DEPARTMENT OF MECHANICAL ENGINEERING OF UNIVERSITY OF BRASILIA, IN PARTIAL FULFILLMENT OF THE REQUIREMENTS FOR THE DEGREE OF DOCTOR OF PHILOSOPHY IN MECHANICAL SCIENCES

APPROVED BY:

_____

Prof. Fábio Comes de Castro, D.Sc. (ENM/UnB)
(Advisor)

_____

Prof. Jorge Luiz de Almeida Ferreira, D.Sc. (ENM/UnB)
(Internal examiner)

_____

Prof. Raphael Araújo Cardoso, D.Sc. (MEC/UFRN)
(External examiner)

_____

Prof. André Luis Pinto, D.Sc. (ENG/IFB)
(External examiner)

FEBRUARY 2024.

CARD CATALOG

MATOS, IAN DE MEDEIROS

Fatigue life prediction of overhead conductors and their wires: Experimental and numerical investigations.

[Distrito Federal] 2024.

xxi, 170p., 210 x 297 mm (ENM/FT/UnB, PhD, Ciências Mecânicas, 2024)

Tese de Doutorado – Universidade de Brasília

Faculdade de Tecnologia.

Departamento de Engenharia Mecânica.

1. Overhead conductor 2. Aluminum wire

3. Fretting fatigue 4. Life prediction

BIBLIOGRAPHIC REFERENCE

MATOS, I. M., (2024) Fatigue life prediction of overhead conductors and their wires: Experimental and numerical investigations. Tese de Doutorado em Ciências Mecânicas, Publicação ENM-DM xx/2024, Departamento de Engenharia Mecânica, Universidade de Brasília, Brasília, DF, 170p.

ASSIGNMENT OF RIGHTS

AUTHOR: Ian de Medeiros Matos.
TITLE: Fatigue life prediction of overhead conductors and their wires: Experimental and numerical investigations.
DEGREE: PhD YEAR: 2024

Ian de Medeiros Matos
SQS 109 Bloco D Apto 404
70372-040 – Brasília - DF - Brasil
ian.m.matos@gmail.com

Acknowledgements

First of all, I would like to thank my parents, Simone and Kleuber, my brothers, Vitor and Gabriel, and my girlfriend, Carolina. Thank you so much for your love and unconditional support during my studies. Thank you for always believing in my success and for motivating me to overcome all adversity.

I would like to express my thanks to my supervisor, Prof. Fábio Castro, who has been guiding me with my research since my master's degree. Thank you for all your teaching, attention, patience and encouragement. Thank you to all the other professors and staff at University of Brasilia (UnB) who, in some way, contributed to my personal and professional learning process during my studies.

I would like to thank Prof. Sébastien Lalonde, who mentored me during my research internship at École de Technologie Supérieure (ÉTS) in Montreal. Thank you for welcoming me into your laboratory and for your valuable guidance regarding the three-dimensional modeling of the conductor-clamp system. I am very grateful for the collaboration and all the meetings we had during the internship.

I would like to thank my friends André Pinto, Giorgio Oliveira, Gabriel Juevenal, Remy Kalombo and Miguel Garcia from the Fatigue, Fracture, and Materials group of UnB for all the conversations and experiences we shared during my research. I would also like to thank my friend Pedro Rocha for all his help during my research internship in Montreal and for the good times we had together.

Finally, I would like express my gratitude to the Coordenação de Aperfeiçoamento de Pessoal de Nível Superior – Brasil (CAPES) – Finance Code 001, and to École de Technologie Supérieure (ETS) for the financial support provided for this research.

Abstract

The fatigue behavior of overhead conductors is a complex problem, involving hundreds of contact regions, localized plasticity, wear, and friction. The increase in computing power and the recent advances in finite element (FE) 3D modeling of conductor-clamp systems have motivated researchers to pursue FE-based approaches for the fatigue damage analysis of the conductor. These approaches are based on a combination of a global-scale analysis of the conductor-clamp system with a local-scale analysis of the wires under fretting fatigue. However, research is still required to improve the accuracy of these approaches considering different conductor geometries, wire materials, and loading conditions. In this context, this thesis aims to propose new methodologies for life prediction of overhead conductors and their wires by means of experimental and numerical analyses.

This thesis is organized as a collection of three research papers by the author and collaborators, which have already been published or are under the process of submission/review. In the first paper, fretting fatigue tests under constant amplitude loading (CAL) were performed using 1120 aluminum alloy (AA) wires of an AAAC (All Aluminum Alloy Conductor) 823 MCM conductor. A tension test and axial fatigue tests on smooth and V-notched wire specimens were also carried out. The fatigue test data were used to compare the AA1120 with the AA1350 and AA6201, two alloys typically used to manufacture the wires of conductors. Under tension, the AA1120 displayed an intermediate ultimate tensile strength between the ones from the AA1350 and the AA6201. For the same stress amplitudes, the AA1120 wires used in the axial fatigue tests had longer lives than the AA1350 wires but considerably shorter lives than the AA6201 wires. However, under fretting fatigue, both AA1120 and AA6201 wires had similar fatigue strength. The test data were also used to evaluate a life prediction criterion for wires under fretting fatigue based on the Theory of Critical Distances (TCD). Most of the predicted lives were within a factor of 3 of the measured lives. The accuracy of the predictions was similar to that observed in previous studies, in which the same methodology was applied to data from fretting fatigue tests on AA1350 and AA6201 wires. These results show that the methodology can be a reliable tool for the fatigue damage analysis of wires made of different materials subjected to fretting fatigue and CAL.

In the second paper, fretting fatigue tests under variable amplitude loading (VAL) were carried out on AA6201-T81 wires of an AAAC 900 MCM conductor. The amplitude variation was represented by a three-block loading history. The loading conditions were defined using vibration measurements from an operating transmission line located in the center-west region of Brazil. Two methodologies for life prediction of wires were extended to VAL conditions and were evaluated using the fretting fatigue test data. One of the methodologies is the same TCD-

based criterion considered in the first paper, while the other is based on a master fatigue curve. Both methodologies provided life predictions within factors of 4 of the measured lives. The accuracy achieved in this study supports the use of the proposed methodologies for predicting the lives of wires under VAL conditions.

The third paper is concerned with the life prediction of an ACSR (Aluminum Conductor Steel Reinforced) Ibis 397.5 MCM conductor under high-low and low-high loading sequences. To this end, a life prediction methodology based on finite element 3D modeling of conductor-clamp systems was extended to include VAL conditions. Firstly, the methodology was applied to CAL fatigue test data to assess whether it can accurately describe the fatigue failure of the ACSR Ibis conductor. Subsequently, the methodology was evaluated using the data from fatigue tests conducted under a two-block loading history. Most life predictions were within factors of 3 of the measured lives. For the VAL tests, the methodology accurately took into account the effect of loading sequence on fatigue failure, providing longer life estimates for the tests under high-low sequence than for those under low-high sequence. Additionally, the methodology was capable of predicting the positions of the wire breaks for the VAL tests in accordance with the experimental observations. These results suggest that the methodology can be extended to VAL conditions and be used to accurately predict the lives, the loading sequence effects, and the fatigue critical regions of conductors.

Keywords: overhead conductor; aluminum alloy wire; fretting fatigue; life prediction; variable amplitude loading

Resumo

O comportamento em fadiga de cabos condutores é um problema complexo, envolvendo centenas de regiões de contato, plasticidade localizada, desgaste e atrito. O aumento no poder de computação e os avanços recentes na modelagem 3D em elementos finitos (FE) de sistemas condutor-grampo motivaram pesquisadores a buscar abordagens baseadas em FE para a análise de dano por fadiga do condutor. Essas abordagens são baseadas em uma combinação de uma análise em escala global do sistema condutor-grampo, com uma análise em escala local dos fios sob fadiga por fretting. Entretanto, pesquisas ainda são necessárias para melhorar a acurácia dessas abordagens considerando diferentes geometrias de condutor, materiais de fio e condições de carregamento. Nesse contexto, essa tese visa propor novas metodologias para previsão de vida de cabos condutores e seus fios por meio de análises experimentais e numéricas.

Essa tese é organizada como uma coleção de três artigos científicos do autor e de colaboradores, que já foram publicados ou estão sob processo de submissão/revisão. No primeiro artigo, ensaios de fadiga por fretting sob carregamento de amplitude constante (CAL) foram realizados utilizando fios da liga de alumínio (AA) 1120 de um condutor AAAC (Cabo de Alumínio Liga) 823 MCM. Um ensaio de tração e ensaios axiais de fadiga em corpos de prova de fio lisos e com entalhe em V também foram realizados. Os dados dos ensaios de fadiga foram utilizados para comparar o AA1120 ao AA1350 e ao AA6201, duas ligas tipicamente utilizadas para fabricação dos fios de condutores. Sob tração, o AA1120 exibiu um limite de resistência à tração intermediário aos do AA1350 e do AA6201. Para as mesmas amplitudes de tensão, os fios de AA1120 utilizados nos ensaios axiais de fadiga tiveram vidas mais longas que os fios de AA1350, mas consideravelmente mais curtas que os fios de AA6201. Entretanto, sob fadiga por fretting, tanto os fios de AA1120 quanto de AA6201 tiveram resistência à fadiga similar. Os dados dos ensaios também foram utilizados para avaliar um critério de previsão de vida para fios sob fadiga por fretting baseado na Teoria das Distâncias Críticas (TCD). A maior parte das vidas previstas estiveram dentro de fatores de 3 das vidas medidas. A acurácia das previsões foi similar à observada em estudos prévios, nos quais a mesma metodologia foi aplicada a dados de ensaios de fadiga por fretting em fios de AA1350 e AA6201. Esses resultados mostram que a metodologia pode ser uma ferramenta confiável para a análise de dano por fadiga de fios de diferentes materiais submetidos à fadiga por fretting e a CAL.

No segundo artigo, ensaios de fadiga por fretting sob carregamento de amplitude variável (VAL) foram realizados em fios de AA6201-T81 de um condutor AAAC 900 MCM. A variação de amplitude foi representada a partir de um histórico de carregamento de três blocos. As condições de carregamento foram definidas utilizando-se medições de vibração de uma linha de transmissão em operação localizada na região centro-oeste do Brasil. Duas metodologias de

previsão de vida de fios foram estendidas para condições de VAL e foram avaliadas utilizando os dados dos ensaios de fadiga por fretting. Uma das metodologias é o mesmo critério baseado na TCD considerado no primeiro artigo, enquanto a outra é baseada em uma curva de fadiga mestre. Ambas metodologias forneceram previsões de vida dentro de fatores de 4 das vidas medidas. A acurácia obtida nesse estudo suporta o uso das metodologias propostas para previsão de vida de fios sob condições de VAL.

O terceiro artigo é focado na previsão de vida de um condutor ACSR (Cabo de Alumínio com Alma de Aço) Ibis 397,5 MCM sob sequências de carregamento high-low e low-high. Para isso, uma metodologia de previsão de vida baseada em modelagem 3D em elementos finitos de sistemas condutor-grampo foi estendida para incluir condições de VAL. Primeiramente, a metodologia foi aplicada a dados de ensaios de fadiga com CAL para avaliar se esta é capaz de descrever com acurácia a falha por fadiga do condutor ACSR Ibis. Em seguida, a metodologia foi avaliada utilizando dados de ensaios de fadiga conduzidos sob um histórico de carregamento de dois blocos. A maior parte das previsões esteve dentro de fatores de 3 das vidas medidas. Para os ensaios com VAL, a metodologia levou em consideração o efeito da sequência de carregamento na falha por fadiga de forma acurada, fornecendo estimativas de vida mais longas para os ensaios sob sequência high-low do que para aqueles sob sequência low-high. Além disso, a metodologia foi capaz de prever as posições das quebras de fios para os ensaios com VAL em acordo com as observações experimentais. Esses resultados sugerem que a metodologia pode ser estendida para condições de VAL e ser utilizada para prever acuradamente as vidas, os efeitos da sequência de carregamento e as regiões críticas para falha por fadiga de condutores.

Palavras-chave: cabo condutor; fios de liga de alumínio; fadiga por fretting; previsão de vida; carregamento de amplitude variável

Título: Previsão de vida à fadiga de cabos condutores e seus fios: Investigações experimentais e numéricas

CONTENTS

List of Figures

List of Tables

Nomenclature

A, b, A', b'	fitting constants of the SWT-N_f relation
C, d_L	fitting constants of the L-N_f relation
D_c	critical damage
d	wire diameter
E	Young's modulus
EI	bending stiffness
F_c	clamping force
F_m	mean bulk force
g	gravitational acceleration
H, T	tension force
K	Poffenberger-Swart's factor
L	critical distance
l	lay angle
M	multiplying factor
N	number of cycles applied at a given stress level
N_block	number of cycles in one loading block
N_est	fatigue life estimate
N_f	number of cycles to failure
n	number of wires
P	compressive normal force
Q	tangential force
R	bulk stress ratio

S_{a}	bulk stress amplitude
S_{m}	mean stress
SWT	Smith–Watson–Topper fatigue parameter
V	volume of the fatigue damage zone
w	conductor's weight
Y_{b}	bending displacement amplitude
α	crossing angle between wires
β_0	inclination angle of the conductor at active end
β_{p}	inclination angle of the conductor at passive end
γ	fitting parameter of Walker's equation
ΔD	fatigue damage fraction
$\Delta F/2$	bulk force amplitude
$\Delta\beta$	variation of the angle β_0
θ	surface crack orientation
ν	Poisson's ratio
ρ_{a}	aluminum density
σ	axial stress
σ_{a}	bending stress amplitude
σ_{ax}	axial stress amplitude
σ_{max}	maximum axial stress
σ_{na}	normal stress amplitude
σ_{nmax}	maximum normal stress
σ_{y}	yield stress
$\boldsymbol{\sigma}$	average stress tensor
$\hat{\boldsymbol{\sigma}}$	stress tensor
ϕ	inclination of the crack

1 Introduction

1.1 Motivation

Transmission lines (Fig. 1.1a) are the most commonly used systems for connecting power plants where electricity is produced with the users. The main component of a transmission line is the overhead conductor, which is responsible for transporting the electricity over long distances. Ideally, conductors should provide the best combination of high electrical conductivity, low cost, good mechanical resistance, low density and good resistance to oxidation and corrosion. The two materials that best fit these criteria are copper and aluminum. The first overhead conductors were usually manufactured using copper, as it was cheaper and mechanically more resistant than aluminum. In 1908, the invention of the Aluminum Conductor Steel Reinforced (ACSR) greatly improved the mechanical resistance of aluminum cables. In addition, developments in the aluminum technology from 1938 to 1945 significantly reduced the cost of this material, which spread the use of aluminum conductors in large scale. Over the years, copper wires have been gradually replaced by aluminum and aluminum alloy (AA) wires due to their lower density, better cost-benefit and fewer occurrences of the corona discharge effect, which causes loss of energy along the line (Fuchs, 1977).

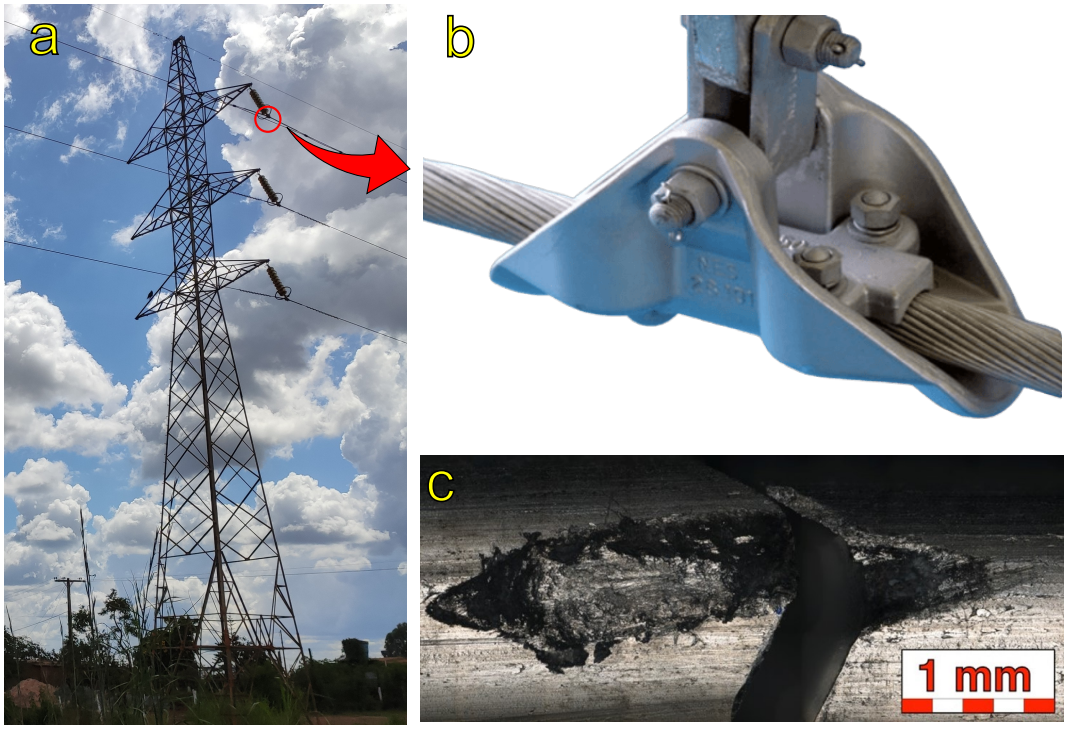

Figure 1.1: (a) Overhead conductors in a transmission tower, (b) suspension clamp (Cosmai et al., 2017), and contact mark between two wires.

During the operation of a transmission line, overhead conductors may be subjected to several types of non sustained and sustained motions. The former are caused by transient phenomena, such as corona vibrations, ice and snow shedding and earthquakes, while the latter are caused by wind forces acting on the conductor. Several studies on damaged or broken conductors taken from transmission lines indicate a clear correlation between wind-induced oscillations and the fatigue failure of the conductor's wires (Azevedo and Cescon, 2002; Boniardi et al., 2007; Chen et al., 2012; Kalombo et al., 2015; Gonzales-Pociño et al., 2018). Among all types of conductor motion, the aeolian vibrations are considered the most critical to fatigue damage. These oscillations can occur on almost all types of transmission lines, during any time of the day or year. The fatigue failures of the conductors wires usually take place near or within devices that restrain the movement of the conductor, such as suspension clamps (Fig. 1.1b), spacer clamps, and dampers. The aeolian vibrations favor the occurrence of fretting fatigue, leading to crack initiation in contact regions of the conductor, and eventually to wire rupture (EPRI, 2006). Fig. 1.1c shows an example of a wire rupture caused by fretting fatigue at the contact region between two wires of adjacent layers of a conductor.

The traditional approach used to evaluate the fatigue failure of conductors is based on obtaining stress-life (S-N) curves using resonant test benches (Kalombo et al., 2017; Fadel et al., 2012; Azevedo et al., 2009; Ouaki et al., 2003). In these tests, the conductor is usually supported by a suspension clamp and is subjected to a cyclic vertical displacement used to represent the aeolian vibrations. This approach can be used not only for obtaining the S-N test data for a given conductor-clamp system, but also as a means of evaluating the influence of parameters such as suspension clamp geometry, high temperatures and presence of lubricants on the failure of the conductor's wires. Additionally, recent studies have considered alternative approaches for investigating the fatigue behavior of conductors based on fretting fatigue tests on wires (Omrani et al. 2022, 2021; Said et al., 2020a, 2020b; Araújo et al., 2020; Matos et al., 2020; Rocha et al., 2019). These approaches are motivated by the fact that one of the main causes of conductor failure is the fatigue damage accumulation that occurs at a local (wire) scale, caused by fretting between wires in contact with each other or with a clamp device.

Despite being used for more than 50 years, the traditional design approach based on S-N curves relies on the fatigue testing of conductors, which can be expensive, time consuming, and dependent on the availability of a resonant test bench. Considering these possible drawback and motivated by the recent advances in computing power and finite element (FE) 3D modeling of conductor-clamp systems, studies over the past five years have aimed to develop a global-local approach to predict the life of the conductor. On a global (structural) scale, a FE model of the conductor-clamp system is employed to identify the fatigue critical region, i.e., the location where wire breaks are expected to occur. Then, the loading and contact conditions in the critical region are estimated and used as input for a local-scale fatigue damage analysis of the wires under fretting fatigue. The local-scale analysis is used to predict the lives of the wires, which can then be associated with the durability of the conductor.

Previous investigations (Rocha et al., 2022, 2023) have shown that these global-local approaches can provide life predictions for conductor-clamp systems in agreement with experimental data. However, the development of these approaches is recent and has been the focus of few investigations. Thus, further research is required to improve their use considering different wire materials, conductor geometries, and loading conditions. In this context, this thesis aims

to propose and evaluate life prediction methodologies for overhead conductors and their wires by means of experimental and numerical analyses.

1.2 Outline of the thesis

This thesis is organized into four main chapters. Chapter 2 is a literature review of the fatigue failure of overhead conductors, while each of the remaining chapters is structured as a research paper. The literature review briefly discusses the three main types of wind-induced conductor motion, but focus is given to the aeolian vibrations and fretting fatigue of the conductors wires. This literature review should provide the reader with a general idea about wind-induced conductor oscillations, the main methods of safe design and assessment of vibration severity, and the main findings from experimental and numerical studies aimed at understanding the fatigue behavior of overhead conductors.

Chapter 3 is focused on the fatigue damage analysis of AA1120 wires under fretting fatigue. This material has a high electrical conductivity and an intermediate ultimate tensile strength compared to other aluminum alloys commonly used to manufacture wires of conductors, such as the AA1350 and the AA6201. These characteristics have led transmission lines in Brazil to be designed with conductors composed of AA1120 wires since the last decade (Hoffman et al., 2015). The growing use of AA1120 wires in overhead conductors in Brazil motivates the present study to further investigate the fatigue behavior of this material. To this end, Chapter 3 aims to compare the fatigue performance of the AA1120 with that of the AA1350 and AA6201, and to evaluate a nonlocal life prediction methodology using data from fretting fatigue tests on AA1120 wires.

Chapters 4 and 5 examine the fatigue performance of conductors and wires under variable amplitude loading (VAL) conditions. The importance of performing fatigue damage analyses under VAL stems from the fact that conductors typically experience significant variations in vibration amplitude during service. These amplitude variations are caused by various environmental factors such as temperature variations, changes in wind speed and velocity, and changes in the landscape where the transmission line is located due to ice or snow accumulation. Des-

pite the numerous reports on vibration amplitude variation (Varney, 1926; Rawlins and Harvey, 1959; Edwards and Boyd, 1963; EPRI, 2006), most studies on the fatigue failure of conductors and wires are limited to constant amplitude loading conditions. In this regard, the present study aims to propose and evaluate life prediction approaches for wires (Chapter 4) and conductor-clamp systems (Chapter 5) under VAL conditions.

1.3 Publications

The following publications have been based on the work contained in this thesis:

In International Journals:

1. **Matos IM**, Araújo JA, Castro FC. Fretting fatigue performance and life prediction of 1120 aluminum alloy wires of overhead conductors. **Theoretical and Applied Fracture Mechanics** (94% percentile in Scopus) 2022;121:103521.

2. **Matos IM**, Araújo JA, Castro FC. Life prediction of 6201-T81 aluminum alloy wires under fretting fatigue and variable amplitude loading. **Tribology International** (94% percentile in Scopus) 2023;183:108407.

3. **Matos IM**, Lalonde S, Araújo JA, Castro FC. Fatigue life prediction of ACSR Ibis conductor under high-low and low-high loading sequences using a finite element 3D model. Submitted to **International Journal of Fatigue** (96% percentile in Scopus).

In International Conferences:

1. **Matos IM**, Araújo JA, Castro FC. Fretting fatigue of 6201 aluminum alloy wires under variable amplitude loading: An initial study. In 26th International Congress of Mechanical Engineering – COBEM 2021.

2. **Matos IM**, Araújo JA, Castro FC. Fretting fatigue of 6201 aluminum alloy wires under variable amplitude loading: Experiments and life prediction. In 10th International Symposium on Fretting Fatigue – ISFF10 2022.

In book chapter:

Araújo JA, Ferreira JLA, Kalombo RB, **Matos IM**, Castro FC. Overhead conductors. In: Liskiewicz T, Dini D, editors. Fretting Wear and Fretting Fatigue - Fundamental Principles and Applications. Cambridge: Elsevier; 2022, p. 565-97.

2 Literature review

2.1 Scope

This literature review is focused on the fatigue failure of conductors due to wind-induced cyclic motions. The review is divided into four main sections to cover the following topics:

- Wind-induced conductor motion (Section 2.2): gives an overall idea about the different types of wind-induced conductor oscillations, their causes and negative consequences to the integrity of the transmission line. Details the occurrence of fretting fatigue in overhead conductors and how it leads to crack initiation and can cause the failure of the conductor. Shows the main characteristics of real transmission line vibration;

- Safe design and assessment (Section 2.3): introduces the Poffenberger-Swart formula, which is widely used to associate the vibration amplitude with bending stresses. Presents the main approaches used for the safe design and assessment of transmission lines with respect to aeolian vibrations;

- Experimental studies (Section 2.4): describes the construction and operation of a resonant test bench for overhead conductors. Details the main findings obtained from fatigue tests performed on these tests benches, as well as from fatigue tests with individual wires and wires under fretting conditions;

- Numerical modeling (Section 2.5): describes the recent advancements in finite element-based analyzes of overhead conductors and fretting wires.

An outline of the topics covered in this review is presented in Fig. 2.1. In the PDF version of this document, this figure contains hyperlinks to each section of this review. The reader may click on any of the topics to go directly to the section where it is discussed.

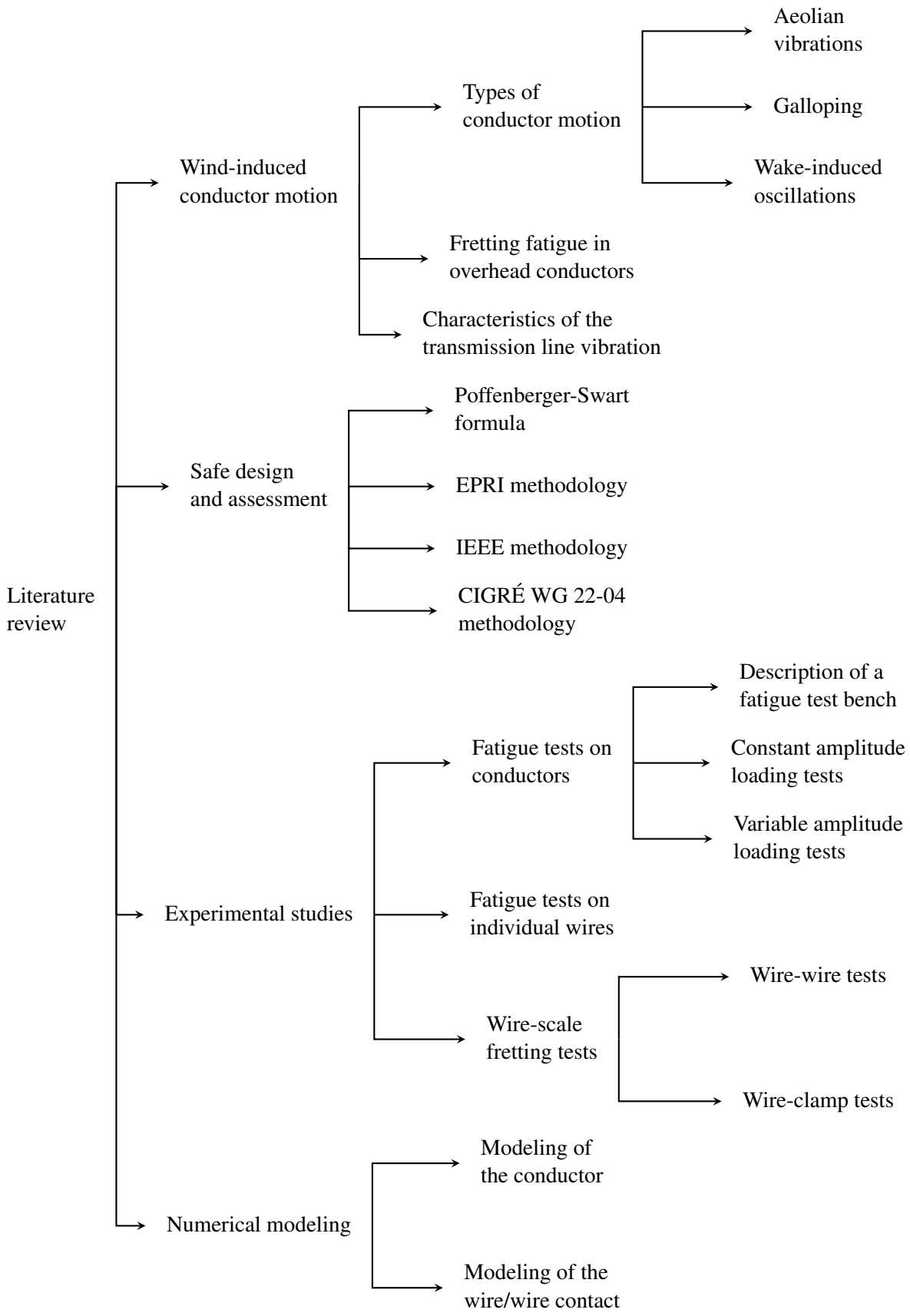

Figure 2.1: Outline of the main topics covered in this literature review.

2.2 Wind-induced conductor motion

Overhead conductors are the main components of transmission lines responsible for transporting electricity over long distances. These components correspond to about 40% of the total cost of a transmission line and are designed to have a lifetime of several years (EPRI, 2006). However, the conductors are frequently subjected to wind-induced cyclic motions, which if uncontrolled can damage the conductor and significantly reduce its durability. Therefore, understanding the different types of wind-induced motion and how they affect conductors is an important step in the safe design of transmission lines.

This section describes the three main types of wind-induced conductor motion, detailing how they occur and the potential failures that arise from each one. Focus is given to the effects of fretting, a contact damage phenomenon caused by conductor oscillations, which is widely associated to the fatigue failure of the conductor. The main characteristics of transmission line vibration are also discussed.

2.2.1 Types of conductor motion

There are three prominent categories of wind-induced cyclic motions in overhead conductors: aeolian vibrations, galloping and wake-induced oscillations. These movements differ from one another in terms of motion pattern, frequency and damage caused to the transmission line. The type of transmission line affected, and the wind and environmental conditions required for these motions to occur are also different for each one.

The aeolian vibrations (Section 2.2.1.1) are considered the most critical motion to the fatigue failure of the conductor. These vibrations can lead to a phenomenon known as fretting fatigue (Section 2.2.2), which can cause crack initiation and eventual rupture of the conductor's wires. Laminar winds flows with slow to moderate speeds may cause aeolian vibrations, making almost all transmission lines susceptible to this motion.

Galloping (Section 2.2.1.2) is considered the conductor motion that can cause the most damage in a short amount of time. This conductor motion can cause the damage and failure of

the conductor, dampers, tie-wires, insulator pins, suspension hardware, crossarm hardware and even lead to the collapse of the transmission tower. Like the aeolian vibrations, galloping can occur on all types of transmission line. In general, galloping only occur on conductors with ice or wet snow deposition, but there are records of non-ice galloping.

Unlike the two other types of conductor motion, the wake-induced oscillations (Section 2.2.1.3) only affect bundled conductors. The movement is caused by moderate to strong winds, which flow by the windward conductor and leave a wake that causes the leeward conductor to move. Part of the movement is also transmitted to the windward conductor through devices that connect both cables, such as a spacer clamp. The wake-induced oscillations typically affect localized sections of the transmission line, causing rapid wear and fatigue to suspension clamps, spacers and other devices.

2.2.1.1 Aeolian vibrations

As wind flows by an overhead conductor, a repeating pattern of alternating vortices can be formed from the top and bottom of the leeward side of the conductor, as illustrated in Fig. 2.2. This pattern is named "von Kármán vortex street" after Theodore von Kármán who developed a theoretical model to describe the phenomenon in 1912. When the wind flows by the conductor, the flow splits around it and the wind loses speed due to friction. Depending on the velocity of the wind, this can create an alternating pressure unbalance, causing the wind to swirl into vortices. The vortex shedding generates forces that make the conductor vibrate in a direction normal to both the direction of wind flow and the conductor's longitudinal direction, which is the primary cause of aeolian vibrations (Cosmai et al., 2017).

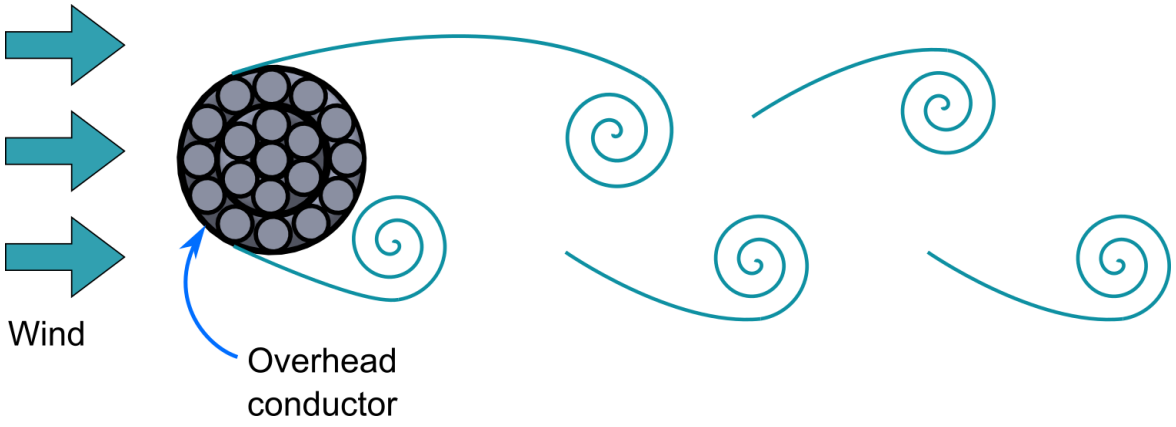

Figure 2.2: Schematic of the "von Kármán vortex street" phenomenon on overhead conductors.

Aeolian vibrations are characterized by their small amplitude, rarely exceeding the diameter of the conductor. Typically, they occur at frequencies of 3 to 150 Hz and are caused by winds flowing at speeds of 1 to 7 m/s. As mentioned, the aeolian vibrations are caused by the vortex shedding that occurs when wind flows by the conductor, in particular when the frequency of the vortices approaches one of the modal frequencies of the conductor. Once the conductor starts to vibrate a locking-in effect occurs, i.e., changes in the wind velocity within a certain range (about 90% to 130% of the initial velocity) do not affect the vibration frequency of the conductor (Cosmai et al., 2017). This happens because once the conductor starts to vibrate at one of its natural frequencies, the vortex shedding is not only affected by the wind speed but also by the vibration frequency of the conductor itself. Once the lock-in effect occurs, the aeolian vibrations develop into waves that travel back and forth in a span. When two opposing waves come across each other, standing vibration loops can be established. Typically, spans will exhibit multiple loops, with nodes (points with minimum amplitude) and antinodes (points with maximum amplitude). The length of these loops can range from less than 1 m up to 30 m depending on the vibration frequency.

The major damage associated with aeolian vibrations is the fatigue failure of the conductor at devices that restrain its movement, such as suspension clamps, deadend clamps, dampers and spacers. As an example, Fig. 2.3a shows the fatigue failure of an ACSR conductor in a metallic suspension clamp. Among these clamping devices, the most critical to fatigue failure is the suspension clamp, because of its rigidity. In this region, the cyclic bending stresses produced

by the aeolian vibrations are combined with static stresses caused by the conductor curvature, the tension force and the clamping force. These loading conditions favor the occurrence of fretting, a process of surface wear caused by minute relative displacement between surfaces in contact, which will be detailed in Section 2.2.2. Aeolian vibrations may also cause loosening of bolts in devices such as the spacer clamp, leading to the rupture of the conductor or the device itself, as shown in Fig. 2.3b.

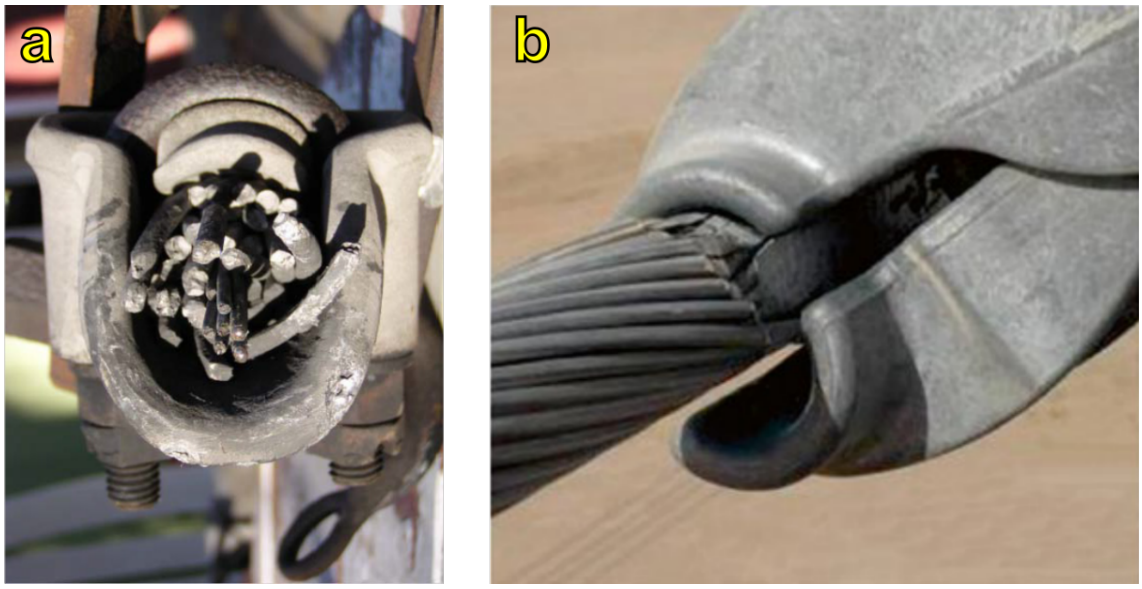

Figure 2.3: Conductor failures caused by aeolian vibrations at (a) a suspension clamp (IEEE, 2015) and (b) a spacer clamp with loosened bolts (Cosmai et al., 2017).

Several factor can affect the aeolian vibrations and consequently influence on the fatigue failure of overhead conductors. IEEE (2015) highlights six of those factors, namely: (i) span length, (ii) horizontal tension/unit weight ratio, (iii) terrain, (iv) local climate, (v) conductor material, and (vi) aeolian vibration entrapment by in-span masses.

The span length and horizontal tension force influence the self-damping of overhead conductors, i.e., their ability to dissipate part of the energy input by the wind. In general, shorter spans are less susceptible to aeolian vibrations than longer spans. This happens because there is less wind energy input in shorter spans, making it easier for the conductor to dissipate this energy trough self-damping. For the same reason, high tension forces can significantly reduce the self-damping capability of the conductor, making it more vulnerable to aeolian vibrations.

Considering the correlation between the tension force applied to the conductor and its self-

damping capability, the definition of maximum admissible tension forces became an important part of the safe design of transmission lines with respect to aeolian vibrations. For this reason, CIGRÉ SC6 defined in 1960 the concept of Every Day Stress (EDS) as the maximum tension force the conductor can sustain without any failure due to aeolian vibrations at or around the temperature that occurs for the longest period during its operation (Barret and Motlis, 2001; CIGRÉ, 2005). EDS is typically expressed as a percentage of the Rated Tensile Strength (RTS). The RTS is defined as the sum of the tensile strengths of the conductor's wires at a specified strain level (usually 1%), multiplied by a rating factor. ASTM Standards defined this rating factors for conductors made of 1350 and 6201 aluminum alloy wires according to the number of wire layers, as summarized in Table 2.1. For ACSR conductors, the same factors are applicable to both steel and aluminum layers (Aluminum Association, 1982; Akhtar, 1988). For example, an ACSR conductor with one layer of steel wires and three layers aluminum alloy wires has its RTS determined by multiplying the strengths of the steel wires by a factor of 96% and of the aluminum wires by 91%.

Table 2.1: Rating factors for conductors made of 1350 and 6201 aluminum alloys.

Nº of wires per conductor	Nº of layers per conductor	Rating factor
7	1	96%
19	2	93%
37	3	91%
61	4	90%
91 or more	5 or more	89%

The EDS has become an important tool for the design of transmission lines and is still used nowadays. Despite that, CIGRÉ (2005) describes a couple of issues related to the EDS. The first issue is that conductors operating below the proposed EDS safe limits may still exhibit fatigue failures. To exemplify this problem, an investigation was performed on bare ACSR conductors in operation. It was observed that approximately 5% of the conductors operating during less than five years presented fatigue failures, and this percentage goes up to almost 60%

for conductors operating during more than 20 years. The second issue is that the EDS concept was proposed in a time when most transmission lines used ACSR (Aluminum Conductor Steel Reinforced) conductors, which made some of the proposed values of EDS insufficient to describe the fatigue failures of more recent transmission lines. For these reasons, CIGRÉ (2005) proposed a different guidance for the conductor tension force based on the catenary parameter, which is the ratio H/w between the horizontal tension force H and the weight per unit length w. This tension force is determined using initial conditions, before wind, ice loading and creep and should be taken using the average temperature during the coldest month.

The terrain in which the transmission line is installed influences the wind turbulence. Aeolian vibrations are critical in laminar flows, which typically occur at open and flat terrains, without obstructions, or near/across large bodies of water. For this reason, CIGRÉ (2005) recommends different magnitudes for the safe design tension force (expressed in terms of the catenary parameter) depending on the terrain characteristics, as shown in Table 2.2. CIGRÉ also notes that the recommended safe tension forces may not be suitable if the span: (i) is extra long, (ii) is exposed to pollutants that decrease the self-damping of the line, (iii) is often covered with ice, (iv) is operated at high temperatures.

Table 2.2: Maximum recommended catenary parameters based on terrain characteristics (CIGRÉ, 2005).

Terrain category	Terrain characteristics	H/w_{adm} [m]
1	Open and flat, with no trees or obstructions and covered with snow; near/across large bodies of water; on flat desert	1000
2	Open and flat, with no obstructions and no snow	1125
3	Open and flat, or undulating, with very few obstacles	1225
4	Built-up with some trees and buildings	1425

Three climate conditions that can affect the aeolian vibrations are temperature, wind intensity and occurrence of ice or snow accumulation. Lines operating at very low temperatures tend to have higher tension forces and are, consequently, more vulnerable to aeolian vibrations. Persistent prevailing winds cause more vibration cycles, which may lead to the fatigue failure

of conductor. Ice and snow accumulation on the conductor can facilitate aeolian vibrations to occur at lower frequencies.

The fatigue failure caused by the aeolian vibrations is affected by the materials used in the conductor's wires. In particular, the material of outer layer wires are significant to the fatigue endurance of the conductor, as most failures occur at these wires. This usually limits the materials used in conductors to steel, copper, aluminum and aluminum alloys. It is important to mention that the fatigue behavior of the conductor cannot be accurately described by simply taking the fatigue resistance of its individual wires, and should preferably be obtained by fatigue tests on a particular conductor-clamp assembly.

Occasionally, additional devices need to be installed on transmission lines. For example, aerial marker balls (Fig. 2.4a) are used to comply with government requests and identify one or more spans on a line. Distributed Series Reactors (Fig. 2.4b) may also be employed on transmission lines to improve voltage unbalance and alleviate overloading problems. The use of such devices can eventually lead to aeolian vibration entrapment, i.e., vibrations between devices that can not be mitigated by the dampers located at the span extremities.

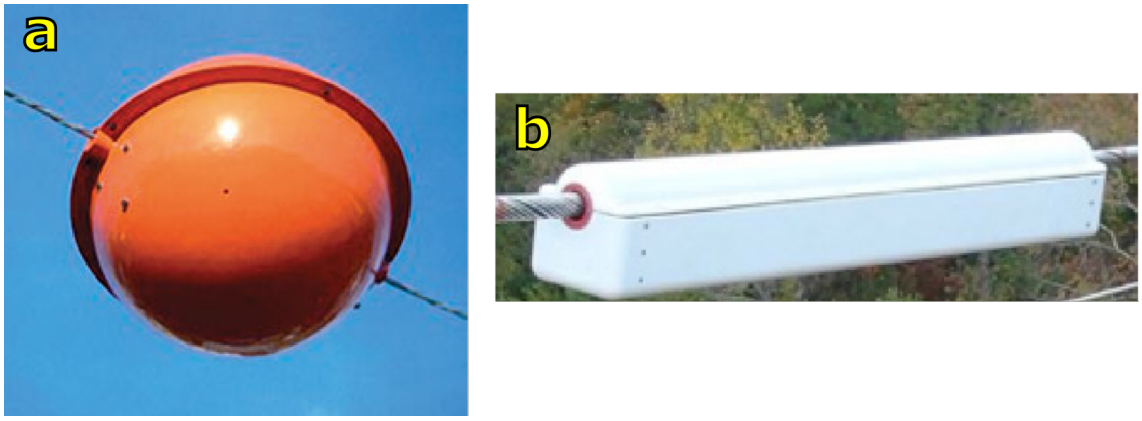

Figure 2.4: Examples of in-span masses: (a) aerial marker ball and (b) Distributed Series Reactor (IEEE, 2015).

2.2.1.2 Galloping

Galloping is a type of wind-induced conductor motion that typically occurs due to thin ice accretion, with a thickness of one to two millimeters. Ice deposition upon the conductor, such as the one illustrated in Fig. 2.5, causes an asymmetric condition for the conductor's cross sectional

shape, which makes the conductor aerodynamically and/or aeroelastically unstable and can lead to galloping. Unlike the aeolian vibrations, galloping is a high amplitude oscillatory motion, with amplitudes that can reach 10 m. It typically occurs at small frequencies of 0.08 to 3 Hz and is caused by wind velocities of 7 to 18 m/s, approximately. The high dynamic loads can cause catastrophic damage in a short amount of time to the conductor, hardware installed on the line and to the transmission towers.

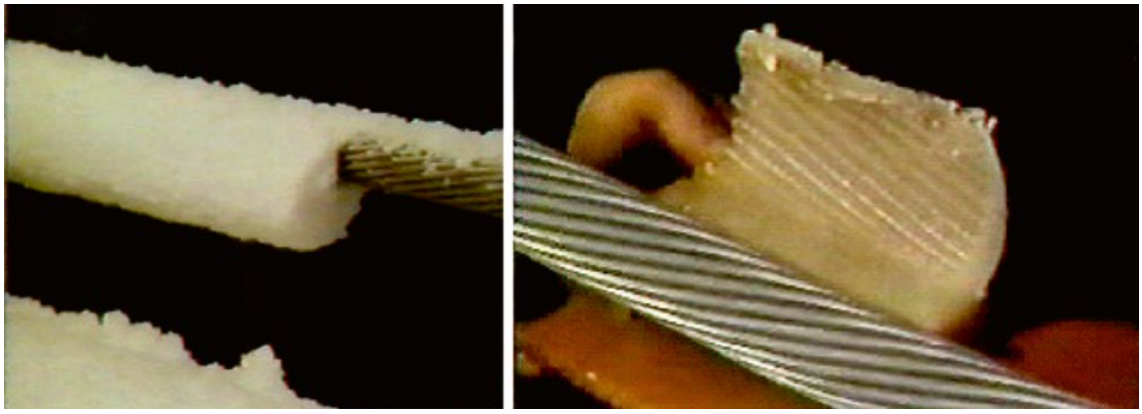

Figure 2.5: Asymmetrical ice accretion in an overhead conductor (Cosmai et al., 2017).

Galloping is usually a vertical motion and can take the form of standing and traveling waves or a combination of both. In some cases, a horizontal component os oscillation can also occur. Both vertical and horizontal components are usually out-of-phase, which can lead some material points in the conductor to display elliptically shaped movements, such as the ones shown in Fig. 2.6. A twisting motion may also take place, with rotations that can exceed 100º.

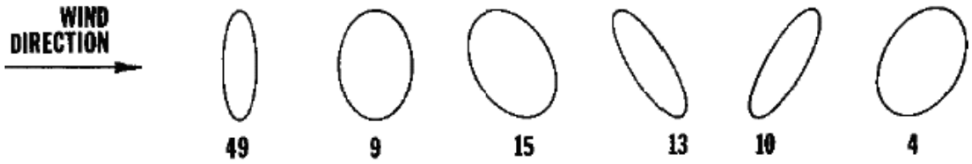

Figure 2.6: Examples of elliptical conductor movements caused by galloping. Numbers bellow each shape indicate percentage of occurrence (EPRI, 2006).

According to EPRI (2006), there is still no reliable method to properly protect the transmission line against galloping, which is applicable to all situations. Even so, there are a few actions that are usually taken by utilities to protect the transmission line against galloping. The main actions are:

- To remove of prevent the formation of ice on the conductor, which is accomplished by ice-melting schemes and mechanical ice removal;
- To prevent galloping from reaching high vibration amplitudes. The installation of interphase ties does not prevent galloping from happening but reduces its movement;
- To design lines more tolerant to galloping, by increasing vertical clearances based on galloping ellipses.

2.2.1.3 Wake-induced oscillations

Wake-induced oscillation is a term used to describe several types of wind-induced cyclic motions that only affect bundled conductors. These oscillations are caused by winds flowing at speeds of 7 to 18 m/s, leading to the aerodynamic shielding of the leeward conductor by the windward conductor. Usually these motions occur at frequencies of 0.15 to 10 Hz, with amplitudes that can reach 2 m. Compared to the other types of wind-induced oscillations, this a relatively recent issue, as bundled conductors were not used until the 1950s. Wake-induced oscillations can cause fatigue and sever wear of the conductor and support hardware.

There are four main types of wake-induced oscillations, which are illustrated in Fig. 2.7. The most common is the subspan mode, where vibrations take the form of elliptical trajectories. The major axes of these ellipses are horizontal, making this movement visible from the ground. The other types of motions are considered rigid-body modes due to the little distortion caused to the bundle cross section. These involve a combination of vertical, horizontal and torsional movements and are classified based on which movement is predominant.

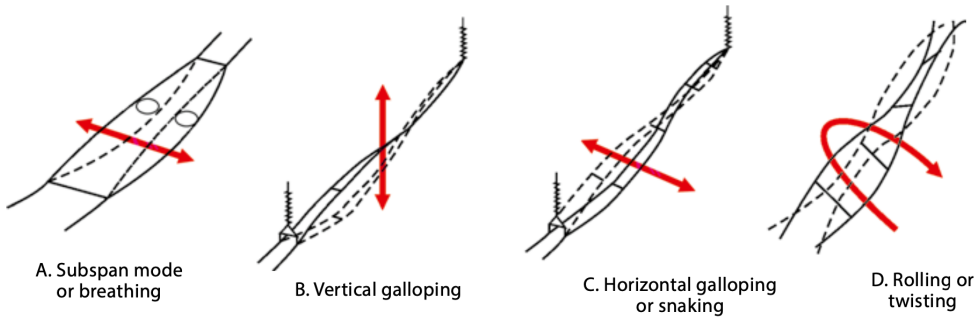

Figure 2.7: Types of wake-induced oscillations (Cosmai et al., 2017).

Several methods have been applied to prevent or mitigate the effects of wake-induced oscillations. Tilting the conductors by angles of more than 20º is a strategy used to place the leeward conductor in a position where it is not affected by the windward conductor's wake. Another strategy is to increase the spacing-to-diameter ratio of the bundled conductors to decrease the motion effect. Some four-conductor bundles have been designed using a diamond configuration, which combines the ideas of placing leeward conductors outside of windward conductors' wakes with an increase in the spacing-to-diameter ratio. In particular for subspan oscillations, the most used protection method is to use subspace staggering schemes and damping spacers, which have been observed to increase wind velocity threshold and reduce vibration amplitudes.

2.2.2 Fretting fatigue in overhead conductors

Fretting is a surface damage process caused by minute relative displacement between surfaces in contact. In overhead conductors, fretting occurs at contact regions between wires of the same or of adjacent layers, and between wires of the external layer with devices that restrain the movement of the conductor, such as suspension clamps. In these critical regions, the oscillatory conductor motions, specially the aeolian vibrations, can cause minute relative displacements between the surfaces in contact. The combination of these displacements with the clamping force applied to these devices favors the occurrence of fretting, eventually leading to crack initiation at the fretting marks. The cyclic bending stresses may cause these cracks to propagate and eventually lead to the rupture of the wires.

It is well known that fretting can significantly reduce the fatigue strength of the components in contact, and there are numerous field and laboratory studies that correlate the occurrence of fretting with the fatigue damage and failure of overhead conductors and devices installed on the line (Ouaki et al., 2003; Boniardi et al., 2007; Azevedo et al., 2009; Kalombo et al., 2015). Despite being a well known problem in conductors for more than 50 years (Fricke and Rawlins, 1968), the fretting fatigue behavior of conductors is still considered a complex phenomenon to characterize based on the mechanical properties of the wires. Hence, the tradi-

tional approach used to describe the fatigue life of a conductor-clamp assembly is still based on performing fatigue tests on a test bench and estimating its S-N curve (Cosmai et al., 2017).

The process of crack initiation from fretting marks can be summarized as follows. Initially, an oxide film is removed from the surfaces in contact. Then, the bare surfaces tend to adhere and form weld junctions that are broken by the minute relative displacements, causing the detachment of debris from the surfaces. In the case of aluminum wires, the released particles react with the air of the environment forming aluminum oxide (Al_2O_3) debris. These dark particles are significantly harder than the aluminum wires, acting as abrasive materials and favoring crack initiation from the fretting marks (Aggarwal et al., 2000; Azevedo et al., 2009).

In a typical conductor-clamp assembly, the contact marks can display three main behaviors, which are affected by their longitudinal distance from the center of the clamp. Marks located between the clamp center and the keeper edge (KE) are usually adhered because of the high pressure produced by the clamp. Between the KE and the last point of contact (LPC) between conductor and clamp, most marks show characteristics of a partial slip fretting regime, with the formation of stick and micro slip zones. One example of such a contact mark is shown in Fig. 2.8. In the stick zone, the surfaces are adhered, while minute relative displacement takes place at the micro slip zones, leading to the formation of aluminum oxide debris. The stick zone is usually positioned towards the KE and is larger for marks located close to it. Finally, most marks ahead of the LPC show characteristics of gross sliding, with the detachment of aluminum oxide debris at the whole contact zone. Fatigue tests performed on conductors have shown that the region between the KE and the LPC is usually the most critical to the fatigue failure of the conductor, as cracks initiate and propagate from the partial slip fretting marks (Zhou et al., 1994a, 1994b; Ouaki et al., 2003). Cracks may also initiate at gross sliding contacts, but vanish due to wear before they propagate (Azevedo et al., 2009).

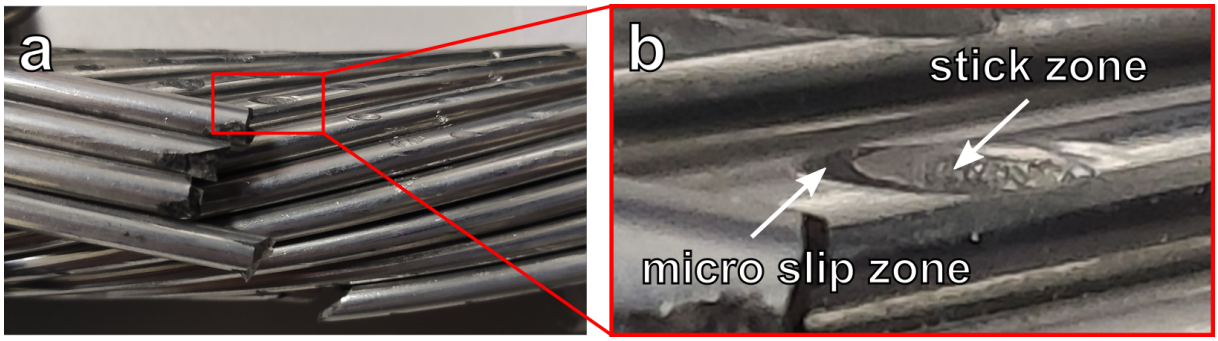

Figure 2.8: Damaged conductor used on a fatigue test: (a) overall view and (b) contact mark where partial fretting slip regime occurred.

There are two main shapes of fretting marks observed on overhead conductors. Fretting marks from the contact between wires of adjacent layers have elliptical shapes (Fig. 2.9a). On the other hand, a line contact shape (Fig. 2.9b) is observed at external layer wires in contact with the support clamp or the keeper, and at the contact between wires of the same layer (Fig. 2.9c). Fatigue tests performed on an ACSR Drake conductor (Zhou et al., 1994b) have shown that the shape of the contact mark can affect the cracking patterns. For the elliptical contact shape (Fig. 2.10a), it was observed that cracks can nucleate simultaneously from both extremities of the contact mark and that these crack propagate at angles of about 30º with respect to the wire surface. As for the line shape (Figs. 2.10b and c), cracks nucleate parallel to each other and propagate at angles close to 90º.

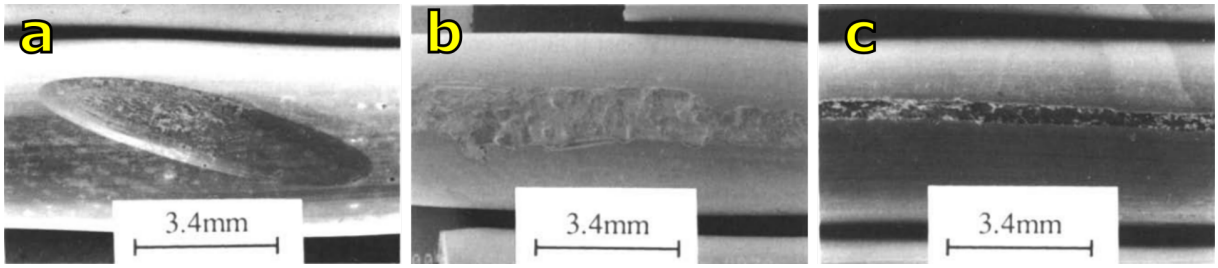

Figure 2.9: Fretting marks obtained from the contacts between: (a) wires of adjacent layers, (b) an external layer wire and the keeper, and (c) wires of the same layer (Zhou et al., 1994a).

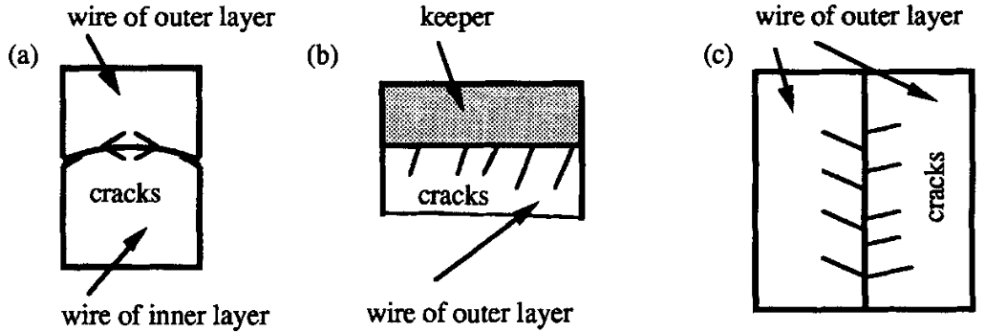

Figure 2.10: Schematic of the crack propagation from the contacts between: (a) wires of adjacent layers, (b) an external layer wire and the keeper, and (c) wires of the same layer (Zhou et al., 1994b).

2.2.3 Characteristics of the transmission line vibration

During the operation of a transmission line, several factors can affect the vibration of an overhead conductor. For example, the wind speed and direction may change during the day or throughout the year, temperature variations can change the line tension force, and dampers can be installed on the line or have their arrangements modified. These factors lead to a complex loading spectrum with significant amplitude variation (Brunair et al., 1988).

Field vibration measurements are an important tool for the safe design and assessment of a transmission line. These data can be used to identify damage sources and the risk of fatigue failure, to assess the remaining lifetime of the conductor, and to evaluate natural damping and damping configurations (IEEE, 2006). Some of the first recordings of vibrations in transmission lines can be found in the work of Varney (1926). The researcher designed an apparatus to measure vibration data using a string connected on one end to an overhead conductor and on the other end to a wooden block attached to a pencil. When the conductor vibrates, the pencil moves up and down in response and the movement is registered in a piece of paper in a wooden slide. Using this device, the researcher obtained short recordings (3 to 11 seconds) of vibration data for different spans and line loads. In most samples, the conductor exhibited a sinusoidal amplitude modulation known as beat pattern, as shown in Fig. 2.11.

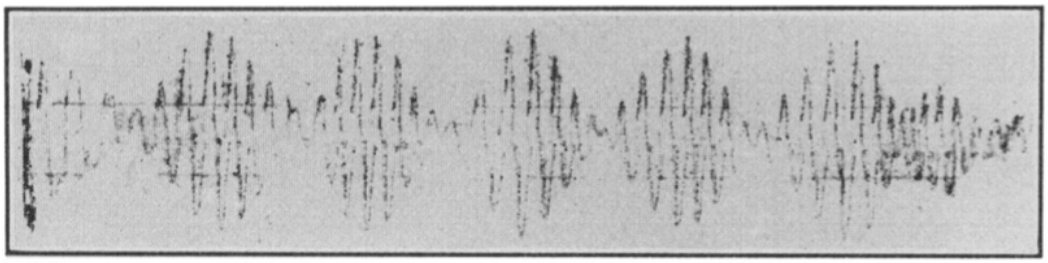

Figure 2.11: Four seconds sample of a transmission line vibration exhibiting beat pattern oscillations (Varney, 1926)

The beat pattern oscillations observed by Varney (1926) are caused by the spatial turbulence of wind along the span of a transmission line. This can lead different points of the conductor to be simultaneously excited at slightly different vibration frequencies. The beat pattern oscillations occur when two or more of these vibrations overlap (Cosmai et al., 2017). With the advancements in vibration recording devices, researchers have been able to record the vibration data of several transmission lines where the same beat pattern oscillations can be observed (Wright and Mini Jr., 1934; Tebo, 1941; Rawlins and Harvey, 1959; Davall et al., 1978).

Noiseux et al. (1987) proposed an analytical model to describe the aeolian vibrations of conductors. According to their model, these vibrations can be described using narrow frequency bands, whose envelopes have a Rayleigh distribution. To evaluate the model, vibration data was obtained from an experimental line located in the Magdalen Islands. The vertical displacements of a material point in the conductor located at a longitudinal distance of 1 m from the suspension clamp were measured in 4 s samples. For each ensemble, i.e., subgroup of samples with the same dominant frequency, the authors compared the distribution of peak values normalized by the ensemble root mean square (Y_c/Y_{rms}) with its probability density function. The results obtained for the ensembles of 11 and 21 Hz are shown in Fig. 2.12. The authors observed that the results compare fairly well with a Rayleigh distribution, especially for the ensemble centered at a frequency of 21 Hz. Thus, it was concluded that the aeolian vibrations can be modeled by narrow frequency bands.

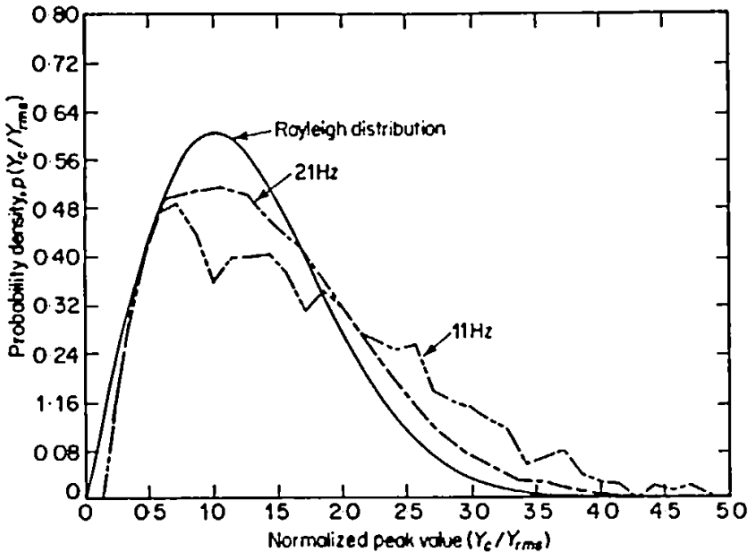

Figure 2.12: Normalized probability density function of the peak displacements of an overhead conductor (Noiseaux et al., 1987)

2.3 Safe design and assessment

This section provides a description of the three main approaches used to assess the vibration severity of overhead conductors. Initially, Section 2.3.1 provides details about the well-known Poffenberger-Swart (P-S) formula. This equation is used to estimate the nominal bending stresses acting on outer layer wires of overhead conductors. The concept of nominal bending stresses or strains is essential to the definition of the endurance limits proposed in the EPRI (Section 2.3.2) and IEEE (Section 2.3.3) methodologies. In the CIGRÉ WG 22-04 methodology (Section 2.3.4), the P-S equation is employed to associate the bending displacements obtained from a vibration recorder matrix with nominal bending stresses, which can then be used to estimate the remaining lifetime of the conductor.

2.3.1 Poffenberger-Swart formula

Since the 1930's, several instruments were developed to measure the relative displacement of overhead conductors, such as the ones shown in the works of (Wright and Mini Jr., 1934; Rawlins and Harvey, 1959; Sproule and Edwards, 1959). Around the same time, strain gauges were being employed to investigate several structures subjected to dynamic loading, and in the

1950's researchers began to apply the technology to non-energized conductors in outdoor and laboratory test spans (Ruhlman et al., 1959; Steidel Jr., 1959).

One of the challenges faced by researchers at the time was the lack of mathematical and experimental evidences that supported the use of relative displacement measurements to estimate the stresses or strains on conductors. This led to the formation of the Task Force on Standardization of Conductor Vibration Measurements by the AIEE Transmission and Distribution Committee in 1961. Their goal was to recommend a standard method for measuring conductor vibration. The Task Force performed a series of experimental tests on different types of ACSR conductors and compared displacement and strain measurements, as reported by (Poffenberger and Swart, 1965). The results from these tests showed that the relation between displacement and strain was affected by the tension force applied to the conductor and the diameter of its individual wires, but not by the vibration frequency.

These experimental results motivated Poffenberger and Swart (1965) to propose a mathematical relationship between differential displacement and bending strain in overhead conductors. Their goal was to provide an analytical solution that could be used for general geometries and materials of the conductor. The formulation was deduced by considering the conductor as a beam fully fixed at one end and subjected to tension force, bending moment and distributed transverse load.

Despite being originally formulated for bending strains, the Poffenberger-Swart formulation is usually expressed as a relation between the bending stress amplitude σ_{a} (zero-to-peak) of an external layer wire at the exit of the clamp mouth and the bending displacement amplitude Y_{b} (peak-to-valley) and can be written as

$$\sigma_{\mathrm{a}} = KY_{\mathrm{b}} \tag{2.1}$$

The bending displacement amplitude used in Eq. (2.1) was defined by IEEE (1966) as the vertical displacement range (peak-to-valley) of a material point of the conductor diametrically opposed to the Last Point of Contact (LPC) between conductor and clamp and located at a longitudinal distance of 89 mm from the LPC, as illustrated in Fig. 2.13.

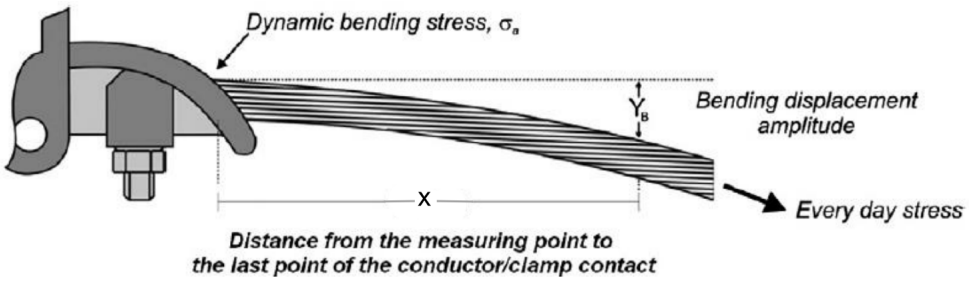

Figure 2.13: Schematic of the conductor-clamp assembly illustrating the measurement of the bending displacement amplitude. Adapted from (Kalombo et al., 2015).

The parameter K in Eq. (2.1) expresses the influence of the applied tension force and the conductor's geometry and material on the relation between bending stress and bending displacement amplitudes. This parameter can be estimated as

$$K = \frac{E_{\mathrm{a}} d_{\mathrm{a}} p^2}{4(e^{-px} - 1 + px)} \tag{2.2}$$

where E_{a} and d_{a} are the Young's modulus and diameter of an aluminum wire located at the external layer of the conductor, respectively, and x is the longitudinal distance between the point in the conductor where the vertical displacement is measured and the last point of contact between conductor and clamp (usually taken as $x = 89$ mm). The parameter p can be calculated as

$$p = \sqrt{\frac{T}{EI}} \tag{2.3}$$

where T is the tension force applied to the conductor and EI is its flexural stiffness.

According to Poffenberger and Swart (1965), the flexural stiffness, EI, in Eq. (2.3) can be determined using three different approaches: (i) by considering that all wires act as individual elements, (ii) that all wires act as if they were welded together, or (iii) somewhere between the other two behaviors. For their analyzes, they only considered the first approach, where the minimum flexural stiffness can be determined by

$$EI_{\mathrm{min}} = n_{\mathrm{a}} E_{\mathrm{a}} \frac{\pi d_{\mathrm{a}}^4}{64} + n_{\mathrm{s}} E_{\mathrm{s}} \frac{\pi d_{\mathrm{s}}^4}{64} \tag{2.4}$$

where n_{a}, E_{a} and d_{a} are the number, Young's modulus and diameter of the aluminum wires, respectively, while n_{s}, E_{s} and d_{s} are the number, Young's modulus and diameter of the steel wires, respectively.

2.3.2 EPRI methodology

EPRI (2006) gathered data from numerous fatigue tests performed on ACSR (Aluminum Conductor Steel Reinforced Cable), AAAC (All Aluminum Alloy Cable), steel and copper conductors. These tests were performed on fatigue test benches, where the conductors were supported by conventional rigid clamps. The bending stresses were estimated from these tests based on either the free-loop amplitude or the bending displacement and the endurance limits were estimated as the maximum bending stresses that could be applied for 500 million cycles without any wire break.

Based on the fatigue test data, EPRI recommended a maximum bending stress of 22.5 MPa for single-layer and 8.5 for multi-layer ACSR conductors. For AAAC conductors, the test data suggested that the same endurance limits could be used for conductors made of 1350 and 5005 aluminum alloys. For conductors made of 6201 or similar alloys, the endurance limits should be approximately 2/3 of the limits proposed for the ACSR conductors, resulting in maximum bending stresses of 15 MPa and 5.7 MPa for single-layer and multi-layer conductors, respectively. Data from tests performed on conductors with armor rods suggest that this fitting does not significantly impact the fatigue performance and the proposed endurance limits may be applied to conductors with or without armor rods (EPRI, 2006; IEEE, 2006).

2.3.3 IEEE methodology

IEEE (1966) proposed a general method to assess the severity of vibrations in overhead conductors using a maximum bending strain limit. Based on field vibration measurements taken from a 54/7 ACSR conductor, it was observed that a peak-to-valley bending strain of 150 microstrains did not produce fatigue damage on the conductor after 30 years of service. The authors observed that this value should only be used as a guide and recommended that a bending

strain of 200 microstrains could also be considered safe. The report concluded that future work would still be required to determine a maximum strain limit more precisely. While this criterion has been shown to generally be conservative, it is still used by utilities worldwide for the safety assessment of lines with damping systems (EPRI, 2006).

The endurance limits given by the EPRI and the IEEE methodologies were initially defined to never be exceeded during the conductor's lifetime. However, IEEE (2006) recognized later that this assumption was overly conservative and that these limits could be exceeded during a limited number of cycles without compromising the fatigue resistance of the conductor. Based on empirical observations, IEEE (2006) proposed the following three criteria:

- The endurance limit should not be exceeded by more than 5% of the cycles;
- The bending stress or strain can exceed the endurance limits by 1.5 times during a maximum of 1% of the cycles;
- The bending stress or strain can not exceed the endurance limit by more than 2 times.

2.3.4 CIGRÉ WG 22-04 methodology

The safe design and assessment methods presented in Sections 2.3.2 and 2.3.3 are based on the definition of endurance limits. On the other hand, the CIGRÉ WG 22-04 method (CIGRÉ, 1979) relies on the use of Miner's cumulative damage rule to estimate the remaining lifetime of overhead conductors. The method requires the use of bending displacement amplitude data, which is typically measured by a vibration recorder and stored in a memory matrix. The vibrations should be measured during a period of at least one second and for a minimum of four times per hour (IEEE, 1966; CIGRÉ, 1995). To obtain a representative description of the conductor's vibrations, IEEE (1966) suggests that the recordings should be obtained during a period of at least two weeks, while CIGRÉ (1995) recommends a minimum period of three months to obtain statistically meaningful results.

The procedure used to obtain the lifetime estimate is illustrated in Fig. 2.14. Initially, the bending displacement amplitude data obtained from the vibration recorder is converted into

bending stress data using Poffenber-Swart formulation and the results are extrapolated to one year. The bending stress data can then be expressed in an accumulated stress curve, relating the bending stresses with the expected number of cycles in one year. Then, Miner's damage rule can be applied by comparing the accumulated stress curve with a reference S-N curve. The fatigue damage, ΔD, produced during one year can be estimated as

$$\Delta D = \sum_{j=1}^{k} \frac{N_j}{N_{\mathrm{f}_j}} \tag{2.5}$$

where k is the number of bending stresses obtained from the vibration data, N_j is the number of cycles expected in one year at the bending stress $\sigma_{\mathrm{a}j}$, and N_{f_j} is the number of cycles the conductor could sustain at the same bending stress based on the reference S-N curve. Finally, the lifetime of the conductor in years, N_{years}, can expressed as

$$N_{\text{years}} = \frac{D_{\mathrm{c}}}{\Delta D} \tag{2.6}$$

where D_{c} is the critical damage, usually assumed to be $D_c = 1$.

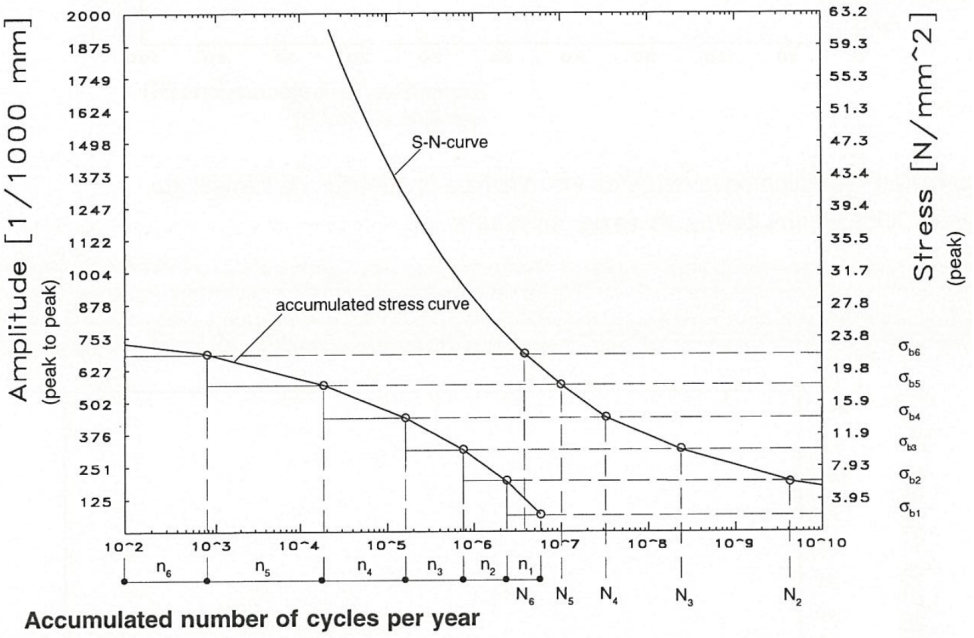

Figure 2.14: Comparison between the accumulated stress curve obtained from vibration measurements with a reference stress-life curve (CIGRÉ, 1995).

There are two main approaches used to obtain the reference S-N curve used in this procedure. The first approach, which is recommended by EPRI (2006), is to perform fatigue tests on the conductor-clamp assembly using different bending displacement amplitudes and express the S-N curve in terms of the number of cycles required for a certain number of wire breaks (usually between one to five). More details about such tests are given in Section 2.4.1. The second approach was proposed by CIGRÉ (1979) and it consists in using the so-called CIGRÉ Safe Border Line (CSBL). The CSBL is an idealized stress-life curve that represents a safe limit for conductors with aluminum or aluminum alloy wires. It was proposed as a means of obtaining conservative fatigue life estimates for the conductor if the S-N curve is unavailable.

The CSBL was derived from a series of fatigue tests performed on individual wires and conductors with and without fittings. The test data were produced by four different institutes using ACSR (Aluminum Conductor Steel Reinforced), AAAC (All Aluminum Alloy Conductor), and pure aluminum conductors. The individual wires were tested under rotating bending and alternating flat bending, while the conductors were tested under alternating flat bending and pulsating tension forces. Figs. 2.15a and b show the experimental setup used for the tests with conductors without and with fittings, respectively. The results were expressed in the S-N curves shown in Fig. 2.15c. Based on these results, CIGRÉ proposed the CSBL as an S-N curve which changes slope at $N_\mathrm{f} = 2 \times 10^7$ cycles. The CSBL can be express by the following equations:

$$\sigma_\mathrm{a} = 450 N_\mathrm{f}^{-0.200}, \text{ for } N_\mathrm{f} \leq 2 \times 10^7 \text{ cycles} \tag{2.7}$$

$$\sigma_\mathrm{a} = 263 N_\mathrm{f}^{-0.168}, \text{ for } N_\mathrm{f} \geq 2 \times 10^7 \text{ cycles} \tag{2.8}$$

where σ_a is the bending stress, in MPa, and N_f is the number of cycles to failure.

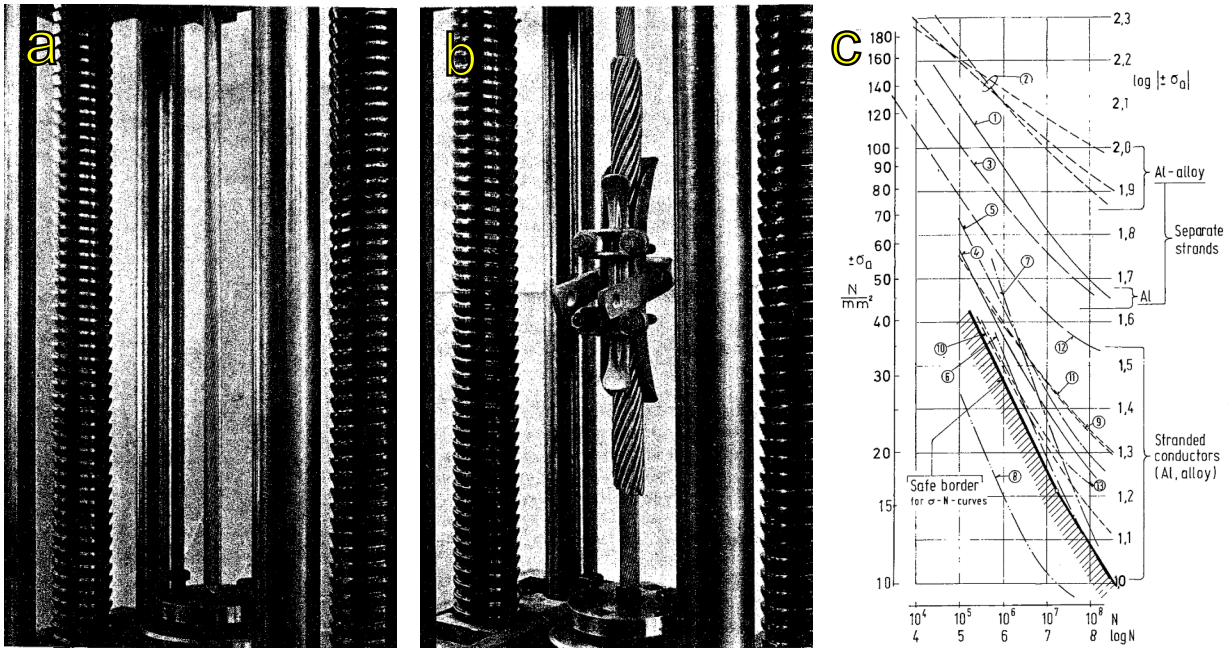

Figure 2.15: Examples of conductor specimens (a) without fittings and (b) with an armor rod and a suspension clamp used to determine the (c) CIGRÉ Safe Border Line (CIGRÉ, 1979).

2.4 Experimental studies

In this literature review, three main experimental approaches used by researchers to investigate the fatigue behavior of overhead conductors were identified. The first and most usual approach (Section 2.4.1) is to perform fatigue tests on conductor-clamp assemblies. In these tests, the conductor is subjected to cyclic oscillations that are representative of the aeolian vibrations in transmission lines. The main objective of these tests is to obtain the S-N curve of a particular conductor-clamp assembly, which can be used for the design and maintenance of transmission lines. Furthermore, these tests can provide a better understanding of the different parameters that can affect the fatigue behavior of the conductor, such as the suspension clamp geometry and the presence of lubricants.

The second experimental approach (Section 2.4.2) is to perform fatigue tests on individual wires taken from overhead conductors, usually containing geometric discontinuities. Notched wires are used to reproduce some of the effects caused by fretting between the conductor's wires. The main objectives of these tests are to investigate the fatigue behavior of wires with notches and to be used as input data for life prediction methodologies of wires under fretting

fatigue.

The third approach (Section 2.4.3) is to perform fretting fatigue tests in a wire scale, i.e., in a wire placed in contact with another wire or with a support used to represent the suspension clamp. These tests can lead to a better understanding of factors that affect the fretting process and crack initiation in wires. The data from these tests can also be used to evaluate methodologies for predicting the lives or fatigue limits of wires under fretting conditions.

2.4.1 Fatigue tests on conductors

The majority of experimental studies on the fatigue failure of overhead conductors consists of laboratory fatigue tests on conductors mounted on suspension clamps. In general, these tests are conducted on resonant test benches. To exemplify the construction and operation of the laboratory equipment used in these tests, a description of the resonant test benches located at University of Brasilia is presented in Section 2.4.1.1. Then, the main findings from fatigue tests performed on such test benches are discussed in Sections 2.4.1.2 and 2.4.1.3. Section 2.4.1.2 is focused on the fatigue tests performed with constant amplitude loading, which comprise the majority of the experimental work, while Section 2.4.1.3 details the tests performed with variable amplitude loading, which propose more realistic representations of the aeolian vibrations.

2.4.1.1 Description of a fatigue test bench

This section provides a brief description of the three resonant fatigue test benches located at the Laboratory of Fatigue and Structural Integrity of Overhead Conductors of the University of Brasilia, shown in Fig. 2.16a. The description presented in this section is specific for these test benches, but the principles of construction and operation are similar to other test benches, such as the ones described in (Cardou et al., 1990; Kubelwa et al., 2017). Each bench is composed of an active (40 m) and a passive (7 m) spans. At one end of the active span, the conductor is assembled in a suspension clamp, rigidly attached to a metallic cradle, as shown in Fig. 2.16b. The inclination of this cradle can be adjusted to reproduce the sag angle of the conductor. At the other end, the conductor is attached to a lever arm with a system of removable dead weights,

responsible for controlling the static tension force.

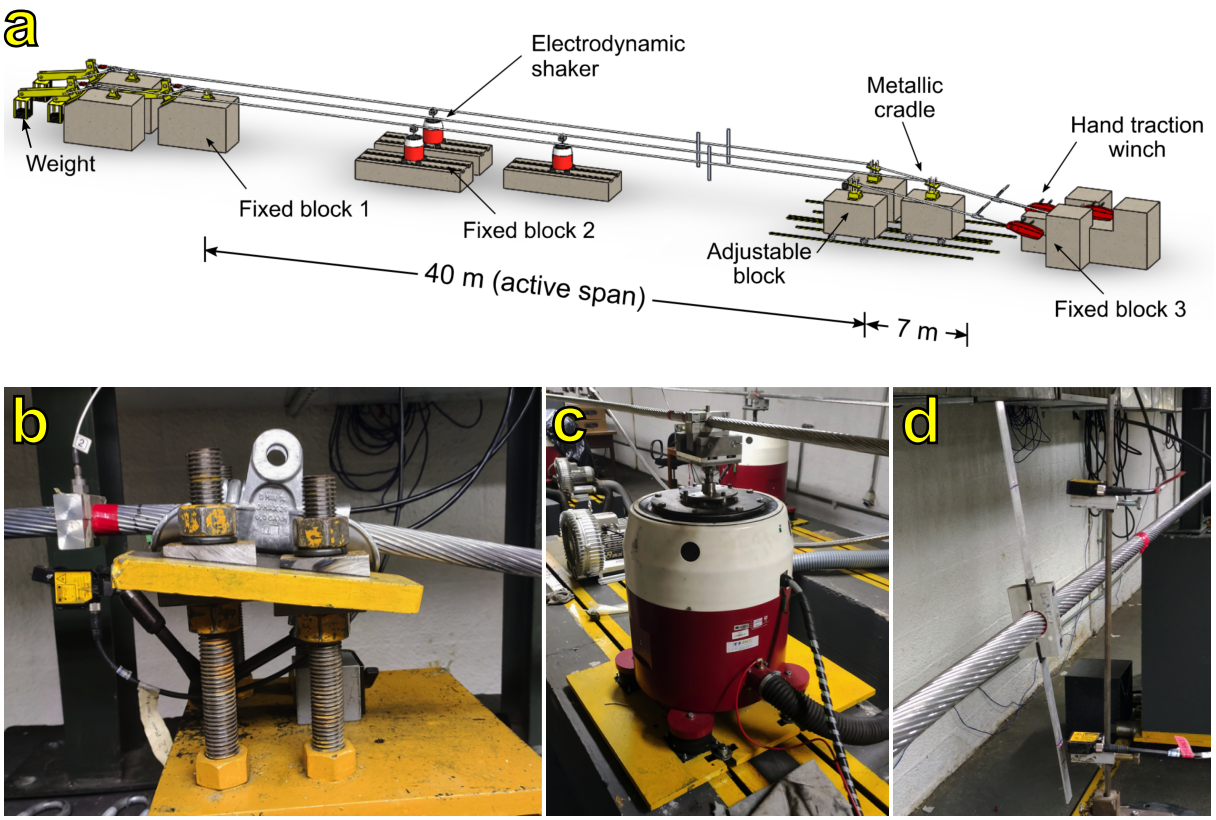

Figure 2.16: Resonant fatigue test benches: (a) schematic overview, (b) conductor/clamp assembly, (c) electronic shaker and (d) rotation sensor.

To perform the fatigue tests, an electronically controlled shaker, Fig. 2.16c, is connected to the conductor within the active span. The shaker is responsible for imposing a vertical cyclic displacement to the conductor, which is used to represent the aeolian vibrations. An accelerometer is installed on the conductor at a point located at a longitudinal distance of 89 mm with respect to the last point of contact between conductor and clamp. The accelerometer and shaker are connected to a closed-loop control system, which is used to ensure that the prescribed bending displacement is maintained throughout the test.

The detection of wire breaks is accomplished by using the rotation sensor shown in Fig. 2.16d, which is placed at the first node from the suspension clamp. The rotation sensor contains two aluminum blades and two laser sensors. The blades are attached to the conductor using a hose clamp. When a wire break occurs, the tangential components of the forces acting on the remaining wires are redistributed, causing the conductor to rotate. As a result, the

aluminum blades also rotate and this movement is detected by the laser sensors. Since the conductor's layers are twisted in alternating directions, rotations can occur on clockwise or counter clockwise directions, allowing the system to identify the layer where the wire break occurred.

2.4.1.2 Constant amplitude loading tests

Most of the tests performed in resonant test benches such as the one described in Section 2.4.1.1 use constant amplitude loading to represent the aeolian vibrations. The main goal of these tests is to obtain the S-N curves of conductor-clamp assemblies, such as the ones exemplified in Fig. 2.17. These curves can be used to estimate the fatigue limit of the conductor, usually assumed to be 500 million cycles. The S-N curves can also be used to compare the fatigue resistance of conductors made with different materials, facilitating the choice of the conductor to be used in a transmission line.

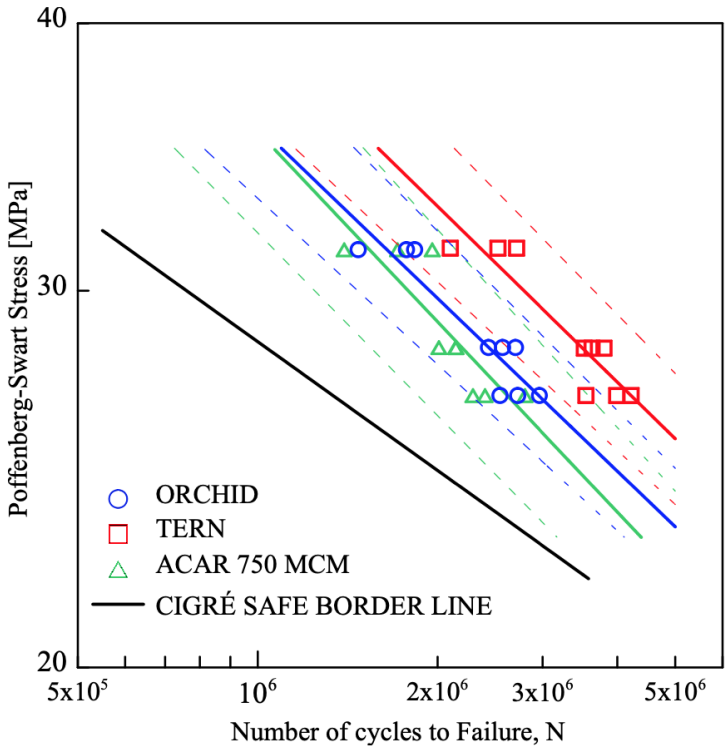

Figure 2.17: Stress life curves of overhead conductors mounted on metallic suspension clamps (Kalombo et al., 2018b)

In addition to obtaining S-N curves, the fatigue tests in resonant test benches have been extensively used to investigate the effect of different parameters on the fatigue failure

of overhead conductors. For instance, most of the current knowledge about fretting fatigue in overhead conductors (previously discussed in Section 2.2.2) was obtained from these types of test. In what follows, this section describes the main findings from several studies, which are organized according to the main parameter being analyzed.

Mean stress

Cardou et al. (1990) performed fatigue tests on an ACSR Bersimis conductor subjected to tension forces of 15%, 25% and 35% of the rated tensile strength (RTS). The tests were performed using a commercial suspension clamp and a steel support similar to a circularly grooved pulley, which was designed to have a good conformity between conductor and groove. One specific objective of these tests was to characterize the behavior of the conductors for long fatigue lives (up to 10^8 cycles). It was observed that the mean tensile load had a significant effect on the fatigue resistance at 10^8 cycles when comparing the tests performed with 15% and 25% of the RTS. However, little difference was observed between the tests with 25% and 35% of the RTS.

Fadel et al. (2012) investigated the effect of mean stress in the fatigue life of an ACSR Ibis conductor. Fatigue tests were performed using tension forces of 20% and 30% of the RTS. The obtained S-N curves showed that the increase in tension force significantly reduced the fatigue life of the conductor for low stress amplitudes (<35 MPa), but had little effect for higher stress amplitudes. Fractography examination revealed the occurrence of quasi-planar, V-type and 45° type of fracture surfaces in all tests. Quasi-planar fractures were predominant at tests with a mean force of 20% of the RTS, while 45° type and V-type of fractures happened more frequently in the tests with 30% of the RTS. The mean stress also influenced the radial distribution of wire breaks. In the tests with 20% of the RTS, an even distribution of wire breaks between external and internal layers was observed, while external layer wire breaks were predominant for the tests with 30% of the RTS.

Recently, extensive research has been carried out by Kalombo et al. (2017, 2018a, 2018b, 2019) to investigate the applicability of the H/w (or catenary) parameter to design safe transmission lines with respect to the stretching force applied to the conductor. Numerous fatigue

tests were performed on AAAC (All Aluminum Alloy Conductor), AAC (All Aluminum Conductor), ACSR (Aluminum Conductor Steel Reinforced), and ACAR (Aluminum Conductor Alloy Reinforced) overhead conductors. It was observed that the H/w parameter can have a significant effect on the fatigue lives of all studied conductors. Comparisons between the S-N curves obtained for different conductors subjected to the same level of the H/w parameter showed significant differences in the fatigue resistance of the conductors. For instance, the fatigue lives observed for the ACSR Tern were about four times longer than those observed for the AAAC 900 MCM conductor under the same load conditions. Thus, the authors concluded that a single value of the H/w parameter should not be used to design all types of conductors, and that specific catenary parameters could be defined for the different conductor configurations (AAAC, AAC, ACSR or ACAR).

Kalombo et al. (2017) also used the following linear equation to correlate the mean stress, S_{m}, acting on the aluminum wires of the external layer of conductors with the H/w parameter:

$$S_{\mathrm{m}} \cong g\rho_{\mathrm{a}}\frac{H}{w} \tag{2.9}$$

where g is the gravitational acceleration and ρ_{a} is the aluminum density. This equation was evaluated by performing static tension tests on AAAC 900 MCM and ACSR Tern conductors. In these tests, strain gages were glued to external layer wires on the region opposed to the last point of contact between conductor and clamp. Using Hooke's law, the measured strains were associated with mean stresses and compared to the predictions given by Eq. (2.9). For both conductors and magnitudes of the catenary parameter used in their study, the estimates obtained by the equation were in good agreement with the stresses estimated from the strain measurements, with differences below 10%.

Type and geometry of the clamp device

As mentioned in Section 2.2.2, fatigue failures in overhead conductors usually occur in the contact between the conductor and clamp devices that restrain its movement. Most studies take this into account by performing fatigue tests on conductor-clamp assemblies. However,

tests are usually performed using only one type and geometry of clamp device. In this context, some studies (Miranda et al., 2022; Cardou et al., 1992; McGill and Ramey, 1986) have focused on evaluating the influence of the clamp device on the fatigue behavior of the conductor.

Possibly the first study to focus on suspension clamp geometry was performed by McGill and Ramey (1986). The authors carried out a series of static and fatigue tests on an ACSR Drake conductor. Clamps were developed with three different cross-sectional radius. Deep and shallow grooved variations of the cross-sectional fit were used, the first one presenting more resemblance to a real conductor conformation. In both static and fatigue tests, strain gages were glued to external layer wires near the clamp. In the static tests, the measured strains varied in an inverse manner to the cross-sectional radius of the clamp. The same behavior was observed in the fatigue tests regarding the strain amplitude. In terms of cross-sectional fit, the deep grooved fit presented lower strain measurements in static tests, but both fits provided, on average, the same number of broken wires in the fatigue tests.

While most studies are performed on conductor-suspension clamp assemblies, Cardou et al. (1992) focused on the fatigue behavior of an ACSR Bersfort conductor connected to two types of spacer clamps. The first type was a pre-twisted rod spacer clamp with an X shape, while the second type was a home-made bolted clamp. It was observed that the pressure imposed by the bolted clamp to the conductor is significantly higher than the pressure caused by the rod clamp. Hence, the fatigue strength of the conductor was smaller for the tests performed using the bolted clamp. The longitudinal and radial distributions of the crack initiation sites were also investigated. For the rod clamp, the researchers observed that wire breaks occurred inside the clamp and in its vicinity, while almost all wire breaks occurred inside the bolted clamp. In terms of radial distribution of wire breaks, it was observed that most of them occurred on the bottom portion of the conductor.

Miranda et al. (2022) evaluated the fatigue behavior of an AAAC 823 MCM and an AAAC 900 MCM conductors mounted with the metallic and elastomeric suspension clamps. To investigate the applicability of Poffenberger-Swart's formulation to both types of clamp, the authors estimated a conversion factor by plotting the bending stresses (obtained using Hooke's law from strain measurements) and the bending displacements, and fitted the test data by a linear

function. This analysis showed that the Poffenberger-Swart equation provided reasonable bending stress estimates for the metallic clamp, but overestimated the stiffness of the elastomeric clamp. The obtained S-N curves indicated a higher fatigue strength for the conductors mounted with the elastomeric clamp, which the authors attributed to higher compliance and less contact pressure and friction between conductor and clamp. The type of clamp device also influenced the distribution of crack initiation sites. In terms of longitudinal position of wire beaks, almost all failures occurred inside the metallic clamp. Most failures also occured inside the elastomeric clamp, but a larger dispersion was observed. As for the radial distribution of wire breaks, most failures occurred on the outer layer for the metallic clamp and on the intermediate layer for the elastomeric clamp. The majority of failures happened at the top portion of the conductors for both materials, except when using the metallic clamp with the AAAC 823 MCM conductor.

High temperatures

Costa et al. (2020) designed a system to control the heat of the conductor-clamp assembly used in test benches. The idea was to represent the heating of the conductor due to the high voltages experienced in real transmission lines, and verify the effect of the higher temperatures in the fatigue behavior of the conductor. The researchers designed an open heating system that was installed around the clamp of the test bench. A proportional–integral–derivative controller and an infrared camera were used to control and measure the temperature in the heating equipment. The system was designed to be capable of raising the temperature of the conductor-clamp assembly from 20 to 150 ºC. To evaluate the proposed system, fatigue tests were performed on an Orchid conductor using a temperature of 75 ºC in the clamped region, and the results of these tests were compared to previously obtained ones under room temperature. The authors observed a significant reduction of fatigue life when the temperature was raised to 75 ºC.

Lubricants

Studies on the effect of lubrication in the fretting damage of cables have usually been limited to steel cables, as most researchers are concerned with lifting systems such as those used in the mining industries (McColl et al., 1995; Sun et al., 2020; Xu et al., 2021). Few

studies have tried to evaluate the effect of lubricants on the fatigue behavior of conductors, with the major contributions being attributed to the extensive work of Zhou et al. (1995, 1996, 1999), The researchers performed several fatigue tests on ACSR Zebra conductors in both dry and lubricated conditions, using a spacer clamp to support the conductor.

As mentioned in Section 2.2.2, there are three main contact behaviors observed on typical conductor-clamp assemblies: stick, partial slip and gross sliding. However, Zhou et al. observed that the use of a lubricant resulted in a fourth type of behavior, where the contact displays slight wear but there is no formation of aluminum oxide debris because of the grease protection. The contact marks that displayed this behavior were located close to the clamp, between the marks in stick and in partial slip conditions.

In terms of failures caused by fretting fatigue, it was observed that the lubricant provides significant improvements to the durability of the conductor. The researchers observed that fewer and smaller contact marks were developed on the lubricated conductor in the critical region near the suspension clamp. In addition, it was observed that crack propagation was more severe for the dry conductor than the lubricated one for contact marks under partial slip fretting regime. As a result, for the same number of loading cycles, cracks would initiate on both dry and lubricated conductors but would only lead to wire rupture on the dry conductor. Despite these advantages, the authors note that the durability of the lubrication can be an issue since fretting can remove the lubrication film and even if replenished, the grease may not be able to access the inner region of the contacts.

2.4.1.3 Variable amplitude loading tests

As discussed in Section 2.2.3 the aeolian vibrations in overhead conductors have a variable amplitude nature. Despite that, few studies have attempted to reproduce these amplitude variations in fatigue tests of conductors. Among the variable amplitude loading (VAL) tests discussed in this section, the majority has been performed on resonant test benches, using a conductor-clamp assembly. The only exceptions are the tests described in (CIGRÉ, 1979), which were performed on conventional hydraulic testing machines.

The main approaches used by researchers to represent the amplitude variations in these

fatigue tests consist in applying loading blocks (CIGRÉ, 1979; Ramey and Silva, 1981; Brunair et al., 1988; Goudreau et al., 2005; Murça, 2011) or in using random loading spectra (Goudreau et al., 2005; Ferreira et al., 2023). Usually, these studies combine Miner's damage rule with the rainflow cycle counting method (when necessary) to calculate the fatigue damage fraction ΔD produced by the loading history. The damage fraction is then used to estimate the critical damage D_{c}, i.e., the cumulative damage that leads to the conductor's failure.

Table 2.3 presents the range of critical damages estimated from the VAL tests. Typically, Miner's damage rule is applied for fatigue life prediction by considering a critical damage $D_{\mathrm{c}} = 1$. Based on the results shown in Table 2.3, the use of a critical damage $D_{\mathrm{c}} = 1$ seems to be appropriate to represent the fatigue failure of overhead conductors subjected to variable amplitude loading. It is worth noticing that the loading sequence affects the critical damage values obtained in the tests with loading blocks. In these tests, it has been observed that Miner's damage rule is in general conservative ($D_{\mathrm{c}} \geq 1$) for tests with decreasing loading sequences, and non conservative ($D_{\mathrm{c}} \leq 1$) for increasing loading sequences.

Table 2.3: Summary of the critical damages estimated from VAL tests on conductors.

Conductor	Loading type	Critical damage	Reference
AlMgSi	Block loading	1.06–2.14	CIGRÉ (1979)
AlMgSi	Block loading	0.71–2.27	CIGRÉ (1979)
ACSR Drake	Block loading	0.67–3.38	Brunair et al. (1988)
ACSR Drake	Block loading	0.86–1.79	Brunair et al. (1988)
ACSR Bersfort	Block loading	0.4–1.7	Goudreau et al. (2005)
ACSR Crow	Loading spectrum	0.3–1.7	Goudreau et al. (2005)
ACSR Ibis	Loading spectrum	0.44–0.89	Ferreira et al. (2023)

2.4.2 Fatigue tests on individual wires

The fatigue failures of wires in overhead conductors usually happen due to cracks that initiate at fretting marks and propagate due to the cyclic bending stresses caused by wind-induced oscillations. The fretting wires share common features with notched components, such as stress concentration and stress gradient. These similarities have led researchers to perform

fatigue tests on individual wires taken from overhead conductors. These wires are usually machined to produce reduced cross sections or geometric discontinuities. The main objectives of these tests are to investigate the fatigue behavior of wires subjected to characteristics that are common to notched components and fretting wires, and to propose methodologies for life estimation that are applicable to notched components and that could be extended to the fretting problem.

In the study performed by Achiriloaiei et al. (2016), the effect of the plastic deformation caused by the contact between two crossed wires on fatigue life was investigated. The researchers used a fixing device to compress one wire against the other, causing the plastic deformation. Different normal forces and crossing angles were adopted in this procedure. Then, tension and fatigue tests were performed on plain wires and on the plastically deformed wires. The authors observed that for fatigue lives in the order of 10^5 cycles, the plastic deformation did not present a significant effect on fatigue life. However, for fatigue lives longer than 10^6 cycles, the plastic deformation caused a noticeable reduction in fatigue life. In these cases, the crossing angle between the wires plays a significant role on fatigue performance, with lower crossing angles resulting in shorter fatigue lives.

Martínez et al. (2018) performed an experimental-numerical methodology to estimate the fatigue life of 6201-T81 aluminum alloy wires containing a transverse hole. The life prediction model made use of the point method variation of the Theory of Critical Distances (TCD). The critical distance was considered as a function of fatigue life and, to calibrate this relation, the researchers used stress-life curves obtained from fully reversed axial fatigue tests on plain and V-notched wires. A finite element model of the wire containing a transverse hole was developed and used to estimate the fatigue damage based on the maximum principal stress in a material point located in the vicinity of the notch root. The authors observed that the model was capable of estimating the fatigue lives with reasonable accuracy for tests in which the fatigue life was in the order of 10^6 cycles. However, less accurate fatigue lives were estimated when the experimental fatigue lives were lower than 10^5 cycles. In this case, the estimated lives were always conservative.

The procedure presented in (Martínez et al., 2018) was extended by Adriano et al. (2018).

In their work, the fatigue lives of V-notched wires, wires with a blind hole and wires with a transverse hole were estimated. Fatigue tests were performed using V-notched wires and wires with a blind hole. The point and volume methods of the TCD were used to estimate the fatigue lives. Two distinct procedures were adopted to calibrate the relation between the critical distance and the fatigue life. The first calibration procedure was identical to the one performed in (Martínez et al., 2018), using one stress-life curve from the test data of the plain wires and the other from the V-notched wires. The second calibration procedure also used two stress-life curves, but in this case both curves are determined from tests with notched specimens. For their research, the authors used the test data from the V-notched wires and from the wires containing a transverse hole. It was observed that the point and the volume method variations yielded similar life estimates, regardless of the calibration procedure adopted. However, the fatigue lives estimated using the second calibration procedure had better agreement to the experimental results.

2.4.3 Wire-scale fretting tests

Recent studies have been focused on investigating the fatigue behavior of overhead conductors by means of wire scale fretting tests, in which a wire is placed in contact with another wire or with a pad (used to represent the suspension clamp) and is subjected to a cyclic loading or displacement. These tests attempt to reproduce the loading conditions on the contact between wires of adjacent layers (Section 2.4.3.1) or between an external layer wire and the suspension clamp (Section 2.4.3.2). The main objectives of these studies are (i) to better evaluate the influence of different parameters on the fretting fatigue of the conductor's wires, and (ii) to provide wire/wire or wire/clamp fretting fatigue test data, which can be used in global-local approaches for fatigue life prediction of overhead conductors.

2.4.3.1 Wire-wire tests

In Section 2.4.1.2, the effect of lubricants on fretting fatigue was discussed based on the studies performed by Zhou et al. (1995, 1996, 1999). To further analyze the effects of

lubricant on fretting, the researchers performed additional fatigue tests on wires in contact under lubricated and dry conditions. In these tests, the wire specimen is stretched by a tension force. Then, two identical wires are pressed against the specimen at a crossing angle of 29º, and a cyclic displacement is imposed to one end of the specimen. It was observed from these tests that the influence of grease on fretting damage increases as the compressive force or cyclic displacement is increased. In particular for gross sliding conditions under high compressive forces, it was observed that the grease film is rapidly removed from the contact mark, leading to similar fretting damage for both dry and lubricated wires.

Rocha et al. (2019) proposed a finite element-based methodology to predict the fatigue life of wires under fretting fatigue. The methodology combines the use of the Theory of Critical Distances with a stress-based version of the Smith–Watson–Topper fatigue parameter to quantify the fatigue damage. To investigate the accuracy of the proposed model, the authors conducted fretting fatigue tests between 1350-H19 aluminum alloy wires and compared the experimental lives to the ones estimated by the model. They observed that the model was capable of estimating the fatigue lives of the wires with reasonable accuracy, with estimated lives falling within factors of three of the observed lives.

The life estimation methodology proposed by Rocha et al. (2019) was further evaluated by Araújo et al. (2020) and Matos et al. (2020) using the 6201-T81 aluminum alloy. In these studies, the authors proposed the inclusion of an elastic-plastic constitutive behavior into the finite element contact model of the wires, in addition to the linear elastic model that was initially used by Rocha et al. (2019). They observed that, for the 6201-T81 aluminum alloy wires, the use of a linear elastic contact model provided overly conservative life estimates, while the elastic-plastic model significantly improved life estimates. The Smith–Watson–Topper parameter was also used in (Matos et al., 2020) to estimate the orientations of the critical planes. Overall, a reasonable agreement was obtained between the measured critical plane orientations and the predictions yielded by the fatigue parameter.

A similar strategy was used by Said et al. (2020a) to predict the endurance limit of the wires in contact. Initially, the researchers performed finite element simulations of the conductor-clamp assembly to estimate the compressive, tangential and fatigue forces on the contact marks.

Then, the estimated loads were employed into a finite element-based analysis of the wire-wire contact configuration. The simulations were used to assess the fatigue damage of the wire, using the point method variation of the Theory of Critical Distances and the Crossland fatigue parameter. To validate the proposed model, the authors performed wire-wire fatigue tests, using quasi-pure aluminum wires. They observed that the model was capable of accurately predicting the crack initiation site and whether cracks would initiate or not. However, the initial assumption used in their model that any initiated crack would eventually propagate and break the wire was not observed experimentally. The authors attributed this behavior to the occurrence of a crack arrest phenomenon, and to verify this hypothesis, they performed 3D-surface-crack simulations. Some preliminary analyses suggested that the crack arrest phenomenon took place.

The conclusions taken about the crack arrest phenomenon by Said et al. (2020a) motivated the researchers to further investigate this phenomenon in (Said et al., 2020b). For that, new fretting fatigue tests were conducted using the same quasi-pure aluminum wires. Once again, the loading conditions imposed in these fretting tests were based on finite element simulations of the conductor-clamp assembly. The researchers investigated the orientation and size of the cracks from specimens that did not break during the fretting tests. Using these measurements, they implemented a model of the cracks into the finite element simulations of the wires. Based on these new simulations performed with a crack model, they concluded that, even in a fully compressive state, the crack can propagate due to in-plane shear stresses. Finally, a Stress Intensity Factor threshold was proposed, below which crack arrest phenomenon occurs.

Pereira et al. (2020) performed fretting fatigue tests between two wires of the aluminum alloy 1350-H19 using three different normal forces: 250, 500 and 1000 N. Five different mean stress models were used to estimate the fatigue life of the wires used in the wire-wire fatigue tests: Goodman, Gerber, Morrow, Smith–Watson–Topper and Walker. To perform the fatigue life estimation, the researchers considered that the equivalent fully reversed stress amplitude can be related to the fatigue life by a power law function. One of the parameters of said function was determined based on the maximum von Mises stress near the contact region and an equivalent radius of the notch root for the contact surface. Both of these properties were estimated based on finite element simulations of the wire-wire fatigue tests. For Goodman, Morrow

and Smith–Watson–Topper models, the fatigue life estimations were generally conservative. In these models, fatigue life estimations had a better agreement with experimental data for the tests performed with a normal force of 500 N. The same behavior was observed when using Walker's model with a fitting parameter $\gamma = 0.6$. For Gerber's model, fatigue life estimations had a good agreement with experimental data. However, for the normal loads of 500 N and 1000 N, the accuracy of the life estimations decreased with longer fatigue lives. The best agreement with experimental data was observed when using Walker's model with a fitting parameter $\gamma = 0.75$.

2.4.3.2 Wire-clamp tests

Steier et al. (2018) performed fretting wear tests on 1350-H19 aluminum alloy wires tested against flat discs, used to represent suspension clamps. The wires were extracted from an Ibis conductor, while the disc material was extracted from a casted suspension clamp made of SAE 305 aluminum alloy. Two surface modifications were applied to the discs: Diamond Like Carbon (DLC) coating and anodization method. For each surface modification, three fretting wear tests were performed by compressing the wire specimen into the flat disc and then imposing a cyclic displacement. The authors observed a high amount of material transfer from the wire specimen to the disc when the anodised coating was applied, while no material transfer happened when the DLC coating was applied. Furthermore, they observed that the DLC coating significantly reduced the wear damage of the wire and the disc.

Section 2.4.3.1 described some studies focused on the development of a global-local approach for life prediction of the conductor-clamp system based on the wire-wire contact configuration. The study performed by Omrani et al. (2021) follows the same topic, but focuses on the wire-clamp contact condition. In addition to the standard fretting fatigue tests with axial fatigue loading, biaxial fretting tests were performed, where the wire specimen was subjected to cyclic axial and transverse loadings. The researchers considered that the biaxial condition was more representative of the fatigue behavior of the conductor, based on results from previously performed finite element simulations of the conductor-clamp assembly. The loading conditions applied in the fretting tests were defined based on the potential crack initiation sites identified during finite element simulations of the conductor-clamp system. The methodology was evalu-

ated by comparing the fatigue lives obtained from the fretting tests with the number of cycles to first wire rupture obtained from fatigue tests with an ACSR Bersfort conductor. Overall, the fretting fatigue tests provided fatigue lives in good agreement to the ones observed in the fatigue tests with the conductor, despite being slightly non-conservative.

Fretting tests were performed by Omrani et al. (2022) to estimate the transition sliding amplitude between partial slip and gross sliding, and the friction coefficient in the wire-clamp contact. Two test configurations were used: variable displacement amplitude (VDA) and constant displacement amplitude (CDA). In both types of test, the wire specimen was stretched and put into contact with a pad. In the VDA tests, a cyclic displacement was imposed to the specimen and its amplitude was repeatedly increased after a predetermined number of cycles. The CDA tests were similar, but a different specimen was used for each increment. From the VDA tests, the researchers estimated the transition sliding amplitude as the one that resulted in a noticeable change of the shape of the hysteresis loops. A similar result was obtained by visually examining the contact marks produced in the CDA tests and identifying the displacement amplitude required for the occurrence of wear in the center of the contact area. To estimate the coefficient of friction, the researchers plotted the ratio between tangential force amplitude and normal contact force, Q/P, as a function of the displacement amplitude. It was observed that the ratio Q/P increases linearly with the displacement amplitude, reaching a maximum value at the transition between partial slip and gross sliding, followed by a quick decrease and then stabilization. The maximum magnitude of the ratio Q/P was considered the static friction coefficient. The results were almost identical regardless of the normal contact force applied in the tests.

2.5 Numerical modeling

2.5.1 Modeling of the conductor

The finite element simulation of a conductor-clamp assembly is a complex task. The conductor geometry involves helically stranded wires organized in layers, which produces multiple

contact regions where local plasticity, fretting and wear may take place. For these reasons, the analyzes of the fatigue behavior of overhead conductors have traditionally been limited to field investigations, laboratory fatigue tests and analytical models for many years. It was only in the last decade that technological advances allowed researchers to develop complex finite element (FE) three-dimensional models of overhead conductors (Frigerio et al., 2016; Baumann and Novak, 2017; Lalonde et al., 2017a, 2017b, 2018; Al Aqil and Kopsidas, 2020; Said et al., 2020a; Omrani et al., 2021). The development of these FE models of the conductor was inspired by previous models of steel wire ropes, usually focused on cables used in bridges and prestressed structures (Nawrocki and Labrosse, 2000; Ghoreishi et al., 2007; Judge et al., 2012).

A crucial aspect in finite element simulations is the choice of the type of element that defines the model's mesh. In the studies evaluated in this section, two types of element were identified: solid and beam. The solid elements (Fig. 2.18a) have a comparatively high computational cost and may require some simplifications in the simulations in terms of the length of the model or the complexity of the load conditions applied. Despite that, this element is still the preferred choice for some studies as it can lead to a more accurate representation of the contact interactions between the conductor's wires. The beam elements (Fig. 2.18b) have a considerably lower computational cost, which allows the modeling of a longer portion of the conductor, while still obtaining estimates of bending displacements, stresses and strains in good agreement with experimental data.

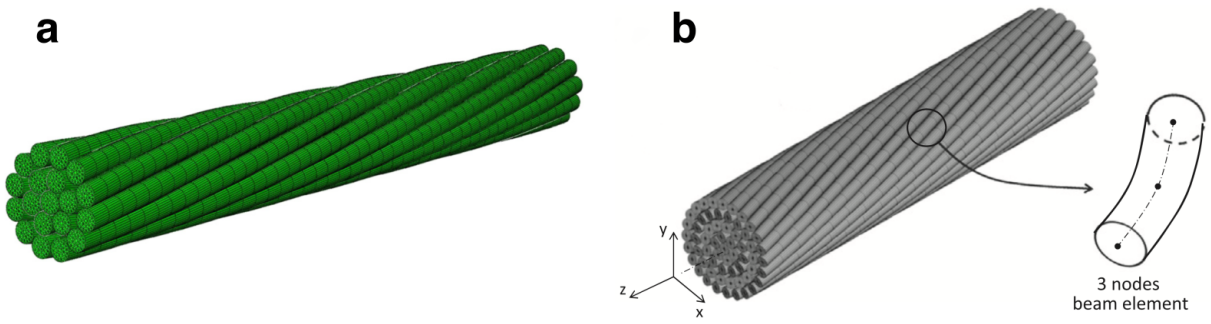

Figure 2.18: Finite element models of overhead conductors using (a) solid and (b) beam elements (Frigerio et al., 2016; Lalonde et al., 2017a).

Regarding the components being modeled, two different approaches have been used. Initially, studies were limited to modeling only a portion of the conductor at the exit of the clamp

mouth (Fig. 2.19a). However, some more recent studies (Lalonde et al., 2018; Omrani et al., 2021) have implemented models containing both the conductor and the suspension clamp. With these models, researchers are able to investigate the effect of suspension clamp geometry and clamping pressure on the conductor, as well as evaluate potential crack initiation sites that may result from the contact between outer layer wires with the suspension clamp.

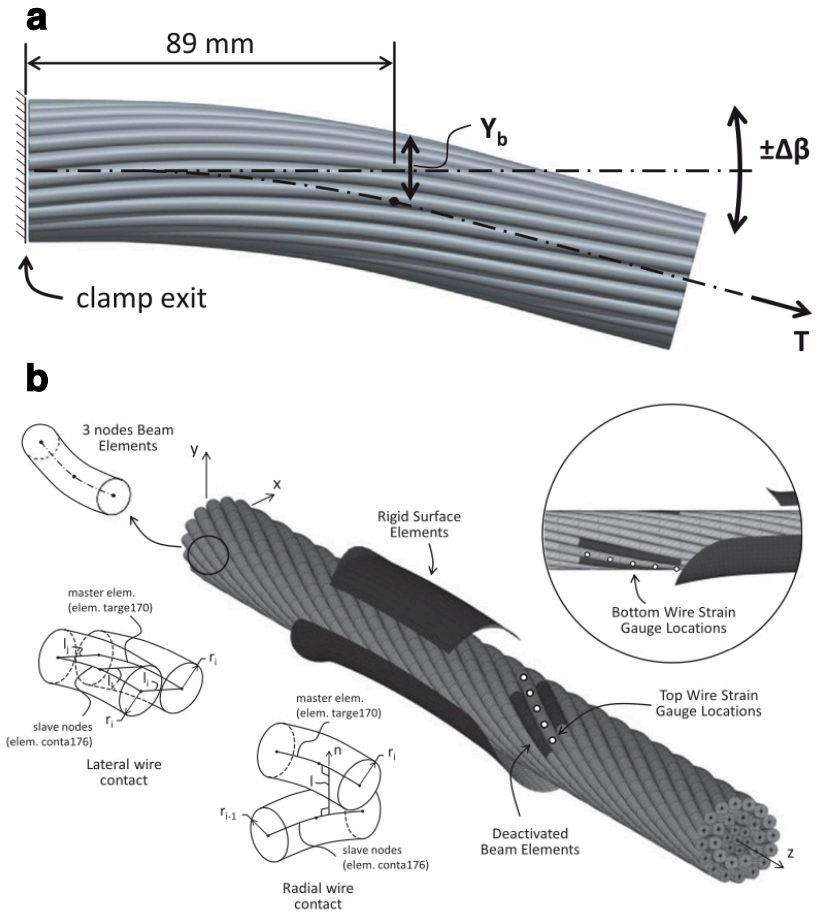

Figure 2.19: Finite element models of (a) the conductor at the clamp exit and (b) the conductor-clamp assembly (Lalonde et al., 2017b, 2018).

Table 2.4 summarizes the main parameters used in the finite element simulations of overhead conductors, as well as the data obtained from the simulations. As it can be seen from the table, the studies have been focused on estimating the contact conditions to identify critical regions for crack initiation and the bending displacements, stresses and strains, which are usually compared to experimental data to validate the model. It is worth noticing that almost all studies were carried out considering ACSR conductors with circular wires. Analyzes

involving other types of conductors and wire shapes are still unusual and could be the subject of future research. Regarding the models that involve the conductor-clamp assembly, it is worth noticing that the simulations were carried out in order to represent conventional metallic suspension clamps. Additional studies could be performed to consider elastomeric suspension clamps, for example, and other types of clamp devices. The effect of clamp geometry on the fatigue behavior of the conductor is also a topic that could be explored from this type of simulation.

Table 2.4: Summary of the main characteristics and obtained data for the finite element models of overhead conductors

Conductor type	Finite element geometry	Element type	Obtained data	Reference
ACSR Bersfort	Conductor-clamp	Beam	Contact forces Bulk forces	Omrani et al., 2021
ACSR (unspecified)	Conductor-clamp	Solid element (conductor) Shell element (clamp)	Contact forces Bulk forces	Said et al., 2020a
ACSR Raven ACSR Bersfort ACSR Flicker (round) and trapezoidal wires)	Conductor	Solid element	Bending displacements Bending stresses	Al Aqil and Kopsidas, 2020
ACSR Bersfort ACSR Drake	Conductor-clamp	Beam element (conductor) Rigid surface element (clamp)	Static and cyclic strains Bending stresses	Lalonde et al., 2018
ACSR Cardinal	Conductor	Beam element	Bending displacements	Lalonde et al., 2017a
ACSR 1/0 ACSR Drake ACSR Crow ACSR Bersfort	Conductor	Beam element	Bending displacements Bending stresses $fy_{\max}$ parameter	Lalonde et al., 2017b
ACSR Drake	Conductor	Beam element	Contact forces Bulk forces Bending displacements	Baumann and Novak, 2017
AAAC Aldrey	Conductor	Solid element	Axial strain Axial stiffness	Frigerio et al., 2016

2.5.2 Modeling of the wire-wire contact

As discussed in Section 2.4.3, recent studies have been focused on the development of a global-local approach for life prediction of conductor-clamp assemblies. One of the key steps in this approach is the contact analysis of potential crack initiation sites, in which a finite element (FE) model of the wire-wire or wire-clamp contact is used to estimate the stress or strain field beneath the contact. So far, most researchers have been concerned with the development of FE

models of the wire-wire contact, as will be detailed in this section.

Fig. 2.20 shows an example of a FE model used to describe the wire-wire contact. As it can be seen from the figure, the wires are modeled as half-cylinders, placed in contact at a certain crossing angle. This strategy is used to reduce the computational cost of the FE simulations and was adopted in all studies investigated in this work. These FE models are also characterized by the use of very refined meshes in the contact regions to properly describe the stress or strain field beneath the contact zone. For the FE model shown in the figure, the strategy used to obtain this refinement was to create refined partitions in the region where the contact marks are expected to be developed.

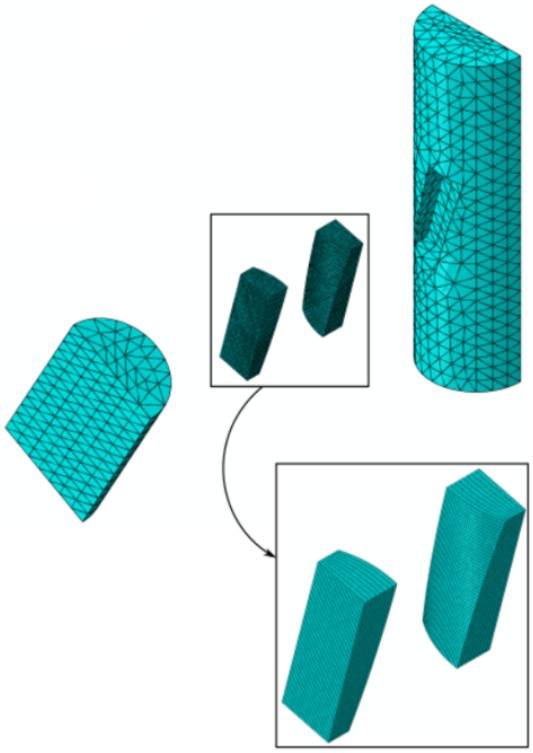

Figure 2.20: Finite element model of two fretting wires (Rocha et al., 2019).

The main characteristics and results obtained by the FE simulations of the wire-wire contact are summarized in Table 2.5. Most of the studies that use this type of simulation are focused on estimating fatigue lives or endurance limits, which is often achieved by combining a fatigue parameter with the Theory of Critical Distances (TCD). Such a combination has also been used to estimate other parameters related to the fatigue failure of the fretting wires. For example,

Rocha et al. (2019) used the Smith–Watson–Topper (SWT) fatigue parameter to estimate the crack initiation site in a wire under fretting fatigue. They observed that the maximum damage estimated by the fatigue parameter would occur at one of the edges of the major axis of the elliptical contact mark, which corresponds to the crack initiation site observed experimentally. Similar results were obtained by Said et al. (2020a, 2020b) using the Crossland fatigue parameter. Matos et al. (2020) used the SWT parameter to estimate the critical plane orientation, i.e., early crack orientation of a wire under fretting, obtaining a reasonable agreement with the critical planes observed on wires used in fretting fatigue tests.

Table 2.5: Summary of the aspects of the wire-wire finite element simulations.

Wire material	Predicted parameters	Fatigue model	Use of a critical distance approach	Material model	Reference
AA1350-H19	Fatigue life Crack initiation site	Smith–Watson–Topper	Yes (volume method)	Linear elastic	Rocha et al., 2019
AA6201-T81	Fatigue life	Smith–Watson–Topper	Yes (volume method)	Elastic-plastic	Araújo et al., 2020
AA6201-T81	Fatigue life Early crack orientation	Smith–Watson–Topper	Yes (volume method)	Elastic-plastic	Matos et al., 2020
AA1350-H19	Fatigue life	Goodman Gerber Morrow Smith–Watson–Topper Walker	No	Linear elastic	Pereira et al., 2020
Quasi pure aluminum	Endurance limit Crack initiation site	Crossland	Yes (point method)	Linear elastic	Said et al., 2020a
Quasi pure aluminum	Endurance limit Crack initiation site Stress Intensity Factor	Crossland	Yes (point method)	Linear elastic	Said et al., 2020b

3 Fretting fatigue performance and life prediction of 1120 aluminum alloy wires of overhead conductors

This chapter is a reproduction of the following publication:

> Matos IM, Araújo JA, Castro FC. Fretting fatigue performance and life prediction of 1120 aluminum alloy wires of overhead conductors. Theoretical and Applied Fracture Mechanics 2022;121:103521.

3.1 Introduction

The main component of a transmission line responsible for transporting electric energy over long distances is the overhead conductor. In the first transmission lines developed at the end of the nineteenth century, conductors were designed with copper wires. Over the years, the materials used to manufacture the conductor's wires have been gradually replaced by aluminum and aluminum alloys (AA), which are widely used nowadays. Among these alloys is the AA1120, a material originally designed in Sweden to be used in overhead conductors. The first major transmission lines to use this material were installed in Sweden in 1977 and in Australia in 1984. Since then, the use of AA1120 has steadily increased in these countries due to its combination of high mechanical and creep resistance and electrical conductivity compared to other aluminum alloys (Barber and Callaghan, 1995). In Brazil, overhead conductors have traditionally been designed using AA1350 and AA6201 wires. However, this scenario has started to change over the last decade with the development of several transmission lines with AA1120 wires, which are in operation nowadays (Hoffman et al., 2015).

One issue that can lead to the interruption of the safe operation of a transmission line is fretting fatigue. Fretting is a surface damage caused by minute relative displacements between

surfaces in contact. In overhead conductors, fretting is usually critical in regions that restrain the movement of the conductor, such as at suspension clamps. In these regions, cracks can initiate at points located within the contact surfaces between wires or between a wire and a clamp. Due to the cyclic bending stresses caused by the aeolian vibrations, these cracks can propagate and eventually lead to wire rupture. This correlation between fretting and fatigue failure of conductor's wires has been supported by many investigations performed both in field and in laboratory (Fricke and Rawlins, 1968; Azevedo and Cescon, 2002; Ouaki et al., 2003; Azevedo et al., 2009; Kalombo et al., 2016).

The safe design, operation and maintenance of overhead conductors against fretting fatigue has traditionally been performed using stress-life (S-N) test data. The tests used to obtain the fatigue data are typically produced in resonant test benches, where the conductor is supported by a suspension clamp and is subjected to a constant vibration amplitude, measured at 89 mm from the last point of contact between the conductor and the clamp. This approach has been employed for more than 50 years and is still the most commonly used engineering approach for identifying fatigue critical regions and defining endurance limits or the remaining lifetime of conductors in operation. In addition to the traditional S-N methodology, the increase of computational power has enabled the simulation of three-dimensional finite element models of conductors. These models have been used to estimate the static and cyclic stresses and strains acting on the conductor's wires in good agreement with experimental data (Frigerio et al., 2016; Baumann and Novak, 2017; Lalonde et al., 2018). Moreover, recent studies have tried to estimate the fatigue damage of conductors by means of fatigue test data of wires combined with finite element simulations of the wire/wire and wire/clamp contact configurations (Rocha et al., 2019; Garcia et al., 2020; Matos et al., 2020; Said et al., 2020a, 2020b; Vieira, 2020; Omrani et al., 2021, 2022). This type of analysis can lead to an understanding at the local scale of the fretting process and the factors that influence wire rupture.

Most of the studies on the fatigue behavior of conductors and their wires have been done using ACSR (Aluminum Conductor Steel Reinforced) conductors, which are usually made of AA1350 wires. Studies (Barber and Callaghan, 1995) have shown that the AA1120 has advantages compared to other aluminum alloys with respect to its electrical conductivity, tensile

strength and creep resistance. However, little has been done to characterize its fatigue strength. Kalombo et al. (2019) performed fatigue tests on conductors made of AA1120 and AA1350 wires. It was observed that under the same stretching forces and bending stress amplitudes, the conductors made of AA1120 wires had longer fatigue lives than the ones with AA1350 wires. Vieira (2020) performed axial fatigue tests on AA1120 and AA6201 wires without contact and under fretting fatigue. The researcher observed that the fretting process caused a reduction of fatigue strength for both materials, but it was more severe for the AA6201 wires. He also noted that the AA6201 wires were significantly more resistant than the AA1120 wires under axial fatigue without contact, but both materials displayed similar strength under fretting fatigue.

To predict fatigue life under fretting conditions, conventional methods based on multiaxial fatigue criteria combined with the Theory of Critical Distances, and other methods based on Continuum Damage Mechanics (CDM), have been considered. The CDM approaches (Bhatti et al., 2018; Sandoval et al., 2020; Shen et al., 2021) typically use a scalar variable to represent the amount of fatigue damage and, due to its incremental formulation, has the advantage of not requiring a cycle counting method. It is noted that the studies on fretting fatigue of wires of overhead conductors have been mostly performed using nonlocal multiaxial fatigue criteria (Rocha et al., 2019; Matos et al., 2020; Said et al., 2020a, 2020b). This approach can provide not only the fatigue lives but also the early crack orientation.

In this work, fretting fatigue tests on a wire/wire contact configuration are performed using AA1120 wires. The fretting fatigue test data are used to evaluate a nonlocal life prediction criterion based on the Theory of Critical Distances. This criterion was previously applied to fretting fatigue data of AA1350 and AA6201 wires and provided good life estimates, which motivates its further evaluation considering AA1120 wires. In addition, a tension test and axial fatigue tests are performed on AA1120 wires. The data from these tests and from the fretting fatigue tests are compared to test data of AA1350 and AA6201 wires to identify potential benefits of using AA1120 wires in transmission lines.

3.2 Experimental work

Aluminum alloy (AA) 1120 wires taken from an AAAC (All Aluminum Alloy Conductor) 823 MCM conductor (Fig. 3.1) were investigated in this study. The AA1120 is a commercially pure aluminum alloy with a chemical composition in weight percentage of 99% Al, 0.40% Fe, 0.20% Mg, 0.20% Cu, and 0.10% Si (Aluminum Association, 2015). Due to its purity, the AA1120 has an electrical conductivity of 59% of that of copper, which is comparable to that of other aluminum alloys commonly used in overhead conductors. For reference, the AA1350 and AA6201 have electrical conductivities of 61% and 53% of that of copper, respectively. The AA1120 also has a high mechanical strength and laboratory tests have indicated that it has a better creep resistance than other aluminum alloy wires (Barber and Callaghan, 1995).

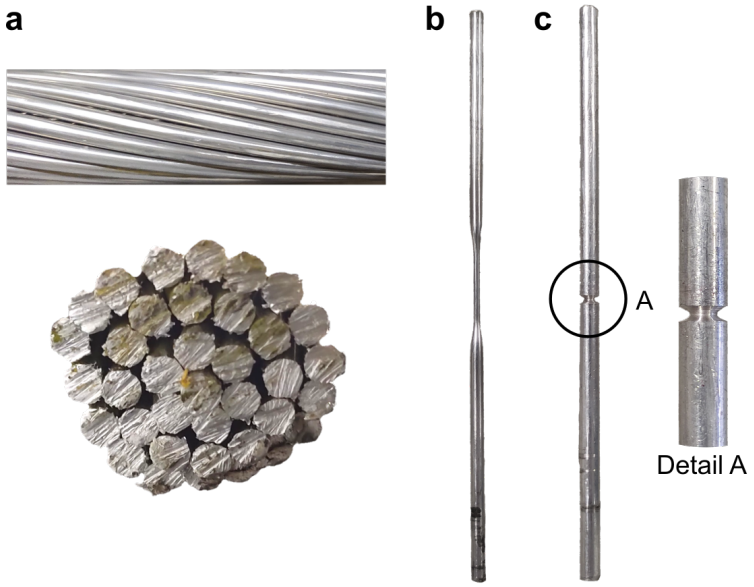

Figure 3.1: (a) AAAC 823 MCM conductor, (b) smooth wire specimen and (c) circumferentially V-notched wire specimen.

A tension test was conducted on a 3.79 mm diameter wire until the complete fracture of the specimen. From the stress-strain curve of the material (Fig. 3.2), the following mechanical properties were obtained: Young´s modulus of 71 GPa, 0.2% offset yield stress of 245 MPa, and ultimate tensile strength of 249 MPa. It should be noted that the ultimate tensile strength is within the range of 230–260 MPa found in the literature (Australian Standard, 1989; Barber and Callaghan, 1995) and informed by the conductor's manufacturer. For reference, the ulti-

mate tensile strengths of the AA1350 and AA6201 are 185 MPa and 311 MPa, respectively (Australian Standard, 1989; Matos et al., 2020).

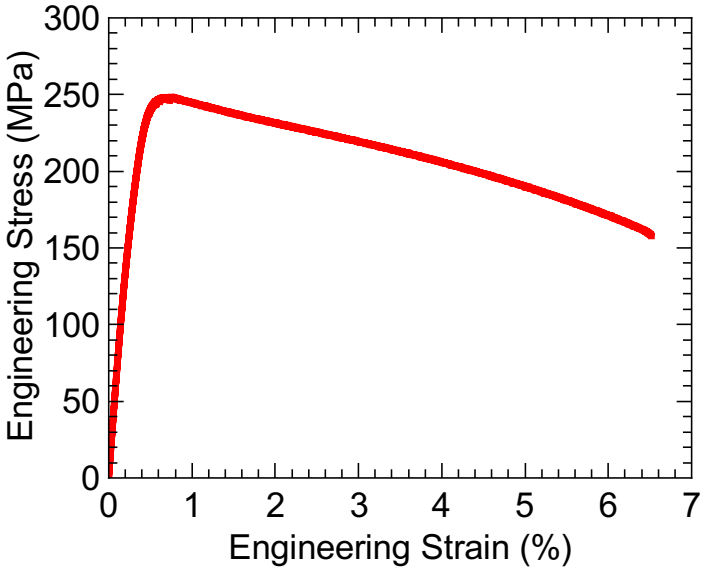

Figure 3.2: Monotonic stress-strain curve of the AA1120 wire.

Smooth and circumferentially V-notched specimens were machined from AA1120 wires with diameter of 3.79 mm. The smooth specimens (Fig. 3.1b) have a minimum diameter of 2 mm while the V-notched specimens (Fig. 3.1c) have a minimum diameter of 2.1 mm, an opening angle of 60º and a notch root radius of 0.17 mm. The tests were performed under fully reversed axial loading. Failure was defined as the complete rupture of the specimen and the run-out condition was defined to be at least 5×10^6 cycles. The fatigue test data are summarized in Tables 3.1 and 3.2, where $\Delta F/2$ is the force amplitude, $\Delta S/2$ is the nominal stress amplitude calculated using the minimum cross-sectional area, and N_f is the number of cycles to failure. The S-N data points are plotted in Fig. 3.3, where run-out tests are indicated by horizontal arrows.

Table 3.1: Fatigue test data of the plain wire specimens.

Test ID	$\Delta F/2$ (N)	$\Delta S/2$ (MPa)	N_{f} (cycle)
P04	404	120	90,518
P06	365	115	212,142
P11	350	112	121,604
P13	338	107	236,447
P12	343	107	403,541
P07	323	105	259,158
P14	338	105	332,035
P15	320	102	714,951
P18	296	100	925,624

Table 3.2: Fatigue test data of the V-notched wire specimens.

Test ID	$\Delta F/2$ (N)	$\Delta S/2$ (MPa)	N_{f} (cycle)
V01	249	72	146,954
V17	236	68	518,460
V16	225	65	674,849
V02	208	60	552,246
V14	204	59	1,444,887
V13	201	58	1,615,094
V06	197	57	1,107,254
V09	194	56	1,313,401
V19	190	55	>10,339,630
V08	187	54	>5,122,455
V07	187	54	>5,763,385
V18	187	54	>10,758,388
V12	184	53	>5,087,613

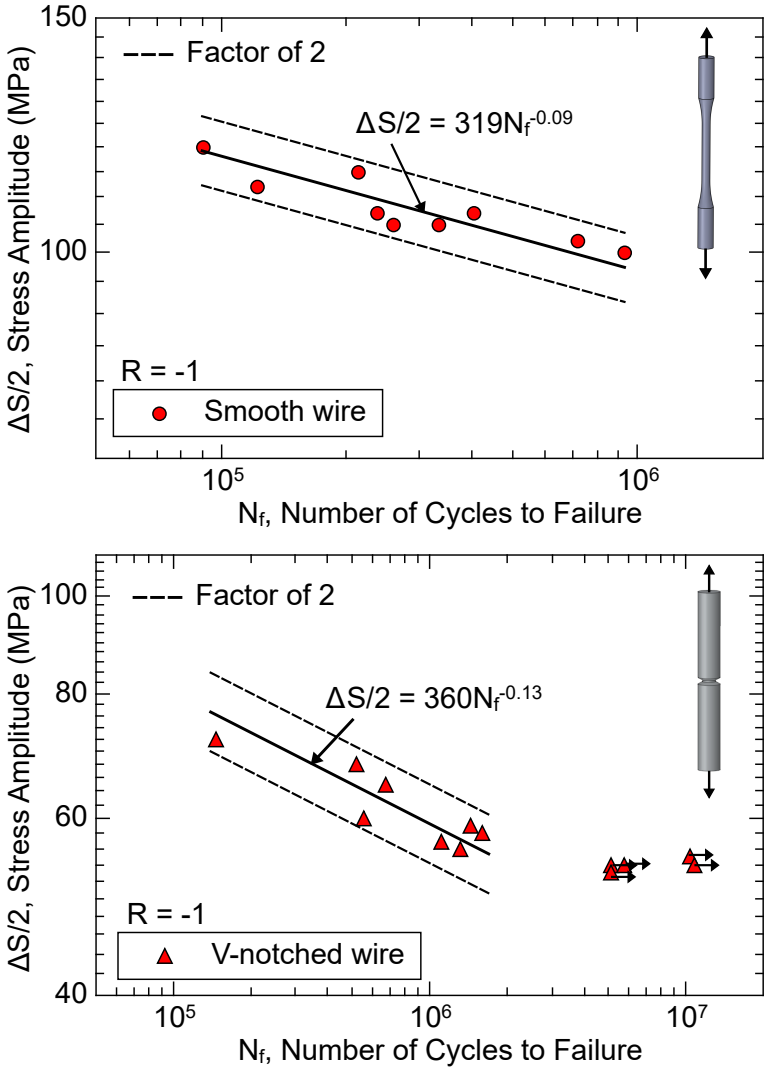

Figure 3.3: Stress-life test data for the (a) smooth and (b) V-notched wire specimens.

Fretting fatigue tests on a wire/wire contact configuration were performed using the apparatus shown in Fig. 3.4a. A cyclic force, $F(t)$, is applied to the lower end of the specimen (vertical wire). This force is controlled by the lower hydraulic actuator and is measured by the lower load cell. The force on the other end of the specimen, $F'(t)$, is measured by the intermediate load cell and the tangential force, $Q(t)$, can be determined as $Q(t) = F'(t) - F(t)$. The contact system used to press the wires against each other is represented in Fig. 3.4b. The compressive force, P, is applied by a pair of pneumatic actuators, which operate simultaneously to push movable blocks over tracks. One block contains a support with the pad (tilted wire) while the other contains a similar support with a bearing. Note that the bearing is free to roll on the wire specimen during the fretting fatigue tests, which reduces the friction between specimen

and bearing. This favors crack initiation at the specimen-pad contact but not at the specimen-bearing contact, allowing the fatigue damage analysis to be focused on the former. The upper hydraulic actuator can be used to impose a cyclic force or displacement to the contact system and, consequently, to the pad and bearing. This cyclic force is measured by the upper load cell and can be used to control the tangential force as it indirectly affects the force $F'(t)$. Additional details about the apparatus can be found in (Garcia et al., 2020).

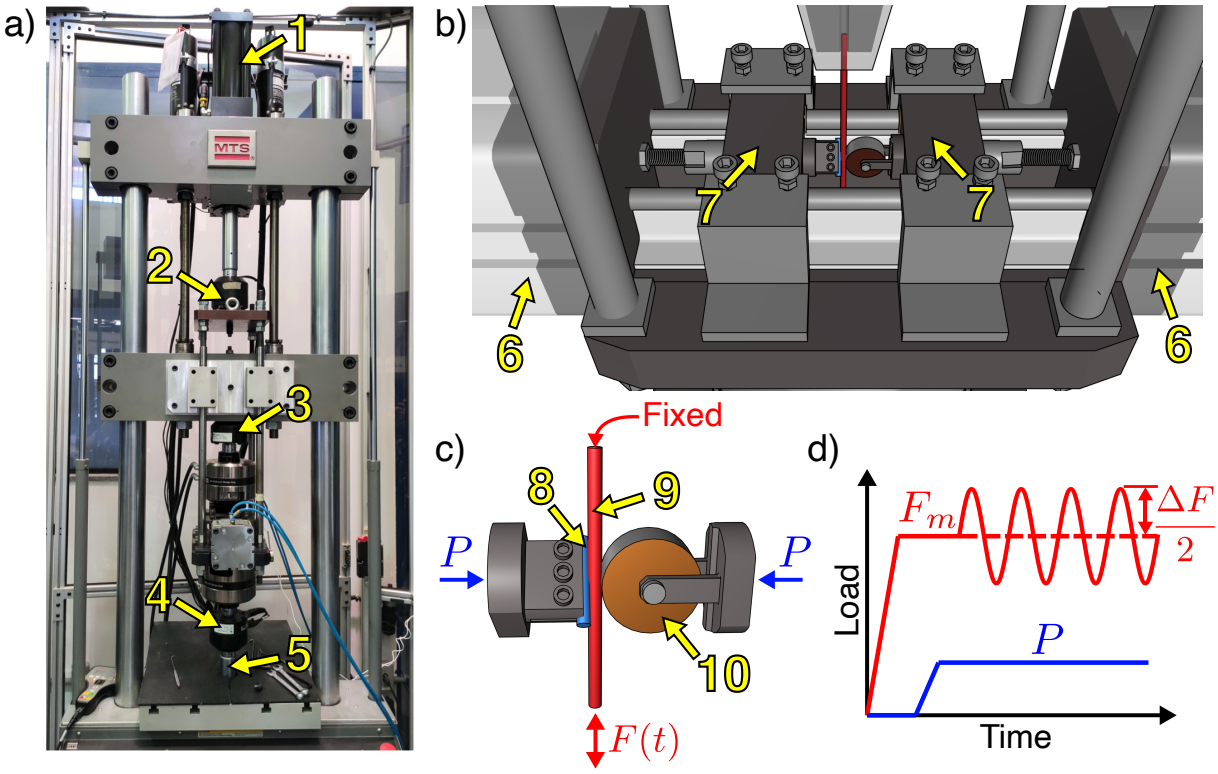

Figure 3.4: Experimental setup for fretting fatigue testing of wires: (a) overall view, (b) system for pressing the wires against each other, (c) detail of the wire/wire contact region, and (d) loading history of the tests.

In the beginning of each test, the support containing the pad is placed at one of the movable blocks. This support contains a pin which is fit into one of the holes of the block. The system of pin and holes is used to position the pad at a certain crossing angle with respect to the specimen, in order to replicate the angle between wires of adjacent layers of the conductor. After positioning the pad, both ends of the specimen are fixed to the testing machine´s grips

and the loads can be applied as represented schematically in Figs. 3.4c and d. Initially, a remote mean force, F_{m}, is imposed by the lower hydraulic actuator to stretch the specimen. Then, the pad and the bearing are pressed against the specimen with a compressive force, P, imposed by the pneumatic system. The remote force is then cycled at a constant amplitude, $\Delta S/2$. In all tests performed in this work, the displacement of the contact system and consequently of the pad and bearing was kept fixed, following the same test procedures used in previous work (Rocha et al., 2019; Garcia et al., 2020; Matos et al., 2020). Although no force is imposed by the upper hydraulic actuator, a cyclic tangential force, $Q(t)$, is produced as a reaction to the remote force applied to the specimen. This tangential force is in phase with the remote force and has a load ratio of about -1.

An important step for carrying out the fretting tests is the planning of the load and contact conditions. More specifically, this planning consists in defining the following four parameters: crossing angle between the wires, stress amplitudes, bulk stress ratio, and normal compressive force. The first two parameters were defined based on the experimental study described in (Kalombo et al., 2019). The researchers performed fatigue tests on an AAAC 823 MCM conductor supported by a suspension clamp using a 47 m resonant test bench. It was observed that in the critical region to fatigue failure, cracks initiated at the contact between wires of adjacent layers and between wires of the external layer in contact with the suspension clamp. In this study, focus has been given to the wire/wire contact interaction. Considering these results, a crossing angle of 20º was chosen for the fretting fatigue tests, as this was the angle measured between wires of the two outermost layers of the AAAC 823 MCM conductor. Stress amplitudes of 27 to 32 MPa were considered, which are similar to the ones used in the fatigue tests performed in (Kalombo et al., 2019).

A bulk stress ratio of 0.7 was chosen for the fretting fatigue tests. The choice for a high load ratio is motivated by the fact that, in a transmission line, the overhead conductor is subjected to a high mean stress caused by the stretching force, and to low bending stress amplitudes due to the aeolian vibrations. This condition can be exemplified by taking the data from the 230 kV transmission line described in (Kalombo et al., 2016). Assuming that the mean stress caused by the stretching force is evenly distributed between the conductor's wires and

that the measured bending displacement amplitudes can be associated with stress amplitudes using the well-known Poffenberger-Swart equation (Poffenberger and Swart, 1965), one can obtain a rough estimate that the conductor's outer layer wires operate at a load ratio of about 0.8 during most of the loading cycles. This characteristic has also been adopted in previous investigations (Matos et al., 2020; Said et al., 2020a), where fretting fatigue tests on wire/wire contact configurations were performed using high load ratios (0.5 to 0.8).

Regarding the normal compressive force, a magnitude of 500 N was chosen for all tests. This force magnitude has been used in several tests on wire/wire and wire/clamp contact configurations (Rocha et al., 2019; Garcia et al., 2020, Matos et al., 2020; Vieira, 2020; Omrani et al., 2021). It is noted that despite the different materials and bulk stresses used in these tests, the contact marks displayed characteristics of partial slip fretting regime, which is usually considered the most critical condition to the fatigue failure of the conductor.

The data of the wires subjected to fretting fatigue tests are listed in Table 3.3, where P is the compressive force, $\Delta F/2$ and $\Delta S/2$ are the force and stress amplitudes, while F_{m} and S_{m} are the mean force and stress, and N_{f} is the number of cycles to failure. As in the axial fatigue tests, failure was defined as the complete rupture of the wires and the run-out condition was set to at least 5×10^6 cycles. The S-N test data are plotted in Fig. 3.5.

Table 3.3: Fretting fatigue test data.

Test ID	P (N)	$\Delta F/2$ (N)	$\Delta S/2$ (MPa)	F_{m} (N)	S_{m} (MPa)	N_{f} (cycle)
F11	500	362	32	2049	181	1,003,951
F08	500	355	32	2010	181	1,154,226
F01	500	355	31	2013	176	1,873,660
F09	500	328	29	1857	164	2,039,350
F10	500	331	29	1874	164	2,169,404
F02	500	311	28	1762	159	1,920,281
F04	500	305	27	1726	153	>5,103,301

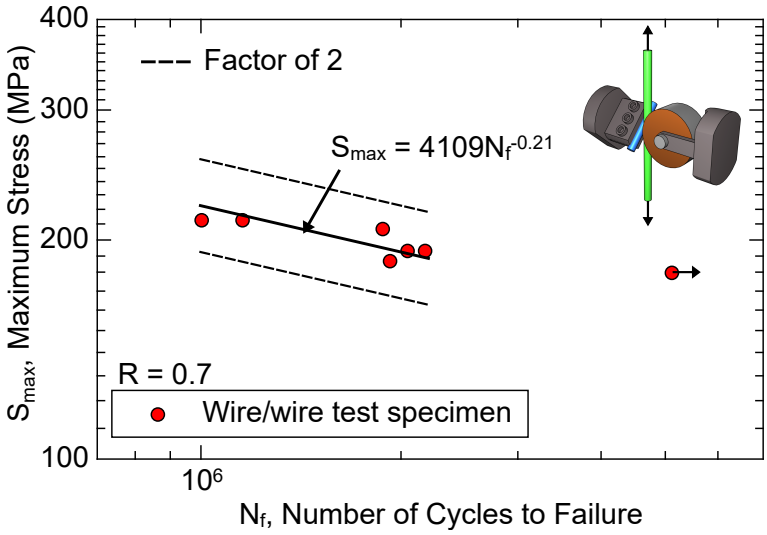

Figure 3.5: S-N data for fretting fatigue tests.

In this work, all fretting fatigue tests were conducted at room temperature. However, during the operation of a transmission line, the conductor's temperature can increase due to solar and Joule heating, the latter being caused by the electric current flowing through the conductor. For instance, Kanálik et al. (2019) measured the temperature of an ACSR conductor used in a 400 kV transmission line in Slovakia during a period of three days and observed that the conductor's temperature was up to 30% higher than the ambient temperature. This temperature increase could lead to a reduction of the fatigue resistance of the conductor, as observed by Costa et al. (2020). The researchers developed a controlled heating system for conductor/clamp assemblies and performed fatigue tests on an AAC Orchid conductor at room temperature and at 75 °C. It was observed that for the same test conditions, the fatigue lives were about 20% shorter in the tests performed at 75 °C. Thus, fretting fatigue tests at higher temperatures could be an interesting topic for future work to evaluate the influence of temperature on the fretting fatigue strength of the conductor's wires.

3.3 Nonlocal fatigue criterion

The introduction of a length scale parameter in continuum damage models is required whenever stress gradient effects become relevant. In fatigue analysis, it is well known that the application of a damage model at the hot spot point of a region under high stress gradient

will result in an inaccurate life estimation. Because of that, various approaches have been developed over the last decades to incorporate the stress gradient effect into fatigue damage analysis. Although the level of rigor of the analytical methods ranges from thermodynamically consistent approaches (Frémond and Nedjar, 1996) to engineering methods such as the Theory of Critical Distances (TCD), all of them involve some length scale, either explicit or implicit.

In this study, the TCD is adopted for being relatively easy to use and generally capable of providing sufficiently accurate results. It started in the 1950s with the pioneering works of Neuber and Peterson (Neuber, 1958; Peterson, 1959) on notches. Then, after its reformulation by Taylor in 1999 (Taylor, 1999), it has steadily been improved and extended. The TCD is an engineering methodology based on the use of a nonlocal stress instead of the stress at the hot spot point. The nonlocal stress is obtained by some averaging procedure of the stresses of a damage zone, whose size is the so-called critical distance. The attractive features of the TCD are:

(i) The critical distance can be determined from fatigue test data obtained by conducting simple tests on standard specimens.

(ii) It can be easily incorporated as a post-processing procedure of a finite element-based stress analysis.

(iii) It can handle three-dimensional problems involving complex multiaxial loading conditions.

The initial development of the TCD was driven by fatigue problems in notched components. In this context, many studies have been carried out involving different types of notch geometries and loading histories. The results obtained have generally indicated that the TCD can provide life estimates with sufficient accuracy for engineering calculations. Later, the TCD was also successfully applied to mechanical assemblies subject to fretting conditions (Araújo et al., 2007, 2020). These studies exploited the fact that contacting surfaces and notches have similar features (e.g., stress concentration, stress gradients, multiaxial stresses) and, therefore, they tried to apply methods originally developed for notches in fretting fatigue problems. Recent studies (Araújo et al., 2020; Pinto et al., 2022) have also shown that it is possible to apply

the TCD in situations where the surface profile is modified due to material loss.

The use of the TCD to estimate the durability of wires of an overhead conductor has recently been investigated. In 2019, Rocha et al. (2019) proposed a nonlocal fatigue criterion in which the stress tensor is defined by averaging the stress distribution over a damage region. It was shown that the characteristic size of the damage zone can be estimated by fitting test data of wires with small notches. By using this methodology, the lives of fretting fatigue tests on AA1350 wires were successfully predicted. Moreover, this approach was also applied to wires made of AA6201-T81, which is a widely used alloy in AAAC (All Aluminum Alloy Conductor) conductors (Matos et al., 2020). For this material, reasonable fatigue lives were also obtained when the input stress data were obtained using an elastic-plastic contact model. Said et al. (2020a, 2020b) have also successfully predicted the fatigue limits of fretting wires using a similar nonlocal fatigue criterion in which the stress tensor from a material point beneath the contact is evaluated.

In what follows, the nonlocal fatigue criterion that will be evaluated later is summarized. The details of the criterion can be found elsewhere (Rocha et al., 2019; Matos et al., 2020). Its starting point is the calculation of an average stress tensor, $\boldsymbol{\sigma}$, associated with a fatigue damage zone. In the volume method of the TCD, the average stress tensor can be expressed as:

$$\boldsymbol{\sigma} = \frac{1}{V}\int_V \hat{\boldsymbol{\sigma}} dV \tag{3.1}$$

where $\hat{\boldsymbol{\sigma}}$ is the stress tensor of a material point inside the damage zone. The shape of this zone was chosen as a hemisphere with volume V, with the center of its flat side positioned at the hot spot. The critical distance, L, corresponds to the radius of the damage zone.

The multiaxial fatigue criterion of Smith, Watson and Topper (SWT) with a critical plane interpretation is used to evaluate the fatigue damage beneath the contact zone. A stress-based version of the SWT parameter can be expressed as

$$\text{SWT} = \sqrt{\sigma_{\text{na}}\langle\sigma_{\text{nmax}}\rangle} = AN_{\text{f}}^{b} \tag{3.2}$$

where σ_{na} and σ_{nmax} are the amplitude and maximum value of the normal stress in a loading cycle, and A and b are fitting constants than can be obtained from smooth wire test data. The Macaulay brackets $\langle\rangle$ are used to ensure that no damage is produced if σ_{nmax} is compressive.

The definition of the critical distance, L, is a crucial aspect for fatigue criteria based on the TCD. As shown by Susmel and Taylor (2007), the TCD can be used to obtain life estimates for medium-cycle fatigue regime by considering that the critical distance is a function of fatigue life. In particular, the following relationship between L and N_{f} was proposed based on test data of notched specimens:

$$L = CN_{\text{f}}^{d_{\text{L}}} \tag{3.3}$$

where C and d_{L} are fitting constants. The procedure to determine the constants of the L-N_{f} relation can be summarized as follows. Initially, the axial fatigue test data from plain wire specimens is fitted by a power law function to obtain the constants of the SWT-N_{f} relation. Then, a datum point is chosen from the notched wire specimen test data, providing a pair of stress amplitude, $\Delta S/2$, and observed fatigue life, N_{obs}. Following that, an estimate is made for the radius of the damage zone, L_{trial}. A stress analysis of the notched wire is performed and the average stress tensor in the damage zone of radius L_{trial} is evaluated. The SWT parameter can then be estimated and applied in the SWT-N_{f} relation to obtain a fatigue life estimate, N_{est}. If the condition $N_{\text{est}} = N_{\text{obs}}$ is reached, the estimated radius can be considered the critical distance and one datum point (L, N_{obs}) is obtained. Otherwise, the procedure must be repeated with a new radius estimate, L_{trial}. After repeating this procedure for all notched wire test data, the (L, N_{obs}) data points can be fitted by a power law function to determine the constants of the L-N_{f} relation.

The implementation of the nonlocal fatigue criterion for life prediction relies on performing a stress analysis of the wire/wire contact problem. Fig. 3.6a shows the finite element (FE) model and the boundary conditions used to perform this stress analysis, where u is the linear displacement. The FE simulations were performed using a linear elastic and an elastic perfectly-plastic material models. The load sequence was defined as follows: initially, a mean

bulk force, F_{m}, is applied to the specimen, then the compressive force, P, is applied to the pad to press one wire against the other and finally the bulk force is cycled at an amplitude $\Delta F/2$. The mesh and element types used in the model are shown in Fig. 3.6b. In order to describe the stress field beneath the contact, partitions with refined meshes were defined in both wires. The bottom and lateral surfaces of these partitions are connected to the bulk of the wires by a tie constraint option, which ensures that there is no relative displacement between the connected surfaces. A surface-to-surface contact approach and a finite-sliding formulation are used to define the contact interaction. The penalty formulation was used for modelling the contact pair. A friction coefficient of 0.6 was chosen, which is within the range of 0.5–0.9 typically used to describe the contact interaction between aluminum wires in finite element-based analyzes of the conductor/clamp assembly (Baumann and Novak, 2017; Lalonde et al., 2018).

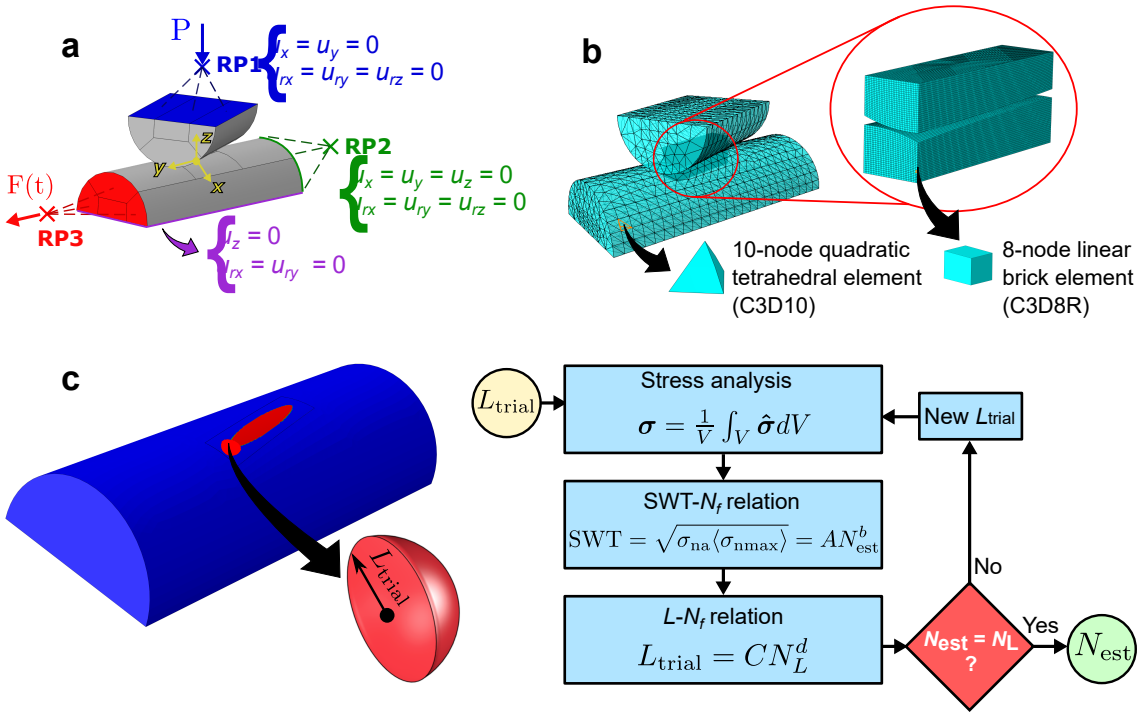

Figure 3.6: Finite element model of the wire/wire contact interaction: (a) mesh and (b) applied loads and boundary conditions.

Fig. 3.6c illustrates the procedure used to estimate the fretting fatigue life of a wire. The hot spot was considered to be located at the lower extremity of the major axis of the elliptically shaped contact mark. This position was chosen because it is physically consistent with the crack initiation site observed in the wire specimens used in the fretting fatigue tests performed

in this work and in previous studies (Rocha et al., 2019; Matos et al., 2020; Vieira, 2020). The procedure starts by defining the bulk and contact forces acting on the fretting wire. Then, an estimate is made for the radius of the damage zone, L_{trial}, and a stress analysis of the wire/wire contact interaction is performed. The average stress tensor over the damage zone outputted from this analysis is used to determine the SWT parameter and obtain a fatigue life estimate, N_{est}. Then, the radius L_{trial} is applied in the L-N_{f} relation to obtain a second life estimate, N_{L}. The estimated lives N_{est} and N_{L} are then compared. If they are different, a new estimate is made for the radius of the damage zone and the procedure is repeated. Otherwise, N_{est} can be considered the life estimate for the wire under fretting fatigue.

3.4 Results and discussion

3.4.1 Fractographic observation of fracture surfaces

This section describes the fractographic observations that were performed on the broken V-notched and fretting wire specimens to evaluate their crack initiation and propagation behaviors. All analyses were performed using a Scanning Electron Microscope. It should be noted that the fracture surfaces of the V-notched and fretting wire specimens did not vary significantly among the specimens. Therefore, for the sake of brevity, only one fracture surface of each type of specimen will be displayed in this section.

Fig. 3.7 shows the fracture surface of the V-notched wire specimen V17 (refer to Table 3.2). Failure occurred at the minimum cross-sectional area where two distinct regions were formed. Details about the microscopic features observed in each region are shown in Fig. 3.8. In Region I, striation marks were found, which characterize the occurrence of crack propagation due to the fatigue loading. Region II is characterized by the formation of a collection of microvoids known as dimples, which indicates that final ductile fracture took place in this region. Therefore, the microscopic features suggest that cracks initiated within Region I and propagated due to the fatigue loading towards Region II, where the final fracture occurred. It should be noted that the size of Region II varied slightly among the specimens, but in all of them, it is

considerably smaller than Region I.

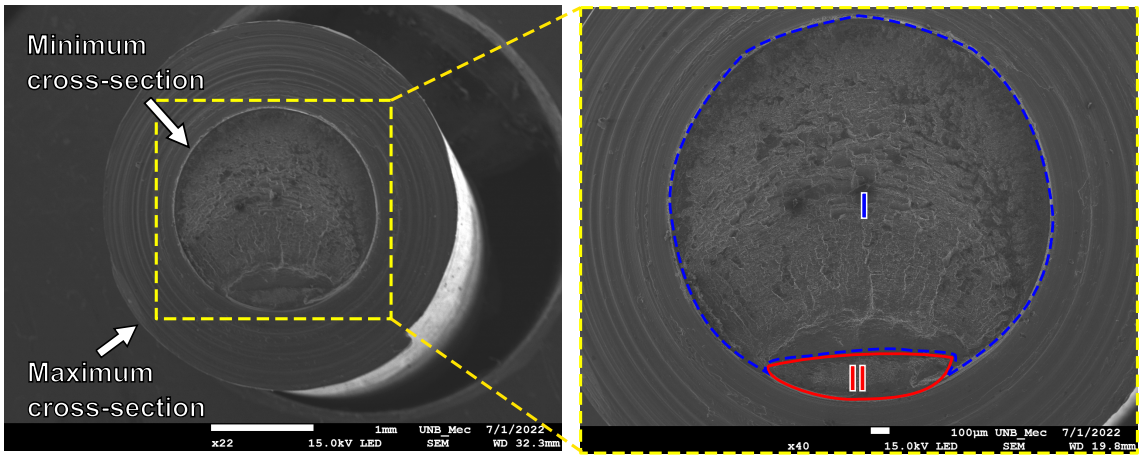

Figure 3.7: Fracture surface of the V-notched wire specimen V17 (refer to Table 3.2).

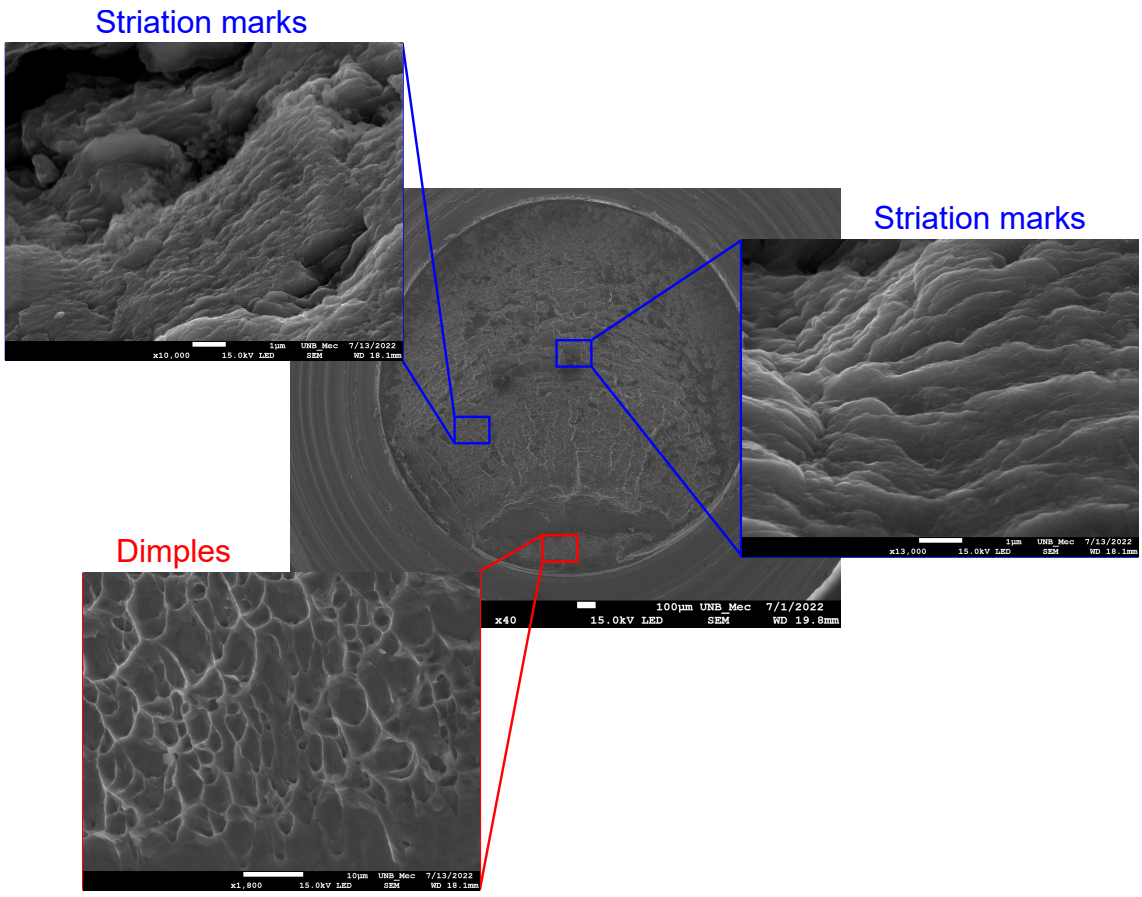

Figure 3.8: Microscopic features observed on the fracture surface of the V-notched wire specimen V17 (refer to Table 3.2).

The contact mark and fracture surface of the fretting wire specimen F09 (refer to Table 3.3) are shown in Fig. 3.9. The elliptically-shaped contact mark displays typical characteristics

of partial slip fretting regime, with a stick zone at its center and a micro slip zone at its edge. The dark color of the micro slip zone is due to the formation of aluminum oxide debris (Ouaki et al., 2003; Azevedo et al., 2009). As with the V-notched specimens, two different regions can be observed in the fracture surface. Region I is formed around the edge of the contact mark while Region II is developed at the rest of the surface. Details about each region are shown in Fig. 10. Striation marks were found in Region I near the contact mark, while dimples were detected in Region II. These microscopic features indicate that the crack initiated from the edge of the contact mark in the micro slip zone, propagated due to fatigue loading in Region I, and lead to a final ductile fracture in Region II. The presence of dimples and striation marks was not evaluated in all specimens. However, all of them displayed a smoother region around the extremity of the contact mark and a rougher region at the rest of the fracture surface, which suggests that the process of crack initiation and propagation was similar for all specimens.

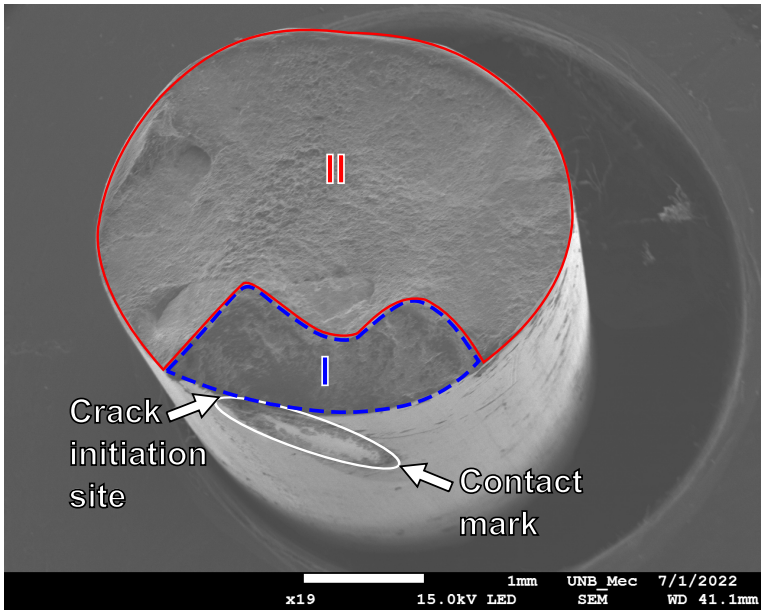

Figure 3.9: Fracture surface of the fretting wire specimen F09 (refer to Table 3.3).

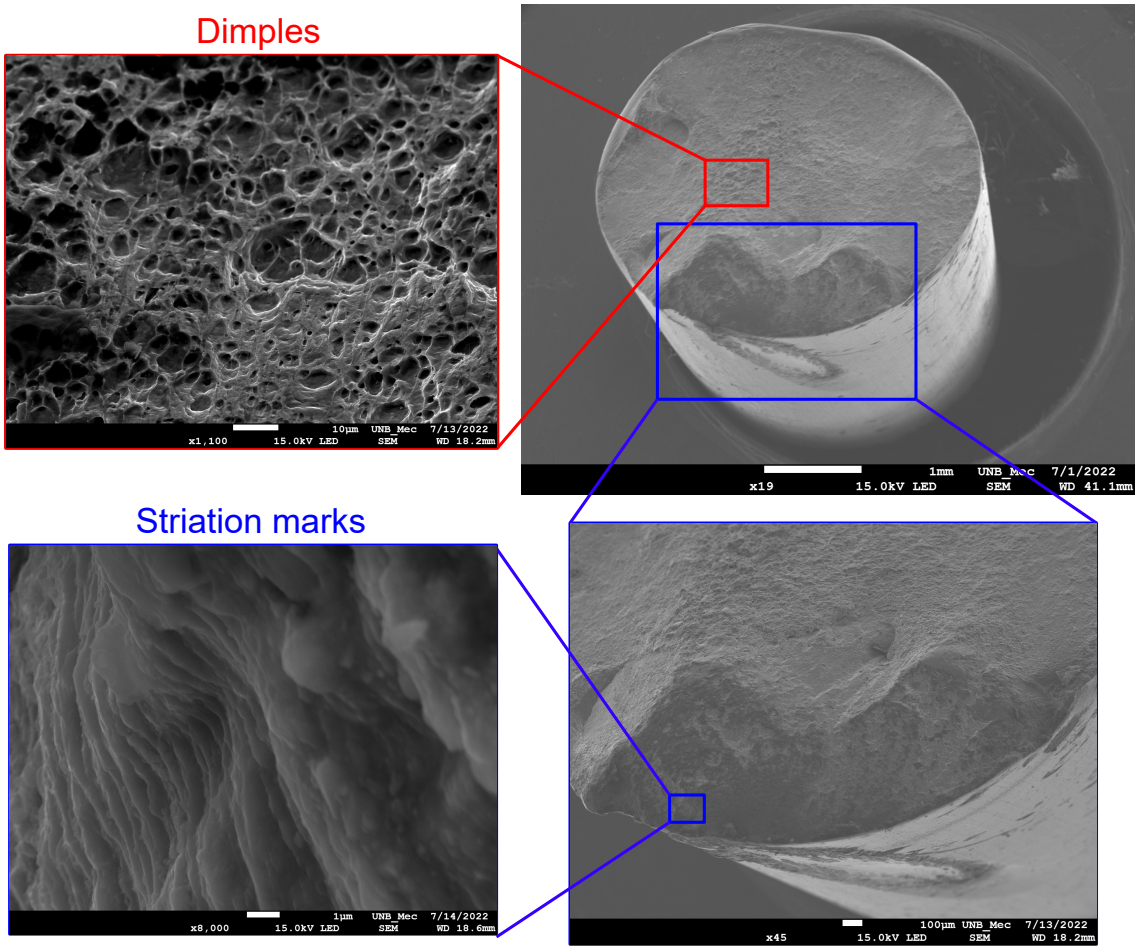

Figure 3.10: Microscopic features observed on the fracture surface of the fretting wire specimen F09 (refer to Table 3.3).

3.4.2 Comparative assessment of aluminum alloy wires

The AA1120 has an ultimate tensile strength of 249 MPa, which is higher than that of the AA1350 (185 MPa) and lower to that of the AA6201 (311 MPa). Having a higher tensile strength means that a higher stretching force can be applied to the conductor at a transmission line, reducing the sag of the span and facilitating the compliance with vertical clearance requirements with respect to roof surfaces. Therefore, a transmission line using a conductor made of AA1120 wires could theoretically be designed with lower transmission towers than one using a similar conductor with AA1350 wires. However, care should be taken when using the ultimate tensile strength of the conductor's wires to define the maximum admissible stretching force, since a high stretching force can reduce the self-damping capability of the conductor, making it more susceptible to aeolian vibrations. Therefore, the choice of the wire material should take

into account not only its tensile strength, but also its fatigue behavior, specially under fretting conditions.

To evaluate the fatigue performance of the three types of aluminum alloys, the following test data of smooth wires subjected to fully reversed axial loading are compared: (i) the AA1120 test data obtained in the present work, (ii) the AA1350-H19 test data reported in (Rocha et al., 2019) using wires from an ACSR Ibis 397.5 MCM conductor, and (iii) the AA6201-T81 test data of wires of an AAAC 900 MCM conductor (Adriano et al., 2018). The S-N data of the three materials are shown in Fig. 3.11. It can be seen that the AA1120 has a higher fatigue strength than the AA1350-H19. For example, for a stress amplitude of 100 MPa, the fatigue life of the AA1120 is about five times longer than that of the AA1350-H19. However, these materials have a considerably lower fatigue strength than the AA6201-T81.

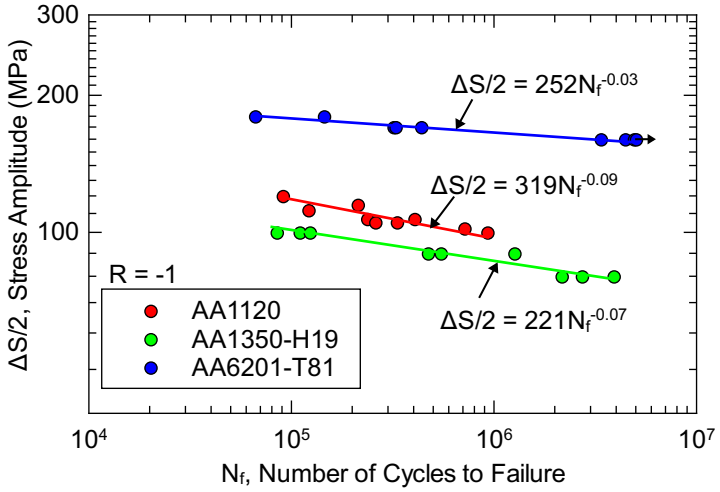

Figure 3.11: Stress-life test data of smooth wires made of 1120, 1350-H19 and 6201-T81 aluminum alloys.

The results from the axial fatigue tests can give a general idea about the fatigue strength of the aluminum alloy wires, but should not be used as a reference for the design of transmission lines. This is because the main cause of failure of overhead conductors is fretting fatigue and, as discussed in (Vieira, 2020), the behavior of an aluminum alloy wire under plain fatigue and under fretting fatigue can be considerably different. To compare the fretting behavior of the aluminum alloy wires, test data of a wire/wire contact configuration obtained from several studies will be used. Table 3.4 summarizes the test conditions adopted in each study, where α

is the crossing angle between the wires, P is the normal contact load, R is the bulk stress ratio, and S_a is the bulk stress amplitude.

Table 3.4: Fretting fatigue test data.

Material	Conductor	α (°)	P (N)	R	S_a (MPa)	Reference
AA1120	AAAC 823 MCM	20	500	0.7	27–32	Current work
AA1120	AAAC 823 MCM	29	250–1000	0.1	62–92	Vieira (2020)
AA1350-H19	ACSR Ibis 397.5 MCM	29	250–500	0.1	32–59	Rocha et al. (2019)
AA6201-T81	AAAC 900 MCM	20	500–750	0.8	24	Matos et al. (2020)
AA6201-T81	AAAC 1055 MCM	29	500–1000	0.1	55–92	Vieira (2020)
AA6201-T81	AAAC 900 MCM	29	250–500	0.1	53–99	Garcia et al. (2020)

The loading conditions in Table 3.4 include low and high bulk stress ratios. To fit the data for each material by a single equation, a nominal stress-based version of the Smith–Watson–Topper fatigue parameter $\mathrm{SWT}_\mathrm{nom}$ is used. This parameter can be expressed as

$$\mathrm{SWT}_\mathrm{nom} = \sqrt{S_\mathrm{a} S_\mathrm{max}} = A' N_\mathrm{f}^{b'} \tag{3.4}$$

where S_a and S_max are the maximum value and amplitude of the bulk stress, respectively, and A' and b' are fitting constants.

The $\mathrm{SWT}_\mathrm{nom}$-$N_\mathrm{f}$ data points for the three aluminum alloy wires are shown in Fig. 3.12. For all materials, the use of a power law relation between the SWT parameter and fatigue life provided an adequate fit for the fretting fatigue test data. As in the plain fatigue tests, the AA1120 displayed a higher resistance than the AA1350-H19 under fretting fatigue. A similar behavior was observed by Kalombo et al. (2019) for fatigue tests of an AAAC 823 MCM conductor made of AA1120 wires and an AAC orchid conductor made of AA1350 wires, where the former exhibited higher fatigue strength. As for the AA6201-T81 wires, its resistance under fretting fatigue is nearly identical to that of the AA1120, which is significantly different than the behavior observed under plain fatigue (refer to Fig. 3.11). The discrepancy between the behavior of the AA6201-T81 wires under plain fatigue and fretting fatigue highlights the importance of performing tests on contacting wires to properly evaluate the durability of wires

of overhead conductors.

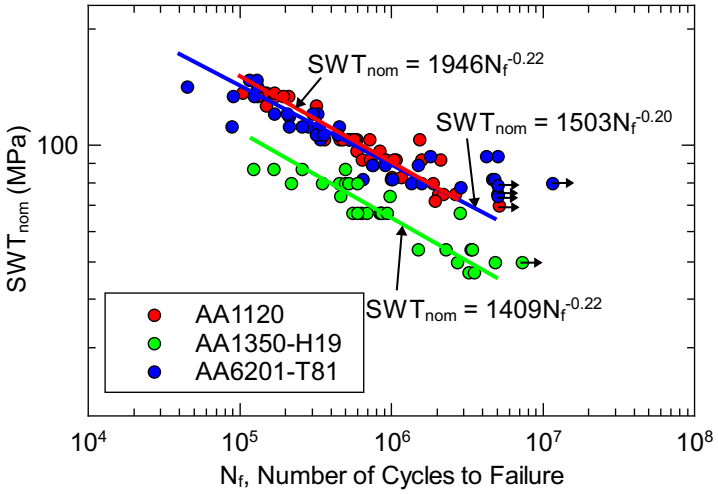

Figure 3.12: SWT_{nom}-fatigue life test data for the fretting fatigue tests performed on 1120, 1350-H19 and 6201-T81 aluminum alloy wires.

The test data in Figs. 3.11 and 3.12 show that the durability of the AA1120 is considerably lower than that of the AA6201 under plain fatigue, but similar under fretting fatigue. As an attempt to explain this behavior, the Vickers hardness of the three aluminum alloy wires were measured. The aim was to evaluate if the surface hardness had a more significant effect on fretting fatigue than on plain fatigue. For instance, in the fretting fatigue tests reported by Sarhan et al. (2013) and by Nishioka and Hirakawa (1972), the specimens with higher surface hardness had slightly longer fatigue lives. However, it should be noted that those tests were performed on carbon steel and aeronautic aluminum alloy specimens, which have significantly higher surface hardness than the materials investigated in this work.

The hardness tests were performed using an indentation force of 1 kgf, which was chosen to ensure that the diagonals of the diamond-shaped indentation marks were longer than 20 μm and at least 1.5 times shorter than the wires' diameters, as recommended by the ISO 6507-1 standard (2018). For each specimen, five indentations were produced and used to determine the Vickers hardness of the wires. Results are summarized in Table 3.5, where HV_i is the Vickers hardness of the i-th test. Note that the AA6201 and the AA1120 had similar fretting fatigue resistances, but the former has a higher surface hardness. Therefore, these results indicate that for the materials and test conditions evaluated in this study, there is no significant influence of

the surface hardness on fretting fatigue strength.

Table 3.5: Vickers hardness of the 1120, 1350-H19 and 6201-T81 aluminum alloy wires.

Material	Conductor	HV_1	HV_2	HV_4	HV_4	HV_5
AA1120	AAAC 823 MCM	56	59	57	55	56
AA1350-H19	ACSR Ibis 397.5 MC	42	41	41	42	40
AA6201-T81	AAAC 900 MCM	78	80	81	87	87

To evaluate the influence of surface wear on fretting fatigue strength, an experimental procedure performed by Vieira (2020) was considered. The researcher performed fretting fatigue tests on a wire/wire contact configuration using AA1120 and AA6201-T81 wires, with diameters of 3.79 mm and 3.34 mm, respectively. The tests were conducted under a bulk stress ratio of 0.1, a bulk stress amplitude of 70 MPa, a crossing angle between wires of 29°, and compressive forces of 750 N and 1000 N. After 200,000 cycles, the tests were stopped and the specimens were examined using a Scanning Electron Microscope equipped with Energy Dispersive X-ray Spectroscopy (EDS). The EDS was used to identify the number and distribution of aluminum and oxygen particles along the contact areas.

The EDS color maps for each specimen are shown in Fig. 3.13. All contact marks displayed characteristics of partial slip fretting regime, with a higher concentration of aluminum particles at the center (stick zone) and oxygen particles at the edge (micro slip zone). The latter can be attributed to the formation of aluminum oxide debris. Based on the EDS color maps obtained by Vieira (2020), the contact areas were measured. The results are reported in Table 3.6, where P is the compressive force, and A_{c}, A_{st} and A_{sl} are the areas of the contact mark, stick zone and micro slip zone, respectively. For the same compressive forces, the contact areas were larger in the AA1120 wires. This result is expected based on the Hertz theory of elastic contact, since the test conditions are the same but the AA1120 wire has a larger diameter than the AA6201 wire. However, for the same compressive forces, the areas of the micro slip zones were similar for both materials. This suggests that the process of surface wear and formation of aluminum oxide debris may be similar for both aluminum alloys, which could explain why they exhibit approximately the same fretting fatigue strength. It should be mentioned that this is only a preliminary analysis, performed with few wire specimens. Additional fretting fatigue

tests under different load conditions are still required to better evaluate the effects of surface wear on fretting fatigue resistance.

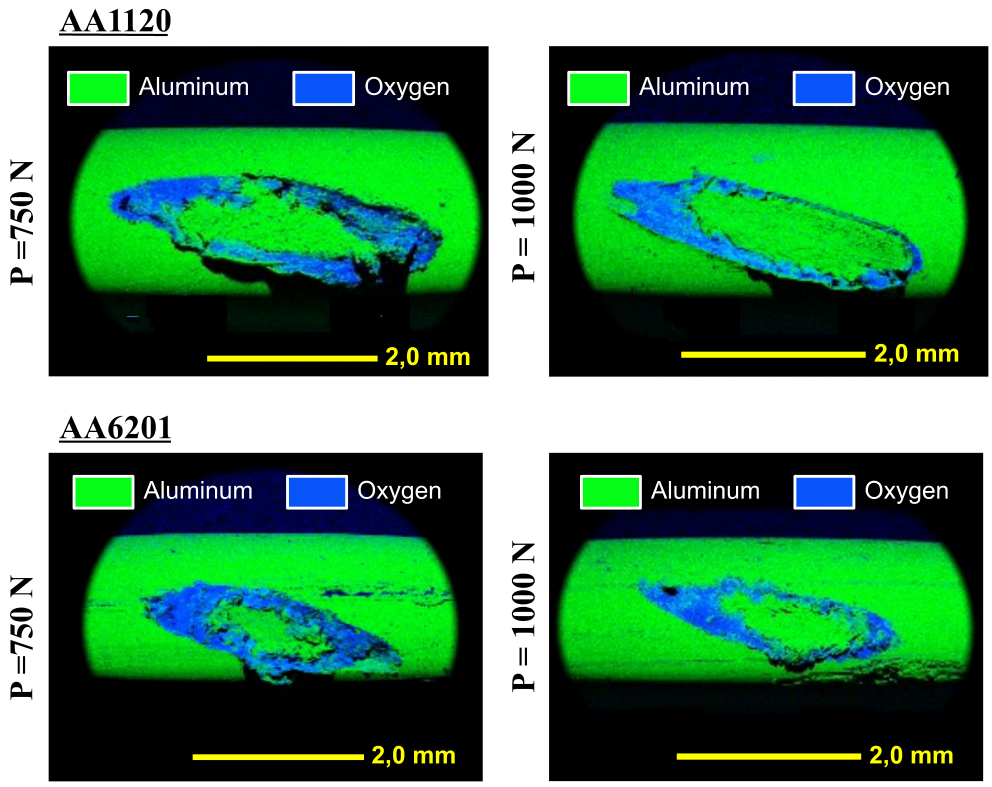

Figure 3.13: SWT_{nom}-fatigue life test data for the fretting fatigue tests performed on 1120, 1350-H19 and 6201-T81 aluminum alloy wires.

Table 3.6: Contact areas of the 1120 and 6201-T81 aluminum alloy wires.

Material	Conductor	P (MPa)	A_c (mm^2)	A_{st} (mm^2)	A_{sl} (mm^2)
AA1120	AAAC 823 MCM	750	2.7	1.0	1.7
AA1120	AAAC 823 MCM	1000	2.4	1.4	1.0
AA6201-T81	AAAC 1055 MCM	750	1.8	0.5	1.3
AA6201-T81	AAAC 1055 MCM	1000	1.5	0.6	0.9

The results presented here suggest that the AA1120 is an appealing alternative for the design of overhead conductors. Compared to the AA1350-H19, the AA1120 has a very similar electrical conductivity, while being considerably more resistant to tension, plain fatigue and fretting fatigue. This implies that conductors made of AA1120 wires, such as the AAAC 823 MCM conductor, could in theory be used to replace aging conductors made of AA1350 wires

with no compromise to the safe operation of the transmission line. Compared to the AA6201-T81, the AA1120 has a higher electrical conductivity, but a smaller tensile strength. While the AA1120 exhibited a smaller fatigue strength than the AA6201-T81 under axial loading, both materials had near identical fatigue strengths under fretting fatigue. Therefore, both materials are expected to have a similar performance when subjected to aeolian vibrations and the choice for one of them will depend on the specific requirements of a transmission line for better tensile strength or electrical conductivity.

The comparison between the fretting fatigue performance of aluminum alloy wires presented in this study indicate that the AA1120 has a resistance comparable to that of other materials used in overhead conductors. However, it is important to mention that these results were obtained considering only the wire/wire contact interaction and may not reflect the resistance of the AA1120 wires in contact with the suspension clamp. As a matter of fact, the wire/clamp contact can also be critical to wire rupture, depending on the type of suspension clamp used. For instance, Miranda et al. (2022) performed fatigue tests on a resonant test bench using an AAAC 823 MCM conductor supported by metallic and elastomeric suspension clamps. In the tests with the metallic clamp, it was observed that about 80% of the wire ruptures occurred at outer layer wires in contact with the clamp, while the opposite happened in the tests with the elastomeric clamp, where about 80% of the failures occurred at the contact between wires of the two outermost layers. Therefore, additional fretting fatigue tests on a wire/clamp contact interaction are still desirable to better evaluate the AA1120 wires.

3.4.3 Evaluation of the life prediction methodology

The application of the nonlocal life prediction methodology requires, as a first step, the determination of the constants of the SWT-N_f and L-N_f relationships given by Eqs. (3.2) and (3.3), respectively. The constants of the SWT equation were obtained by fitting smooth wire test data. Since the tests were performed under fully reversed loading, the SWT parameter is equal to the stress amplitude, $\Delta S/2$, used in the tests. Therefore, the constants can be directly determined from the power law fit shown in Fig. 3.3a, resulting in SWT $= 319N_\mathrm{f}^{-0.09}$. The

constants of the L-N_{f} relationship were calibrated using the V-notched wire test data, following the procedure described in Section 3.3. This resulted in the L-N_{f} data points shown in Fig. 3.14. Note that the estimated critical distances ranged from 102–134 μm. This small variation motivated the use of two different approaches to estimate the lives of the wires used in the fretting fatigue tests: (i) using a constant critical distance $L = 115$ μm, which is the mean value of the critical distances obtained, and (ii) considering the power law equation $L = 65303N_{\mathrm{f}}^{-0.47}$.

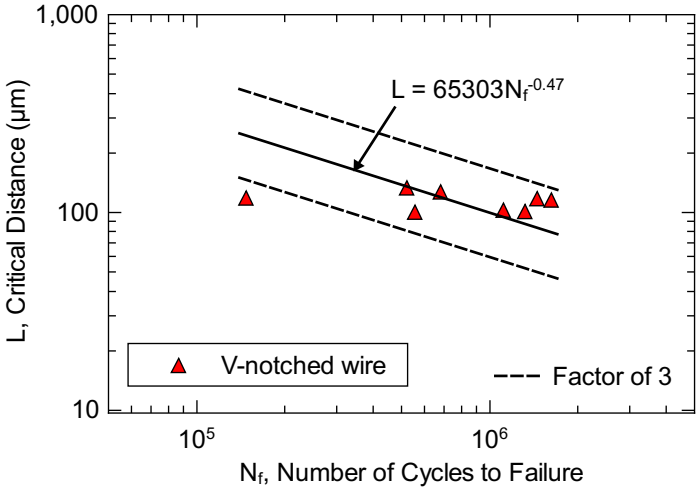

Figure 3.14: Critical distance vs. fatigue life for the V-notched wires.

After the calibration of the fatigue criterion using test data from smooth and V-notched wires, the lives of the fretting fatigue tests were predicted following the procedure represented in Fig. 3.6. For a better evaluation, the fretting fatigue data reported in (Vieira, 2020) for a bulk stress ratio of 0.1 and normal contact load of 500 N were included in the analysis. Fig. 3.15 shows a comparison between the predicted and observed fatigue lives. The life estimates in Fig. 3.15a were obtained using a constant critical distance $L = 115$ μm, while in Fig. 3.15b the power law relation $L = 65303N_{\mathrm{f}}^{-0.24}$ was considered. In both approaches, the linear elastic model was not adequate to describe the stress response of the material, resulting in excessively conservative life estimates. For the tests performed with a bulk stress ratio of 0.1, the life estimates are not shown in Fig. 3.15, but were just as conservative as the ones obtained for $R = 0.7$. The introduction of the plasticity effect significantly improved the life estimates, which were mostly within factor-of-five boundaries when using the constant critical distance, and factor-of-three boundaries when the L-N_{f} relationship was employed. It is clear from these

results that the second approach had, in general, a better agreement to the test data. Additional tests on V-notched wires with lives of 100,000 to 400,000 cycles are still required to better describe the variation of critical distance with fatigue life. However, previous studies (Rocha et al., 2019; Matos et al., 2020) performed on AA1350-H19 and AA6201-T81 wires have shown that the use of a power law relation between critical distance and fatigue life provides an adequate description of the test data, and thus, the same is expected for the AA1120 wires. It is worth mentioning that for the run-out test (specimen F04 in Table 3.3), the estimated life is at least four times shorter than the observed life. This discrepancy could be associated with the plain fatigue test data used to calibrate the life prediction criterion. Note that the lives of the smooth and V-notched wires (refer to Tables 3.1 and 3.2) are mostly in the range of 10^5 to 10^6 cycles. Therefore, the estimated constants of the SWT-N_f and L-N_f relationships should only hold for this range of fatigue lives, which might explain why the prediction was less accurate for this specimen than for the other fretting fatigue tests. It is also noted that satisfactory life predictions were obtained for both low and high bulk stress ratios, which indicates that the SWT parameter was able to correctly predict the mean stress effect.

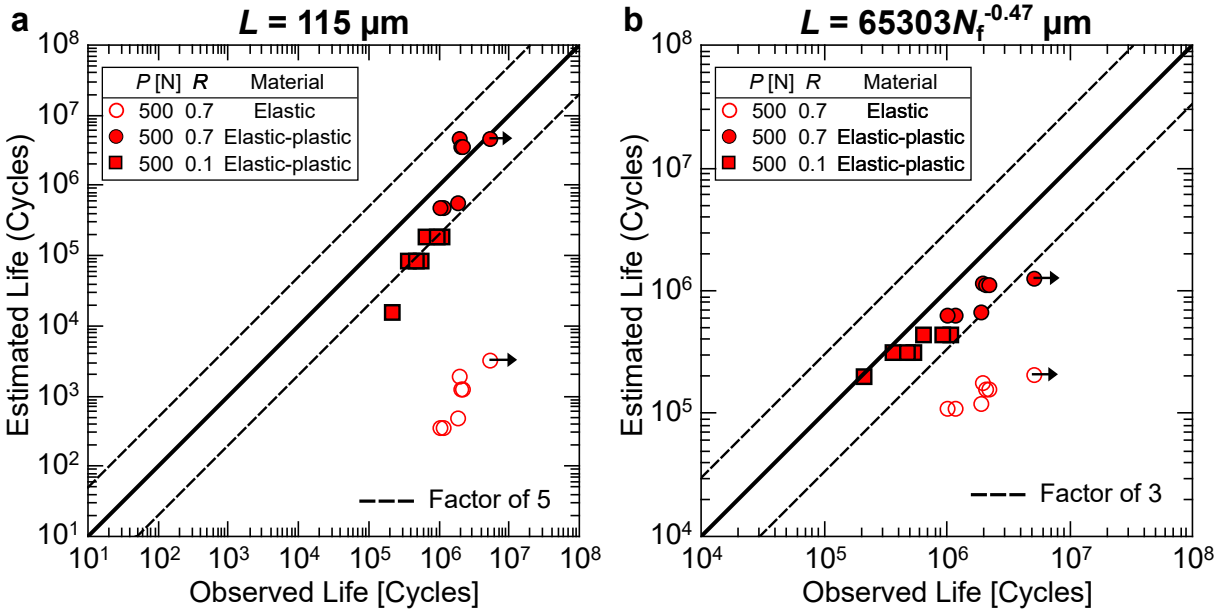

Figure 3.15: Observed vs. estimated lives for the fretting fatigue tests on AA1120 wires considering (a) constant and (b) life-depend critical distances.

The life estimates shown in Fig. 3.15 for the AA1120 and obtained in previous studies for the AA1350-H19 (Rocha et al., 2019) and AA6201-T81 (Matos et al., 2020) show that

the nonlocal fatigue criterion is capable of estimating the lives of fretting wires with acceptable accuracy for different materials and load conditions. It is worth mentioning that for the AA1120 and AA6201-T81, the use of stresses from a linear elastic contact model provided life estimates more than ten times shorter than the observed lives, while most predictions were within a factor of three of the observed lives for the AA1350-H19. The reason for this discrepancy is not yet clear, but it could be related to the fretting fatigue resistance of the aluminum alloys. As observed in Section 3.4.2, the AA1120 and AA6201 have similar resistances under fretting fatigue and both materials are considerably more resistant than the AA1350. These results suggest that the failure of the AA1350 wires is mostly affected by the fretting process, while for the AA1120 and AA6201 wires, both fretting and plasticity play important roles on crack initiation and eventual failure.

3.5 Conclusions

Fretting fatigue tests, plain fatigue tests and a tension test were conducted on AA1120 wires of an AAAC 823 MCM conductor. The test data were used to evaluate a nonlocal life prediction criterion. Also, a comparative assessment between the fatigue performance of the AA1120 with the traditional AA1350-H19 and AA6201-T81 was carried out. The main conclusions of this study are summarized as follows:

(1) The ultimate tensile strength of the AA1120 is about 30% higher than that of the AA1350 and 30% lower than that of the AA6201. In comparison with the AA1350, the fatigue lives of the AA1120 wires were up to five times longer under axial fatigue and four times longer under fretting fatigue. The AA1120 and AA6201 displayed approximately the same fretting fatigue resistance.

(2) The life estimates obtained using a linear elastic contact model were excessively conservative, with most predictions being more than ten times shorter than the observed lives. The use of an elastic-plastic contact model significantly improved the life estimates, which were mostly within a factor of 3 of the observed lives.

(3) Satisfactory life predictions were obtained for the fretting fatigue tests conducted under bulk stress ratios of 0.1 and 0.7, indicating that the Smith–Watson–Topper damage parameter was capable of appropriately describing the mean stress effect.

(4) The life estimates obtained for the AA1120 and in previous studies for the AA1350-H19 and AA6201-T81 demonstrated the capability of the nonlocal fatigue criterion to handle different materials and load conditions and to provide life predictions with acceptable accuracy for engineering calculations.

4 Life prediction of 6201-T81 aluminum alloy wires under fretting fatigue and variable amplitude loading

This chapter is a reproduction of the following publication:

> Matos IM, Araújo JA, Castro FC. Life prediction of 6201-T81 aluminum alloy wires under fretting fatigue and variable amplitude loading. Tribology International 2023;183:108407.

4.1 Introduction

During the operation of a transmission line, overhead conductors may undergo wind-induced oscillations known as aeolian vibrations. Near or within devices that restrain the movement of a conductor (e.g., suspension clamps), the combined effects of aeolian vibrations, clamping pressure, stretching load, and weight of span may lead to wire rupture due to fretting fatigue (Azevedo and Cescon, 2002; Boniardi et al., 2007; Kalombo et al., 2015). To assess the structural integrity of conductors against aeolian vibrations, transmission line utilities have used vibration recorders since the 1920s (Varney, 1926; Wright and Mini Jr, 1934; Edwards and Boyd, 1963; Hardy and Brunelle, 1991). These devices are designed to measure the vertical displacement amplitude of the conductor (usually near a clamp device) and the vibration frequencies. Vibration data recorded from transmission lines (Varney, 1926; Wright and Mini Jr, 1934; Edwards and Boyd, 1963, Cosmai et al., 2017) have shown that the conductor oscillations have a variable amplitude nature, often following a sinusoidal amplitude modulation known as a beat pattern.

To assess the effect of variable amplitude loading on the durability of conductors, block loading histories were used in the fatigue tests performed in (Ramey and Silva, 1981; CIGRÉ,

1979; Brunair et al., 1988; Murça, 2011). These tests were designed to evaluate the effects of increasing or decreasing the loading amplitude on conductor lifetime. To evaluate the benefits of adding damping systems to transmission lines in operation, Ramey and Silva (1981) applied high-low sequences of bending displacement amplitude on three types of ACSR (Aluminum Conductor Steel Reinforced) conductors. The tests were performed by initially subjecting the conductors to a constant amplitude vibration until the rupture of about one to four wires, and then reducing the amplitude to a second level and keeping it constant for up to 100 million cycles. For comparison, fatigue tests with no amplitude reduction were also performed. The researchers observed that about half of the aluminum wires broke during the tests performed under constant amplitude loading. On the other hand, most tests performed using loading blocks exhibited no wire breaks after the amplitude was reduced, suggesting that the addition of dampers could extend the durability of damaged conductors. Similar fatigue tests were performed in (CIGRÉ, 1979; Brunair et al., 1988; Murça, 2011) with low-high and high-low sequences in order to evaluate the use of Miner's rule for overhead conductors. Additionally, CIGRÉ (1979) and Brunair et al. (1988) conducted tests in which the vibration amplitude was alternated periodically between two to four levels. In general, the results from these studies have indicated that Miner's rule can provide reasonable life estimates for design purposes.

More realistic representations of aeolian vibrations have been pursued by (Goudreau et al., 2005; Ferreira et al., 2023) using random loading spectra. Goudreau et al. (2005) defined the spectrum using an approximate Rayleigh distribution, which was discretized into a histogram with 15 stress amplitudes applied at random. Two types of plots were used to represent the test results: a stress-life curve and a D Rayleigh-Miner diagram. For each test, the Rayleigh distribution used to define the loading spectrum can be characterized by a single stress amplitude σ_{aR}, which corresponds to the stress amplitude where the probability density function is maximum. The stress-life curve was then defined using the stress amplitude σ_{aR} in the y-axis and the number of cycles to first wire break in the x-axis. In the D Rayleigh-Miner diagram, the data were plotted using a failure probability function and the damage was calculated using Miner's rule. The researchers observed that the data scatter tended to decrease for higher stress amplitudes and recommended the use of both types of plots to represent the data of tests under

random loading spectra. Ferreira et al. (2023) performed fatigue tests on an ACSR Ibis conductor using narrowband random loading conditions. Time and frequency domain approaches were used to estimate the conductor fatigue life. The time domain approach considers the use of the rainflow cycle counting method and Miner's rule, while the frequency domain approach is based on the moments of a power spectral density function that represents the loading history. The predictions from both approaches were similar and in good agreement with the measured lives.

Turning now to the development of computational models for fatigue life prediction of conductor-clamp systems, progress has been made in the last years (Said et al., 2020a; Omrani et al., 2021; Rocha et al., 2022) but research is still limited to constant amplitude loading. These models are based on analyses performed on two scales. On a global (structural) scale, three-dimensional finite element models of the conductor-clamp system are used to calculate the contact and bulk forces at the contact regions of the conductor. The loading conditions obtained from the global analysis are used as input for a fatigue damage analysis at a local (wire) scale. Different approaches have been considered for the local scale analysis. In (Rocha et al., 2019; Matos et al., 2020, 2022), a combination of the Theory of Critical Distances (TCD) and the Smith–Watson–Topper parameter was used to predict the lives of fretting fatigue tests on wires. A similar analysis was used in (Said et al., 202a) by combining the TCD and the Crossland parameter to predict the endurance limit of the conductor. Omrani et al. (2021) performed fretting fatigue tests on wires and associated the measured lives to the conductor lifetime. An alternative life prediction approach was proposed by Rocha et al. (2022) by using the concept of a master fatigue curve, which represents fretting fatigue data of wires with a single equation. In general, these methodologies have provided good correlations between measured and predicted lives for constant amplitude loading. In particular, the satisfactory life predictions obtained in (Rocha et al., 2019; Matos et al., 2020, 2022) motivated us to give a further step towards the formulation of methodologies applicable to variable amplitude loading conditions.

The goal of the present study was to extend two previously developed methodologies for life prediction of wires to variable amplitude loading conditions: one based on a master fatigue curve (Rocha et al., 2022) and the other on the Theory of Critical Distances (Rocha et al.,

2019). The proposed methodologies were assessed using new fretting fatigue data of 6201-T81 aluminum alloy wires, which were tested under bulk stress histories composed of three loading blocks.

4.2 Experimental program

Wires made of 6201-T81 aluminum alloy (AA), extracted from an AAAC (All Aluminum Alloy Conductor) 900 MCM conductor, were used in this study. The chemical composition of this material, in weight percentage, is 98.54 Al, 0.65 Mg, 0.58 Si, 0.21 Fe, and 0.0012 B (Adriano et al., 2018). The AA6201-T81 has an electrical conductivity of 52.5% IACS (Aluminum Association, 1989) and the following mechanical properties: Young's modulus of 69 GPa, 0.2% offset yield stress of 306 MPa, and ultimate tensile strength of 311 MPa (Matos et al., 2020). During the manufacturing process, this material is solution heat treated, cold worked and then artificially aged, causing the diffusion of Mg and Si atoms, and subsequent formation of magnesium silicide (Mg_2Si) precipitates. These substances restrict the movement of dislocations, increasing the tensile strength and electrical conductivity of the material. The result is an aluminum alloy with slightly lower electrical conductivity but higher tensile strength than other aluminum alloys used in overhead conductors (Davies, 1989; Alshwawreh et al., 2021).

Fretting fatigue tests on wires subjected to variable amplitude loading were performed using the apparatus shown in Fig. 4.1a. The design and operation of the device can be found in detail elsewhere (Garcia et al., 2020; Matos et al., 2022), but for completeness are summarized here. The apparatus contains two hydraulic actuators. The lower one is responsible for controlling the bulk force applied to the specimen (vertical wire), while the upper one controls the tangential force or displacement applied to the pad (tilted wire). A pair of pneumatic actuators are operated simultaneously to press the pad and the bearing against the specimen.

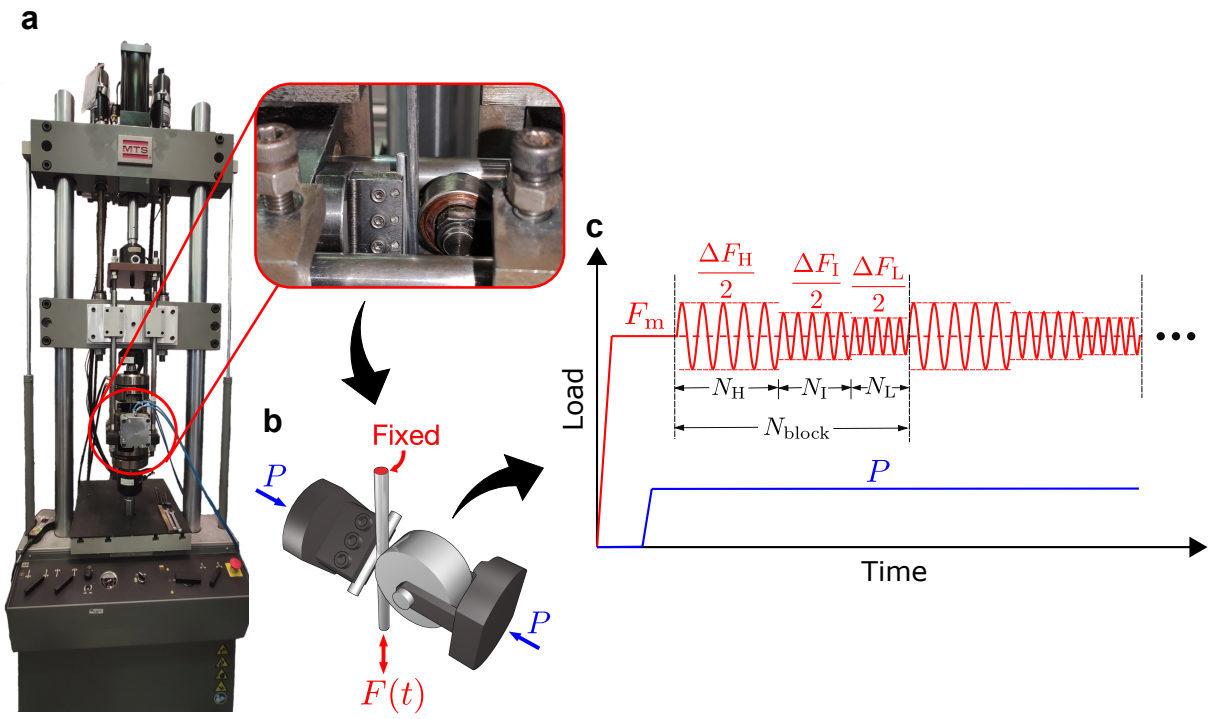

Figure 4.1: (a) Fretting fatigue test apparatus, (b) applied loads, and (c) loading history.

The tests were performed using the loading program illustrated in Figs. 4.1b and 4.1c. First, the pad was positioned at a certain crossing angle with respect to the specimen, in order to represent the crossing angle between wires of adjacent layers of the conductor. Then, the specimen was clamped and subjected to a mean bulk force F_{m}. After that, a compressive normal force P was applied so as to press the pad and bearing against the specimen, and was kept constant during the test. Finally, the specimen was subjected to a cyclic bulk force of variable amplitude until its complete rupture.

The loading program consisted of a main block with N_{block} cycles (see Fig. 4.1c) that was repeated until specimen failure. Each block was composed of three sub-blocks with different amplitudes. The bulk force amplitude $\Delta F/2$ and number of cycles N applied in each sub-block are identified by subscripts H, I and L, which refer to the high, intermediate and low force amplitudes, respectively. All tests were performed by organizing these sub-blocks in a decreasing load sequence. Other studies (Ramey and Silva, 1981; CIGRÉ, 1979; Brunair et al., 1988; Murça, 2011) also exploited the use of loading blocks in fatigue tests of conductors in resonant test benches. Therefore, the choice for this loading history facilitates a comparison

between previous results on conductors with the ones of the present work on wires.

To perform the fretting fatigue tests, the following test parameters have to be defined: (i) crossing angle between wires; (ii) mean bulk stress; (iii) compressive normal force between wires; (iv) bulk stress amplitude of each sub-block; (v) number of loading cycles of each sub-block. The crossing angle between wires was 20°, which was measured in previous studies (Rocha, 2019; Matos et al., 2020) as the angle between wires of the two outermost layers of the AAAC 900 MCM conductor. To define the test parameters (ii) and (iii), the experimental and numerical analysis performed by Rocha (2019) was used as a basis. In his study, fatigue tests on an AAAC 900 MCM conductor were performed using a 47 m resonant test bench. A metallic suspension clamp was positioned close to one end of the conductor, while at the other end, a system of dead weights was used to control the stretching force applied to the conductor. An electrodynamic shaker was connected to the active span of the conductor and was used to control the vibration amplitude. Before each test, strain gages were glued to wires of the outer layer of the conductor near the suspension clamp. All tests were performed under a stretching force of 26 kN, which corresponds to 20% of the breaking strength of the conductor. A total of nine tests were performed, considering three different levels of bending displacement amplitude. The failure condition was defined as the rupture of four wires.

Rocha (2019) observed that the majority of the wire breaks occurred ahead of the keeper edge, at distances of 0.5 to 19 mm from the keeper edge, and most failures occurred on external layer wires, at contact zones with wires of the second outermost layer. Based on these observations, the strain measurements in the fatigue critical region were used to estimate mean bulk stresses considering a linear elastic behavior. In addition, a confocal laser microscope was used to measure the lengths of the major and minor axes of the contact marks. Then, finite element simulations of two wires in contact were performed to estimate the compressive forces between wires required to reproduce the same dimensions observed experimentally. In these simulations, an elastic-perfectly plastic material model was used to account for the plasticity caused by the normal forces. From these analyses, it was concluded that, in the critical region, the mean bulk stresses ranged from 53 to 243 MPa, and the compressive forces were on the order of 100–1270 N. Note that the mean bulk stresses and compressive forces estimated by Rocha (2019) are in a

similar range to those used in the fretting fatigue tests performed in other studies (Rocha et al., 2019; Said et al., 2020a, Matos et al., 2020, 2022; Arnaud et al., 2023).

To define the bulk stress amplitudes and the number of loading cycles of each sub-block, vibration measurements taken on a 230 kV transmission line located in the center-west region of Brazil were considered. The data were recorded at a transmission line composed of two AAAC 900 MCM conductors separated by rigid spacer clamps, as shown in Fig. 4.2a. Each conductor had a total of 37 wires made of AA6201-T81 with a diameter of 3.96 mm, and both conductors were subjected to a stretching force of 26 kN. Additional details about this transmission line can be found in (Kalombo et al., 2015).

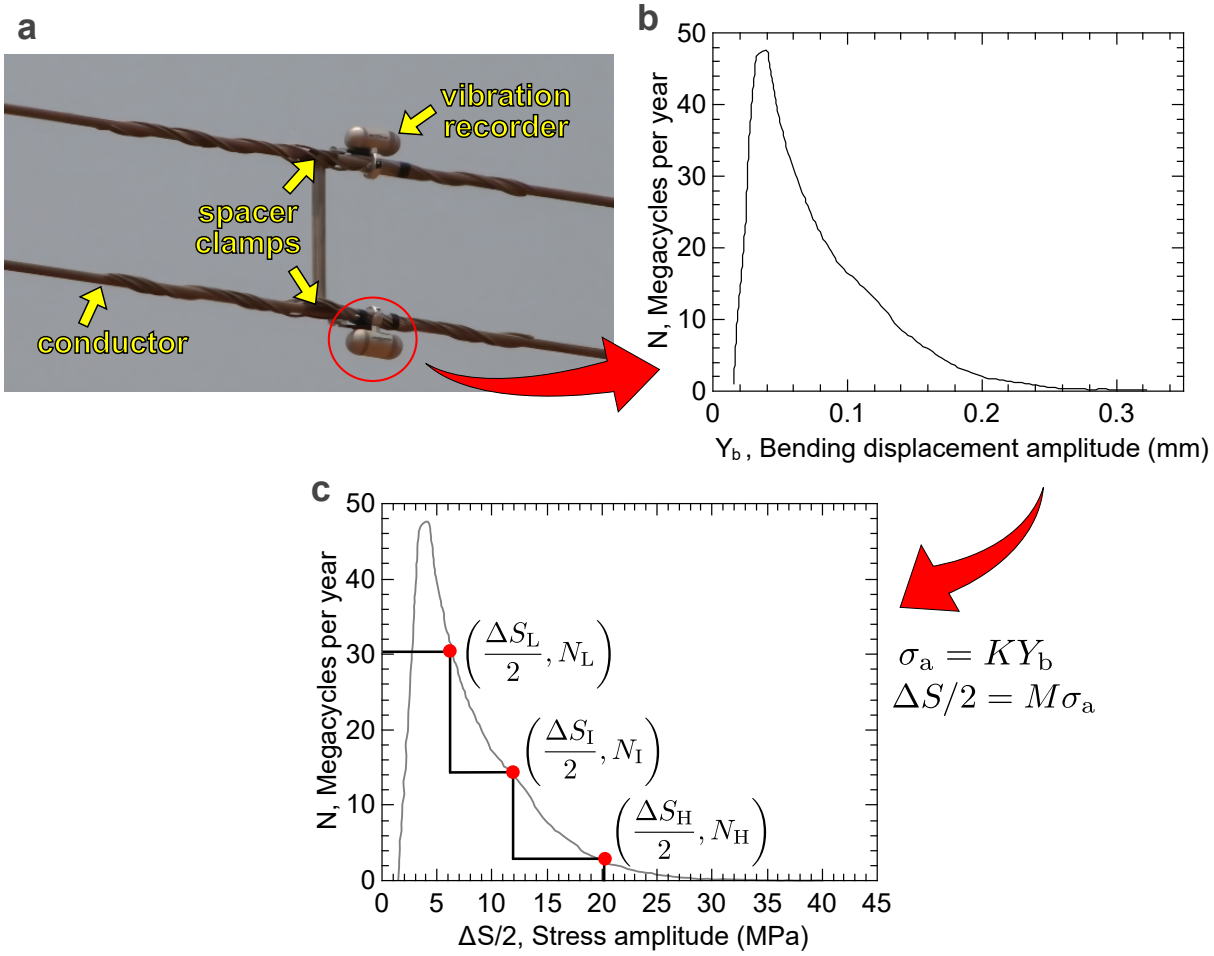

Figure 4.2: Schematic of the procedure for determining the stress amplitudes and loading cycles of the loading block. (a) Transmission line with spacer clamp and vibration recorders. (b) Frequency distribution of bending displacement amplitude over a year. (c) Frequency distribution of bulk stress amplitude.

Two PAVICA vibration recorders were installed near one of the spacer clamps (see

Fig. 4.2a). An schematic of the installation and vibration measurement is shown in Fig. 4.3. Note that the schematic in Fig. 4.3 is representative of a typical conductor-suspension clamp system, which is commonly found in single stranded and bundled conductors. While this configuration does not correspond exactly to the conductor-spacer clamp system shown in Fig. 4.2a, the procedure of measuring the bending displacement amplitude illustrated in Fig. 4.3 is valid for clamp devices in general. The device contains a main cylindrical housing, fixed to the conductor by means of a metallic clamp. A cantilever beam with a length of 89 mm is used to measure the vibration amplitude. One end of this beam has strain gages and is connected to the housing of the recorder, while the other end has a feeler in contact with the conductor. The feeler is placed at a region diametrically opposed to the last point of contact (LPC) between the conductor and the clamp device. The vibration recorder registers the bending displacement amplitude Y_{b} of the conductor, which is defined by IEEE (1966) as the displacement (peak-to-valley) of the point of the conductor diametrically opposed to the LPC and located at a longitudinal distance of 89 mm from the LPC. This point is represented by a red circle in Fig. 4.3. Note that IEEE has traditionally defined the bending displacement amplitude as the difference between the peak and the valley displacements, whereas the fatigue community has defined the amplitude as half the peak-to-valley difference.

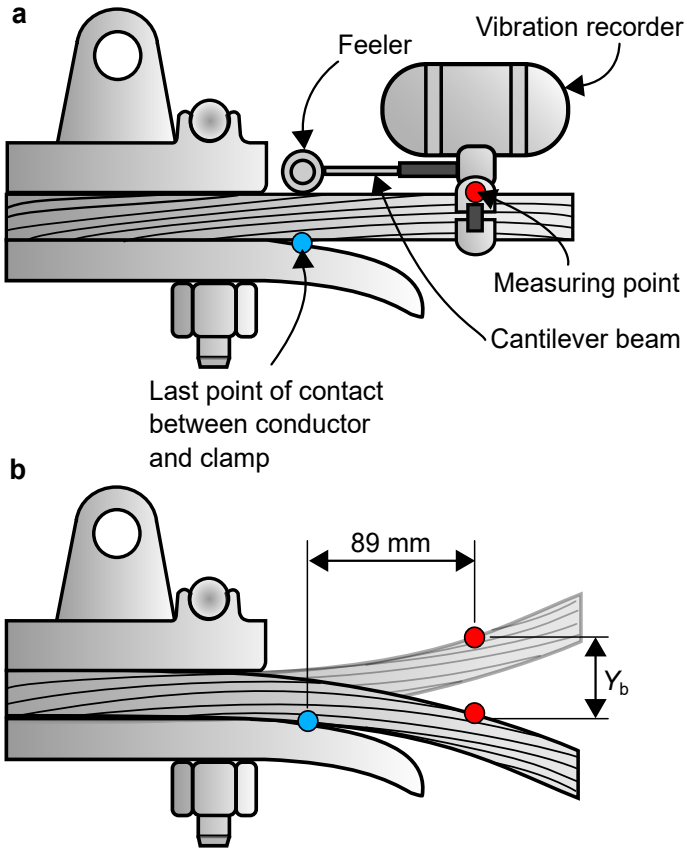

Figure 4.3: Schematic of the (a) positioning of a vibration recorder at a conductor-clamp system and (b) point where the peak-to-valley bending displacement amplitude Y_b is measured.

The vibration data used in the present study were obtained from the lower vibration recorder shown in Fig. 4.2a. The measurements were performed in 2012, between July and August. Ten-second samples were obtained every 15 minutes for 10 days. This procedure follows the recommendations provided by IEEE (1966), which states that, under normal conditions with predominantly steady wind, a record period of one to two weeks long is usually sufficient to record the maximum bending displacement amplitude of the conductor. The vibration data were then extrapolated to a period of one year, as recommended by EPRI (2006). This procedure resulted in the plot of bending displacement amplitude vs. number of megacycles per year shown in Fig. 4.2b. After that, the bending stress amplitude σ_a was calculated from the measured bending displacement amplitude Y_b by using the Poffenberger–Swart relation (Poffenberger and Swart, 1965):

$$\sigma_a = KY_b \tag{4.1}$$

where the parameter K is given by

$$K = \frac{E_{\mathrm{a}} d_{\mathrm{a}} p^2}{4(e^{-px} - 1 + px)} \tag{4.2}$$

where E_{a} and d_{a} are the Young's modulus and the diameter of an aluminum wire of the external layer of the conductor, respectively. For the vibration recorder considered in this study, the distance x between the LPC and the point where the bending displacement was measured was 89 mm. The quantity p is defined by

$$p = \sqrt{\frac{T}{EI}} \tag{4.3}$$

where T is the tension force in the conductor and EI is its bending stiffness. According to Poffenberger and Swart (1965), the bending stiffness can be calculated by considering: (i) that all wires act as a single element and that contact zones are adhered, (ii) that each wire acts as an independent element and that contact zones are in gross sliding condition, or (iii) that the wire interactions are somewhere in between. Hypotheses (i) and (ii) correspond to the conditions of maximum and minimum bending stiffness, respectively. For small levels of bending displacement, which are typical of aeolian vibration, the bending stiffness is expected to be close to its maximum value because there is practically no gross sliding. However, studies (Poffenberger and Swart, 1965; EPRI, 2006) show that a good correlation between theory and experimental data can be obtained even when using a minimum stiffness value, which for AAAC conductors can be determined by the expression:

$$EI = n_{\mathrm{a}} E_{\mathrm{a}} \frac{\pi d_{\mathrm{a}}^4}{64} \tag{4.4}$$

where n_{a}, d_{a} and E_{a} are the number, diameter, and Young's modulus of the aluminum alloy wires. The use of the foregoing relations yielded $K = 35$ MPa/mm for the AAAC conductor under study.

After the calculation of the bending stress amplitude using Eq. (4.1), the nominal stress

amplitude $\Delta S/2$ in the wire was determined as $\Delta S/2 = M\sigma_{\text{a}}$, where M is a multiplying factor. The reason for using this factor is that the bending stress amplitudes are small (between 0.3 and 13 MPa) because the conductor is designed to operate over hundreds of millions of cycles. Thus, to define test conditions that resulted in fatigue failure in a reasonable time duration (i.e., days rather than months), a multiplying factor $M = 3$ was used.

Regarding the number of cycles applied in the main loading block, a value of $N_{\text{block}} = 50,000$ cycles was chosen. This value was defined to provide a high number of repetitions of loading blocks, resulting in several stress amplitude variations during the tests. This procedure followed the suggestion by Sonsino (2007) that the load sequence applied in a variable amplitude loading test should be repeated at least five to ten times to provide an adequate representation of the in-service loading. The definition of the number of cycles applied in each sub-block was made considering the number of cycles of the loading block and the number of megacycles per year for each stress amplitude (Fig. 4.2c). Note that for the transmission line considered in the present study, most of the loading cycles occurred at small stress amplitudes, while few cycles were observed at large amplitudes. To represent this condition, the number of cycles applied in the high, intermediate, and low sub-blocks was defined to correspond to 5%, 15%, and 80% of the number of cycles of the loading block, respectively.

Table 4.1 gives the loading conditions and measured lives of the fretting fatigue tests performed on AA6201 wires. Note that the mean bulk stress is kept constant during the test, while the remote stress amplitude varies between each sub-block. As a result, the bulk stress ratio varies throughout the test, ranging from 0.7 to 0.9. During these tests, all parameters except the bulk stress amplitude of the high-amplitude sub-block are kept constant. The objective was to evaluate how high stress amplitudes affect fatigue life since they occur during a short amount of loading cycles compared to the wire lifetime. In this context, all tests provided fatigue lives of about five to ten million cycles, regardless of the high stress amplitude applied. It should be mentioned that these tests were performed by keeping the displacement of the upper hydraulic actuator fixed. Thus, the tangential force Q is not directly controlled in the tests but arises as a reaction to the cyclic bulk force applied. The tangential force is calculated as the difference between the force measurements from two load cells located near both ends of the

wire specimen. In all tests, the tangential force is in phase with the cyclic bulk force and has a ratio of about -1. The tangential force amplitude varies during the tests, following a similar three-block loading history to that shown in Fig. 4.2c. The minimum and maximum amplitudes registered during the tests were 150 and 270 N, respectively.

Table 4.1: Loading conditions and lives of fretting fatigue tests of AA6201 wires under variable amplitude loading.

Specimen ID	P (N)	S_{m} (MPa)	$\Delta S_{\mathrm{H}}/2$ (MPa)	$\Delta S_{\mathrm{I}}/2$ (MPa)	$\Delta S_{\mathrm{L}}/2$ (MPa)	N_{H} (cycle)	N_{I} (cycle)	N_{L} (cycle)	N_{f} (cycle)
02	500	243	40	24	16	2500	7500	40,000	5,700,581
01	500	243	40	24	16	2500	7500	40,000	7,452,037
05	500	243	36	24	16	2500	7500	40,000	5,650,168
03	500	243	36	24	16	2500	7500	40,000	9,500,092
04	500	243	32	24	16	2500	7500	40,000	4,850,270
08	500	243	32	24	16	2500	7500	40,000	5,400,215

P = compressive normal force; S_{m} = mean bulk stress; $\Delta S/2$ = bulk stress amplitude; N = number of cycles applied in a sub-block; N_{f} = number of cycles to failure.

The loading program studied here was limited to loading blocks with three different bulk stress amplitudes. This is a simple representation of the actual vibrations of conductors in transmission lines, which was adopted as an initial attempt to evaluate the life prediction approaches described in Section 4.3. However, it is important to highlight that the methodology proposed for the definition of the bulk stress amplitudes based on vibration recorder data could also be employed for more complex loading conditions. For instance, tests with more sub-blocks could be defined by taking more points from the graph of frequency distribution shown in Fig. 4.2c. Additionally, tests with a random load spectrum could be defined by considering that each loading cycle would exhibit one of the bulk stress amplitudes shown in Fig. 4.2c, and that the probability of occurrence of a given amplitude would be proportional to the number of megacycles in a year measured for each stress amplitude with the vibration recorder.

4.3 Methodologies for fatigue life prediction

The durability of overhead conductors has traditionally been assessed using stress-life data produced in resonant test benches (see, e.g., Azevedo et al., 2009; Fadel et al., 2012). Taking advantage of today's computational power and finite element (FE) technology, recent efforts have been directed to the development of FE-based procedures for fatigue life prediction of conductor-clamp systems. A major feature of these procedures is the incorporation of the root cause of fatigue failure of conductors, i.e., fretting fatigue in the contact regions of wires. Moreover, they can be useful tools for analyzing the impact of new materials, clamp geometries, and wire cross section configurations on the conductor life.

In addition to a FE model of the conductor-clamp system, the above-mentioned procedures require (i) a reliable methodology for life prediction of wires under fretting fatigue, and (ii) fatigue test data of aluminum alloys typically used in overhead conductors. The authors and collaborators developed two methodologies (Rocha et al., 2019, 2022) for life prediction of wires under fretting fatigue, which provided a good correlation of test data under constant amplitude loading. In this section, these methodologies are extended to variable amplitude loading conditions.

4.3.1 Life prediction based on the Theory of Critical Distances

The Theory of Critical Distances (TCD) is a widely used method for fatigue analysis of notches (Taylor, 2007; Susmel, 2009; Castro et al., 2009). It is based on a nonlocal stress measure, defined by an averaging procedure over a characteristic length, that can account for the stress gradient around the notch to obtain fatigue life predictions. Studies (Araújo et al., 2017, 2020; Kouanga et al., 2018) have shown that the TCD can also account for the stress gradient beneath the contact zone in fretting fatigue. More recently, efforts (Rocha et al., 2019; Said et al., 2020a; Vieira, 2020; Matos et al., 2020, 2022; Araújo et al., 2022) have been made to estimate the durability of wires of overhead conductors using the TCD and a multiaxial fatigue criterion. In particular, the Smith–Watson–Topper criterion with a critical plane interpretation

has provided satisfactory life predictions for aluminum alloys commonly used in overhead conductors (Rocha et al., 2019; Matos et al., 2020, 2022; Araújo et al., 2022) (types 1120, 1350, and 6201). In this section, this approach for fatigue life prediction is extended to variable amplitude loading conditions.

The TCD-based methodology for fatigue life prediction of wires in contact is summarized in the flow chart of Fig. 4.4. The input data consist of the histories of the contact and bulk forces on a wire, and a pair of equations that relate the fatigue parameter and the critical distance with the number of cycles to failure. The fatigue life of the wire is predicted using a critical plane criterion combined with the rainflow method and Miner's rule. However, instead of considering the stress history at the hot spot, a nonlocal stress history is calculated by an averaging procedure over a critical distance. As discussed in previous studies (Rocha et al., 2019; Matos et al., 2020, 2022), the determination of the fatigue life requires an iterative algorithm. It begins by adopting a trial critical distance L_{trial} from which an estimated fatigue life N_{est} is computed. Another estimate $N_{\text{f,L}}$ based on the critical distance vs. fatigue life relation is also obtained. If these life estimates are different, the trial critical distance is updated and the procedure is repeated. Otherwise, N_{est} is taken as the predicted number of cycles to failure. The bisection method is used in this work to update the critical distance L_{trial} at each iteration. To implement this method, the function $f(L_{\text{trial}}) = N_{\text{est}} - N_{\text{f,L}}$ is defined on the interval $[L_{\text{a}}, L_{\text{b}}]$. For the first iteration, values of $L_{\text{a}} = 10\ \mu$m and $L_{\text{b}} = 200\ \mu$m are assumed. The iterative procedure is stopped if the number of iterations exceeds 100 or if the difference between the estimates N_{est} and $N_{\text{f,L}}$ is lower than 1%. The choice for a maximum number of iterations of 100 was based on the initial interval assumed for the critical distance. It is noted that, after 100 iterations, the difference between the values of L_{trial} between two consecutive iterations is lower than 1%, and thus, there is no significant difference between the life estimates obtained from one iteration to the next one. Details of this approach for fatigue life prediction are now presented.

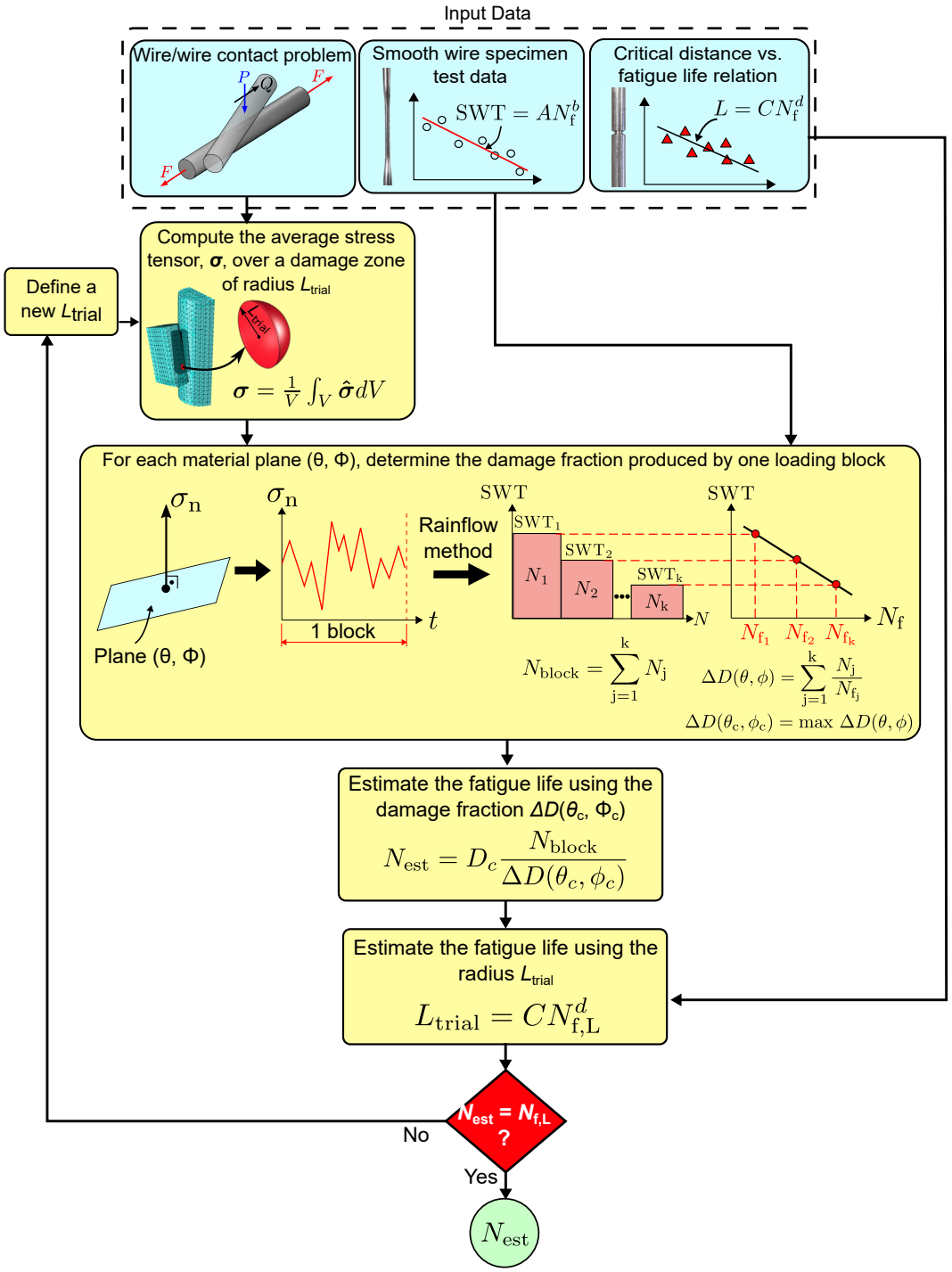

Figure 4.4: Schematic of the TCD-based approach for life prediction of wires under fretting conditions and variable amplitude loading.

In the volume method of the TCD, the average stress tensor $\boldsymbol{\sigma}$ associated with the fatigue damage zone V is given by

$$\boldsymbol{\sigma} = \frac{1}{V}\int_V \hat{\boldsymbol{\sigma}}\, dV \tag{4.5}$$

where $\hat{\boldsymbol{\sigma}}$ is the stress tensor at a point in the damage zone, which has the shape of a hemisphere of radius L (the critical distance). The center of the flat side of the hemisphere is placed at the hot spot, which is the location at the contact surface where a fatigue crack is expected to form. The contact of crossed wires produces an elliptically-shaped contact mark and, as observed in fretting fatigue tests (Rocha et al., 2019; Vieira, 2020; Matos et al., 2020, 2022), cracks typically initiate at one of the extremities of the major axis of the contact mark.

A finite element-based stress analysis is used to calculate the average stress tensor. Details about the finite element model are provided elsewhere (Rocha et al., 2019; Matos et al., 2022) and only a brief description is given here. The specimen and pad are modeled as half-cylinders placed in contact with each other. Partitions are constructed in the contact regions, which allows the construction of a refined mesh in the contact zone and a coarse mesh on the bulk of the wires. An elastic-perfectly plastic material model is used since it was observed to provide more accurate life estimates for AA6201-T81 wires under fretting fatigue than a linear elastic model (Matos et al., 2020). The simulations are performed by initially applying a mean bulk force to the specimen, then a compressive normal force to press the pad against the specimen, and finally by subjecting the specimen to a cyclic bulk force of variable amplitude. To represent the three-block loading history, one loading block is simulated and three loading cycles are applied to each stress amplitude.

As shown in earlier studies (Rocha et al., 2019; Matos et al., 2020, 2022), the SWT parameter with a critical plane interpretation can provide a good correlation of fretting fatigue data of wires. For this reason, this fatigue indicator parameter is adopted here. To calculate the SWT parameter, the normal stresses acting on a material plane are taken as input. The SWT parameter is expressed by

$$\text{SWT} = \sqrt{\sigma_{\text{na}} \langle \sigma_{\text{nmax}} \rangle} = A N_{\text{f}}^{b} \tag{4.6}$$

where σ_{na} and σ_{nmax} are the amplitude and maximum value of the normal stress in a loading cycle and $\langle\rangle$ are the Macaulay brackets. The constants A and b can be obtained by fitting fatigue test data of smooth wires. Typically, the wires of the conductor undergo plastic deformation due to

the manufacturing process, mounting of the conductor on the line, and application of the initial pre-tension. However, the conductors usually operate during hundreds of millions of cycles, which is possible due to a process of elastic shakedown. Thus, the cyclic plastic strains on the wires are expected to be small, which justifies the use of a stress-based fatigue criterion, such as the one expressed in Eq. (4.6). Due to the application of a variable amplitude loading, the normal stress-time history is irregular. Hence, the rainflow cycle-counting method is employed to extract from the normal stress history in a material plane the number of cycles associated with each stress level $(\sigma_{\text{na}}, \sigma_{\text{nmax}})$. The corresponding SWT parameter for each of these pairs is calculated using Eq. (4.6), and the number of cycles in one loading block is determined by

$$N_{\text{block}} = \sum_{j=1}^{k} N_j \tag{4.7}$$

where k is the number of stress levels $(\sigma_{\text{na}}, \sigma_{\text{nmax}})$, and N_j is the number of cycles counted for each of these pairs.

The fatigue damage fraction ΔD produced by one loading block is calculated using Miner's rule, which is expressed by

$$\Delta D(\theta, \phi) = \sum_{j=1}^{k} \frac{N_j}{N_{\text{f}_j}} \tag{4.8}$$

For each stress level, N_{f_j} is the number of cycles to failure determined using Eq. (4.6). The damage fraction is defined as a function of the material plane, which in this work is characterized by a pair of angles (θ, ϕ), where θ indicates the surface crack orientation and ϕ indicates the inclination of the crack. The critical plane $(\theta_{\text{c}}, \phi_{\text{c}})$ is defined as the material plane that maximizes the damage fraction. According to Miner's rule, the damage produced by one loading block is permanent and cumulative, and the failure occurs when this damage reaches a critical value D_{c}. Therefore, an estimated fatigue life N_{est} can be obtained using

$$N_{\text{est}} = D_{\text{c}} \frac{N_{\text{block}}}{\Delta D(\theta_{\text{c}}, \phi_{\text{c}})} \tag{4.9}$$

To implement the fatigue criterion based on the TCD, the critical distance L and the fatigue life N_{f} are assumed to follow the relation

$$L = CN_{\mathrm{f}}^{d_{\mathrm{L}}} \tag{4.10}$$

where C and d_{L} are fitting constants. Eq. (4.10) was initially proposed by Susmel and Taylor (2007) based on fatigue test data of notched specimens and was later used in (Rocha et al., 2019) for life prediction of wires under fretting fatigue. In these studies, the methodologies were calibrated using fatigue test data of smooth and notched specimens under constant amplitude loading (CAL) and were limited to life prediction of notched components and wires under CAL. Later studies (Susmel and Taylor, 2012; Kouanga et al., 2023) demonstrated that the same calibration procedure based on CAL fatigue test data can provide satisfactory life predictions for notches and fretting components under variable amplitude loading. Based on these results, the fitting constants of the SWT criterion and the L-N_{f} relation are obtained in the present work using CAL fatigue test data of smooth and notched wire specimens.

4.3.2 Life prediction based on a master fatigue curve

A methodology to predict the fatigue life and the critical regions of failure of conductor-clamp systems was proposed by Rocha et al. (2022). The methodology relies on (i) stress analysis of the conductor-clamp system based on finite elements, and on (ii) the use of test data of wires under fretting conditions to estimate the durability of the wires of the conductor. To evaluate the methodology, fatigue test data of an AAAC 900 MCM conductor were considered. The predicted lives and critical regions of failure were in good agreement with the experimental results.

The innovative aspect of Rocha's approach was the introduction of a master fatigue curve to represent test data of wires under fretting fatigue. This idea was inspired by the similitude concept of the S-N method. According to this concept, there is a set of test conditions under which a specimen tested in the laboratory will have the same fatigue life as a component in service. In the case of overhead conductors, if a wire specimen tested under fretting conditions

and a wire of the conductor-clamp system share the same material and nominal stress history, the fatigue lives of both should be the same. Thus, the master fatigue curve was suggested for estimating the fatigue life of a wire of the conductor-clamp system. The researchers found that the test data of AA6201-T81 wires under various normal loads and bulk stress ratios could be represented by a master fatigue curve using a nominal stress-based version of the Smith–Watson–Topper (SWT) parameter. The effectiveness of the master fatigue curve approach was attributed to the fact that it takes into account the effects of stress concentration and stress gradients since the curve is defined using fretting fatigue test data. Furthermore, the good fit of the test data obtained using the SWT parameter was attributed to the significant effect of the mean bulk stress on the life of a wire under fretting fatigue.

The concept of a master fatigue curve was later exploited by Matos et al. (2022) for fretting fatigue test data of AA1120, AA1350-H19, and AA6201-T81 wires. It was observed that the data for each material could be represented by a single equation using the SWT parameter. The researchers used this approach to compare the three materials, concluding that the AA1120 and the AA6201-T81 wires had approximately the same fretting fatigue resistance, which was higher than that of the AA1350-H19 wires. The promising results obtained in (Rocha et al., 2022; Matos et al., 2022) motivated us to conduct the present research, which is an attempt to extend the concept of a master fatigue curve to life prediction of wires under fretting fatigue and variable amplitude loading (VAL).

The flow chart in Fig. 4.5 illustrates the life prediction methodology based on a master fatigue curve. The input data consist of the nominal stress history of a wire, and the master curve, which is obtained using test data of wires under fretting conditions. A combination of the rainflow cycle-counting method and Miner's rule is used to estimate the fatigue damage fraction ΔD produced by the nominal stress history. The master fatigue curve is used as a reference for the calculation of the damage fraction, which in turn is used to predict the fatigue life of the wire. In what follows, the new formulation of the methodology is presented.

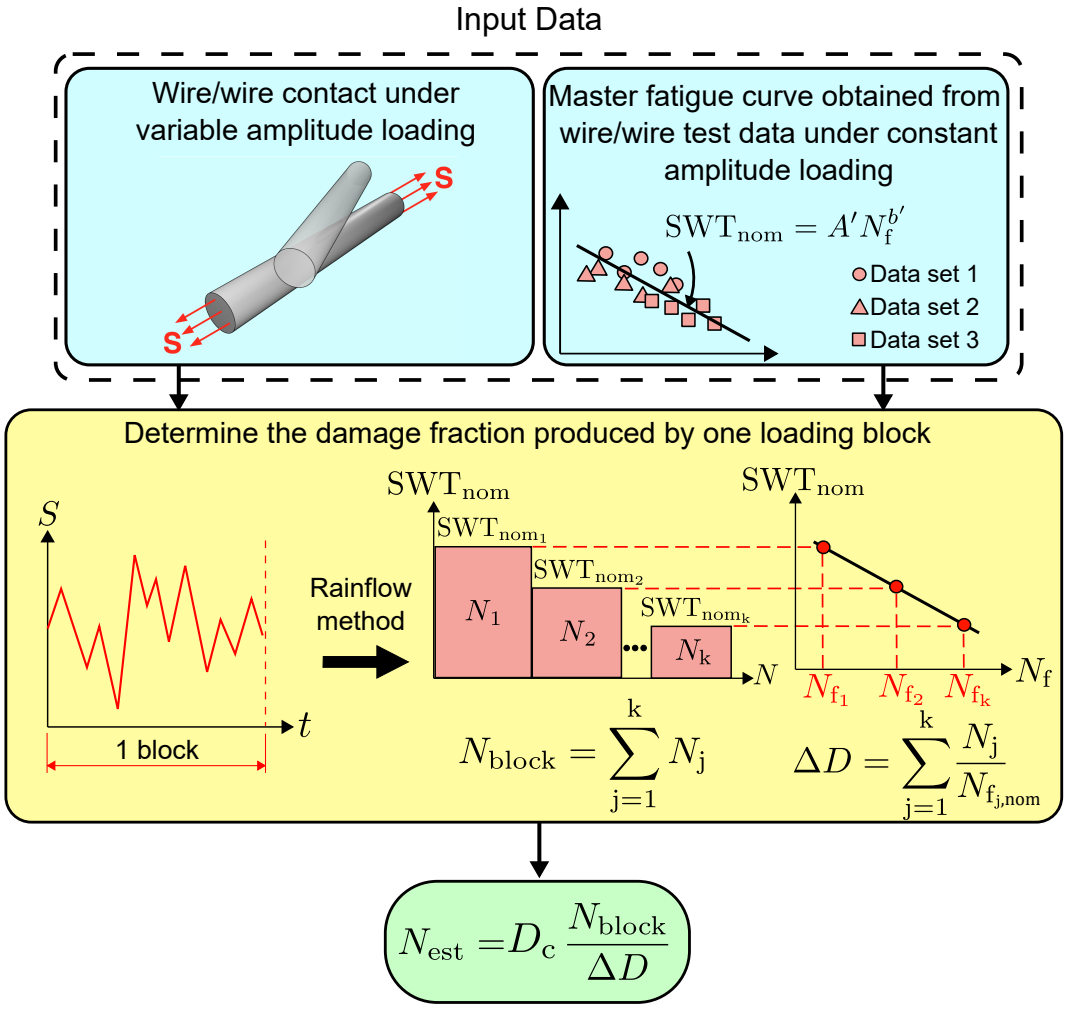

Figure 4.5: Schematic of the master fatigue curve approach for life prediction of wires under fretting conditions and variable amplitude loading.

The starting point of this approach is the representation of fretting fatigue test data of wires under constant amplitude loading as a master fatigue curve. Considering that the SWT parameter provides, in general, a good correlation for stress-life data of aluminum alloys (Dowling et al., 2009; Rocha et al., 2019, 2022; Matos et al., 2020, 2022), the following equation is proposed for the master fatigue curve:

$$\mathrm{SWT_{nom}} = \sqrt{S_\mathrm{a} S_\mathrm{max}} = A' N_\mathrm{f}^{b'} \tag{4.11}$$

where S_a and S_max are the amplitude and maximum value of the nominal stress in a loading cycle, and A' and b' are fitting constants. The rainflow cycle-counting method is used to extract from the nominal stress history a set of stress levels $(S_\mathrm{a}, S_\mathrm{max})$ and the number of loading cycles

N_j associated with each level. Eq. (4.11) is then employed to calculate the corresponding SWT_{nom} parameter for each stress level.

After the application of the rainflow method, the fatigue damage fraction ΔD produced by one loading block is estimated using Miner's rule, which is expressed as

$$\Delta D = \sum_{j=1}^{k} \frac{N_j}{N_{\text{f}_{j,\text{nom}}}} \tag{4.12}$$

where $N_{\text{f}_{j,\text{nom}}}$ is the number of cycles to failure for a given stress level $(S_{\text{a}}, S_{\text{max}})$, determined using Eq. (4.11). Finally, the estimated fatigue life N_{est} is obtained using

$$N_{\text{est}} = D_{\text{c}} \frac{N_{\text{block}}}{\Delta D} \tag{4.13}$$

where D_{c} is the critical damage and N_{block} is the number of cycles in one loading block.

4.4 Results and discussion

Life prediction based on a master fatigue curve requires checking if fretting fatigue test data can be reduced to a single curve, such as that defined by Eq. (4.11). The data used here are summarized in Table 4.2, which includes tests on AA6201-T81 wires subjected to normal loads ranging from 250 to 1000 N, bulk load ratios of 0.1 and 0.8, and bulk stress amplitudes from 15 to 99 MPa. Fig. 4.6 presents a plot of the data in terms of the SWT parameter (calculated using the nominal bulk stress) versus the number of cycles to failure. It is seen that the power-law relation $\text{SWT}_{\text{nom}} = 1840 N_{\text{f}}^{-0.22}$ provided a good fit of the data, which were mostly within factor-of-three boundaries. This result shows that the nominal SWT parameter was capable to reduce fretting fatigue test data of AA6201-T81 wires under various test conditions and covering a wide range of lives (from 4×10^5 to 6×10^6 cycles).

Table 4.2: Fretting fatigue test conditions of AA6201-T81 wires under constant amplitude loading.

α (°)	P (N)	S_a (MPa)	R	Reference
20	500	15–24	0.8	Rocha et al., 2022
20	500–750	24	0.8	Matos et al., 2020
20	250–500	53–99	0.1	Garcia et al., 2020
29	500–1000	55–92	0.1	Vieira, 2020

α = crossing angle between wires P = compressive normal force; S_a = bulk stress amplitude; R = bulk stress ratio

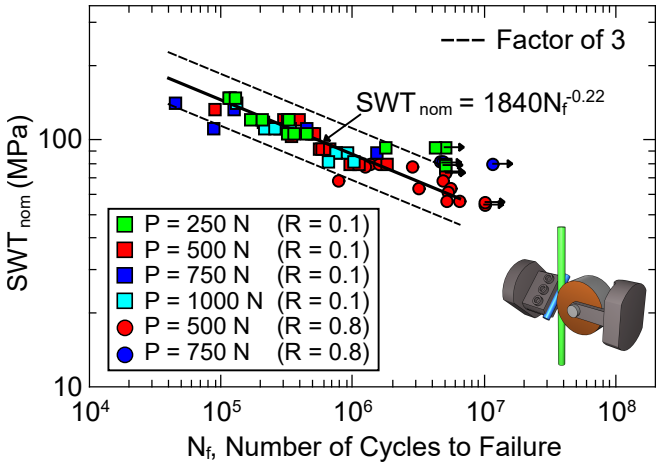

Figure 4.6: Correlation of fretting fatigue test data of AA6201-T81 wires with the SWT parameter calculated using the nominal bulk stress.

For life prediction based on the Theory of Critical Distances, one must first determine the constants of the SWT criterion in Eq. (4.6) and the L-N_f relation in Eq. (4.10). These constants were obtained by fitting the test data of smooth and V-notched wires reported in (Matos et al., 2020), which resulted in the power-law relations SWT $= 252N_f^{-0.03}$ and $L = 1765N_f^{-0.24}$ (see Fig. 4.7).

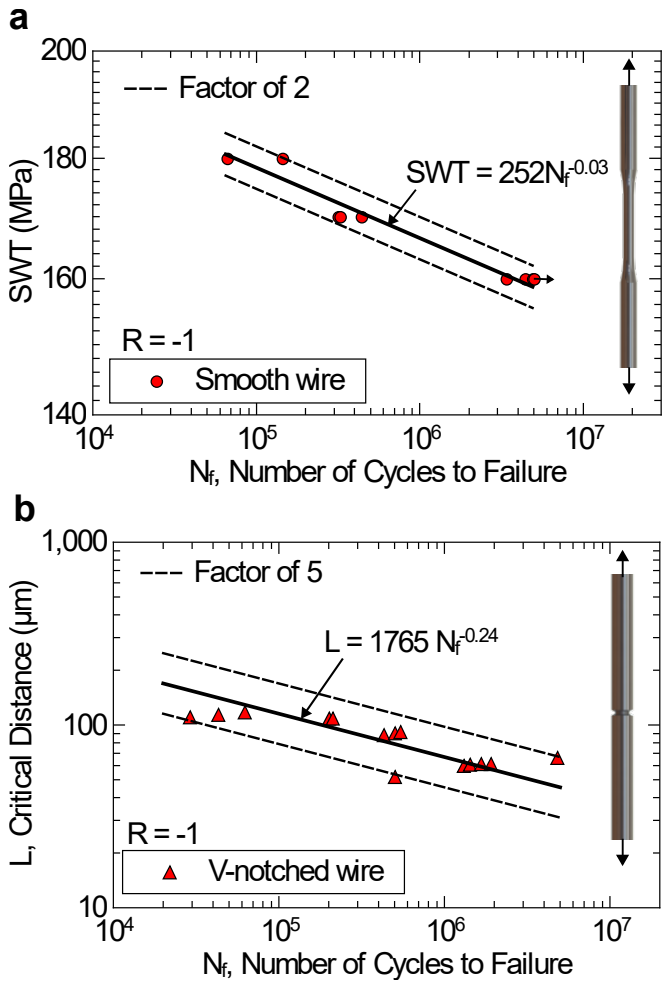

Figure 4.7: (a) SWT parameter vs. fatigue life for the smooth wires. (b) Critical distance vs. fatigue life for the V-notched wires.

The application of the life prediction methodologies also requires the specification of the critical damage D_c. In 1979, CIGRÉ (1979) performed a series of fatigue tests on AlMgSi conductors under variable amplitude loading. It was observed that the critical damage of these tests ranged from 0.7 to 2.3, which lead CIGRÉ to recommend the use of a critical damage $D_c = 1$ for overhead conductors. In later studies (Brunair et al., 1988; Goudreau et al., 2005; Murça, 2011), fatigue tests were performed on ACSR (Aluminum Conductor Steel Reinforced) conductors under variable amplitude loading and similar critical damage values were obtained, ranging from 0.4 to 3.4. In addition, studies (Gandiolle et al., 2016; Pinto et al., 2020; Kouanga et al., 2023) on fretting components under variable amplitude loading have employed a critical damage $D_c = 1$. Based on these results, a critical damage $D_c = 1$ is adopted in the present study.

After calibrating the constants of the fatigue life prediction methodologies, the durability of AA6201-T81 wires subjected to fretting fatigue and variable amplitude loading was predicted. A comparison of measured and predicted lives is shown in Fig. 4.8. The estimates based on a master fatigue curve were all conservative and were within a factor of 4 of the measured lives. The lives estimated using the Theory of Critical Distances (TCD) were evenly scattered with respect to the solid diagonal (perfect correlation) line and were within factor-of-three boundaries. Note that the loading sequence may affect the average stress tensor from the FE simulations and, consequently, the life estimates, which could explain why the TCD-based approach did not display a conservative bias. It should be mentioned that the master fatigue curve was defined in the present study using only nominal bulk stresses. The methodology was purposely designed to be as simple as possible, and still provide reasonable life estimates for design purposes. There are limitations to this methodology, as other test parameters such as the normal and tangential forces, can also affect the lives of wires under fretting fatigue (Matos et al., 2020; Said et al., 2020b; Omrani et al., 2022). Despite the simplifications, the results obtained in the present study show that the methodology can provide life predictions within a similar scatter to the fretting fatigue test data used to calibrate the master curve.

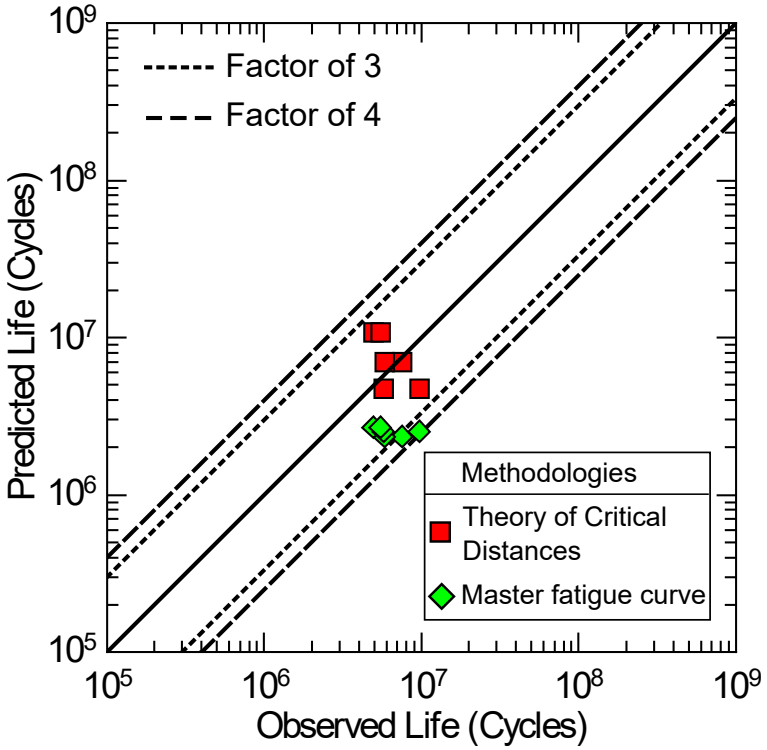

Figure 4.8: Observed vs. predicted lives for fretting fatigue tests on AA6201-T81 wires under variable amplitude loading.

The results in Fig. 4.8 suggest that the two methodologies are promising tools for durability analysis of wires subjected to fretting fatigue and variable amplitude loading. Note that both methodologies were capable to predict fatigue lives reasonably well despite all the influencing factors of the problem (such as plasticity, wear, and loading sequence) and the simplifications made in the formulations. The approach based on a master fatigue curve is easier to implement since it does not require an FE-based stress analysis of the wires in contact. However, fretting fatigue test data of wires are necessary to calibrate the master curve, which in turn requires an experimental apparatus such as that in Fig. 4.1. On the other hand, the methodology based on the Theory of Critical Distances needs a refined FE-mesh in the contact zone, but is calibrated using axial fatigue test data of smooth and notched wires, which can be obtained from conventional servo-hydraulic testing machines.

4.5 Conclusions

Two previously developed methodologies (Rocha et al., 2019, 2022) for life prediction of wires under fretting fatigue were extended to variable amplitude loading conditions. These predictive tools are based on a master fatigue curve and on the Theory of Critical Distances. To evaluate these methodologies, fretting fatigue tests were performed on AA6201-T81 wires using three-block loading histories. Vibration data from an operating transmission line were considered for the definition of the test parameters. Both methodologies had an acceptable level of accuracy for engineering calculations, providing life estimates within a factor of 4 of the measured lives. These results indicate that the two methodologies can be useful tools for fatigue analysis of wires of overhead conductors. One major feature of the methodology based on a master fatigue curve is that it does not require an FE-based stress analysis of the wires in contact. An advantage of the methodology based on the Theory of Critical Distances is that it can be calibrated using data from simple axial fatigue tests on smooth and notched wires.

5 Fatigue life prediction of ACSR Ibis conductor under high-low and low-high loading sequences using a finite element 3D model

This chapter is a reproduction of the following publication:

> Matos IM, Lalonde S, Araújo JA, Castro FC. Fatigue life prediction of ACSR Ibis conductor under high-low and low-high loading sequences using a finite element 3D model. Submitted to International Journal of Fatigue.

5.1 Introduction

Overhead conductors used in transmission lines are exposed to oscillatory motions caused by the wind, which can lead to the fatigue failure of their wires. The failures typically take place near devices that restrict the movement of the conductor, such as suspension clamps. At these critical regions, fretting fatigue can occur at the contact zones of the wires, leading to crack initiation and eventually to wire rupture (Azevedo et al., 2009; Cosmai et al., 2017). To monitor the conductor oscillations, power utilities generally use a vibration recorder attached to the conductor or to the suspension clamp. The vibration data recorded by these devices can then be used to assess the risk of conductor fatigue failure and to estimate its remaining lifetime. Vibration measurements from operating transmission lines have shown that the conductor is usually subjected to oscillations of varying amplitudes, which often follow beat patterns, as reported in (Rawlins and Harvey, 1959; Edwards and Boyd, 1963; Cosmai et al., 2017). Such variations can be caused by several factors related to the environment and to the hardware installed on the line. For example, the wind speed and direction can change during the day or throughout the year, the conductor's tension force can be modified by temperature variations,

the landscape can be affected by snow and ice, and dampers can be installed on the line or have their arrangement modified (Brunair et al., 1988; CIGRÉ, 1995).

The most common approach used to investigate the fatigue behavior of conductors is to perform fatigue tests using resonant test benches. In these tests, the conductor is usually supported by a suspension clamp and is subjected to cyclic vertical displacement that is used to represent the aeolian vibrations. The standard test procedure can be found in (IEC, 2015) and examples of investigations performed on resonant test benches can be found in (Azevedo et al., 2009; Lévesque et al., 2010; Kubelwa et al., 2017; Araújo et al., 2022). Although significant progress has been made in understanding the fatigue failure of the conductor and its influencing factors, most studies have been performed using constant amplitude loading (CAL) and few have tried to reproduce more realistic loading conditions. To represent the amplitude variations typical of the aeolian vibrations, some studies have considered the use of loading blocks (CIGRÉ, 1979; Ramey and Silva, 1981; Brunair et al., 1988; Murça, 2011), while others adopted random loading spectra (Goudreau et al., 2005; Ferreira et al., 2023). These studies have shown that life estimates of conductors under variable amplitude loading (VAL) based on Miner's rule agreed well (within factor of 3 boundaries) with the test data. Moreover, the use of time and frequency domain approaches provided life estimates with similar accuracy.

Nowadays, fatigue testing of conductors is still a widely used approach for the design and maintenance of transmission lines. However, this type of test can be expensive, time consuming, and dependent on the availability of a resonant test bench. As a result, recent studies (Said et al., 2020a, 2023; Omrani et al., 2021; Rocha et al., 2022, 2023) have aimed to develop alternative approaches to predict the durability of conductor-clamp systems that require simpler and less expensive laboratory infrastructure. These new approaches benefit from recent advancements in finite element (FE) 3D modeling of conductor-clamp systems (Frigerio et al., 2016; Baumann and Novak, 2017; Lalonde et al., 2017a, 2017b, 2018), since the FE models are capable to calculate loading conditions at the local (wire) scale. These loading conditions are then employed into a local-scale fatigue damage analysis of the wires. To perform this local-scale analysis, some studies (Rocha et al., 2019; Said et al., 2020a, 2023; Araújo et al., 2020, 2022, 2023; Matos et al., 2020, 2022) have proposed the use of FE simulations of wires under fretting

fatigue. These simulations are used to evaluate a multiaxial fatigue parameter below the contact surface, which is associated with the life of the wire. In (Omrani et al., 2021), the local-scale analysis relies on performing a fretting fatigue test on a wire specimen, and associating the measured life with the failure of the conductor-clamp system. Rocha et al. (2022, 2023), proposed an approach for the local-scale analysis based on master fatigue curves, which are defined using test data of wires under plain and fretting fatigue. These master curves are used to associate the local loading conditions with the lives of the conductor's wires. The approach proposed in (Rocha et al., 2022, 2023) is remarkable due to its simplicity, since it does not require any FE-based stress analysis of the wires in contact. Although the results of these studies have indicated that the proposed methodologies are promising tools for the safe design of transmission lines, it should be noted that all of these analyses were limited to CAL conditions.

Regarding the local-scale fatigue damage analysis, a previous study by the authors (Matos et al., 2023) investigated the applicability of life prediction methodologies for wires under fretting fatigue and VAL. The study proposed to extend two previously developed methodologies (Rocha et al. 2019, 2022) to VAL conditions: one based on the Theory of the Critical Distances and the other on a master fatigue curve. To evaluate the methodologies, fretting fatigue tests were performed on 6201-T81 aluminum alloy wires subjected to a three-block loading history. Most of the lives predicted from the methodologies were within factors of 4 of those measured in the fretting fatigue tests. The accuracy obtained from these predictive tools motivates a more in-depth evaluation of how they could be applied to the life prediction of conductor-clamp systems under VAL, using a two-scale approach such as those employed in (Said et al., 2020a, 2023; Omrani et al., 2021; Rocha et al., 2022, 2023).

In this study, the life prediction approach proposed by Rocha et al. (2022, 2023) is extended to account for VAL conditions. The methodology is evaluated considering fatigue test data from two studies performed on an ACSR (Aluminum Conductor Steel Reinforced) Ibis 397.5 MCM conductor (Murça, 2011; Fadel et al., 2012). The tests in (Fadel et al., 2012) were carried out under CAL, while those in (Murça, 2011) were under VAL. Therefore, the proposed methodology will be first applied to the CAL fatigue test results to ensure it provides life estimates for the ACSR Ibis conductor with an accuracy similar to that obtained in previous studies with

ACSR Tern and AAAC 900 MCM conductors (Rocha et al., 2022, 2023). Then, the application of the methodology will be extended to VAL conditions by comparison to the test results in (Murça, 2011) in order to access if it still provides accurate life estimates.

5.2 Fatigue test data of ACSR Ibis conductors

This section describes the fatigue tests performed in (Murça, 2011; Fadel et al., 2012) on an ACSR Ibis conductor. The test data will be used to evaluate the life prediction methodology detailed in Section 5.3. The ACSR is a conductor composed of steel and aluminum wires. Its design dates back to 1907, when most conductors were made of only copper or aluminum wires. The desire for conductors with higher strength-to-weight ratio led to the development of the ACSR, a conductor that combines the light weight and high electrical conductivity of its aluminum wires with the high mechanical resistance of its steel wires. These characteristics led to the gradual replacement of copper and aluminum conductors with ACSR conductors, starting in Germany in 1920 and quickly spreading to other countries over the next decade (Kiessling et al., 2003). Nowadays, the ACSR is still one of the most widely used type of conductors (Lequien et al., 2021; Zhang et al., 2020).

The geometric and mechanical characteristics of the ACSR Ibis conductor are listed in Table 5.1. This conductor is composed of a core and one layer of steel wires, and two layers of 1350-H19 aluminum alloy (AA) wires. The AA1350 is characterized by its high electrical conductivity (approximately 62% of that of copper) and low density. These properties have favored the use of AA1350 wires in ACSR conductors since the early 20th century, and it remains the primary alloy used in overhead lines today (Sanders and Staley, 2019). The suspension clamp used in the tests was made of A413.0 aluminum alloy. This material has high corrosion resistance and excellent castability, which allow this alloy to be used in various applications that require complex shapes and thin-walled castings (Anderson et al., 2019). Details about the geometry and dimensions of the clamp can be found in (Rocha et al., 2022).

Table 5.1: Geometric characteristics of the ACSR Ibis 397.5 MCM conductor.

Layer	Material	n	d (mm)	l (°)	E (GPa)	ν
Core	Steel	1	2.44	-	207	0.3
1	Steel	6	2.44	6.2	207	0.3
2	AA1350-H19	10	3.14	10.1	69	0.33
3	AA1350-H19	16	3.14	13.9	69	0.33

n = number of wires; d = wire diameter; l = lay angle; E = Young's modulus; ν = Poisson's ratio.

Fig. 5.1 shows the resonant test rig and the loading histories applied in the tests. The test procedures followed the guidelines provided in (CIGRÉ, 2010; IEC, 2015). During the experimental setup, the conductor was assembled to the suspension clamp, which was attached to a metallic cradle. The cradle was adjusted to have angle of 10° between the clamp and the horizontal position of the conductor, so as to represent the sag angle in a transmission line. Dead blocks and a winch were used to apply a tension force of $T = 14.5$ kN to the conductor, and a torque of 50 N·m was applied the bolts of the clamp, resulting in a clamping force of $F_{\text{c}} = 59$ kN. The cyclic vertical displacement of the conductor was applied by an electrodynamic shaker, which operated in conjunction with an accelerometer positioned 89 mm from the last point of contact (LPC) between the conductor and clamp. The shaker and accelerometer were connected to a closed-loop system designed to control the bending displacement, i.e., the vertical displacement of the conductor at the position where the accelerometer was installed.

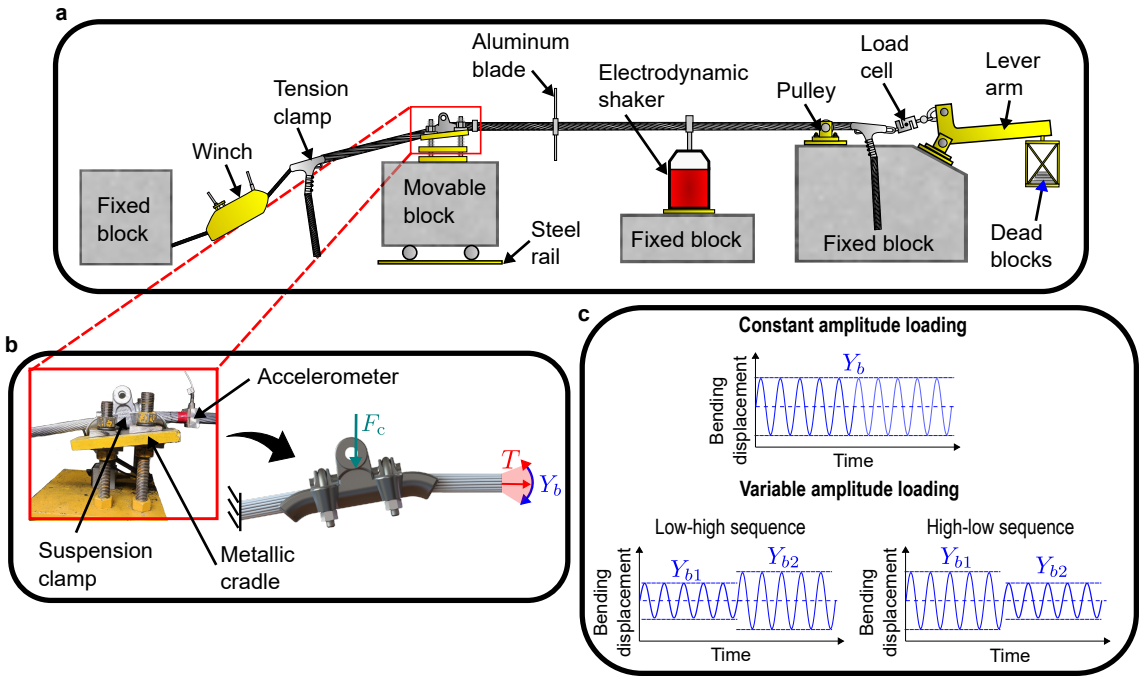

Figure 5.1: Schematic of the (a) fatigue test bench, (b) applied loads, and (c) loading histories.

The loading histories used in the fatigue tests are shown in Fig. 5.1c. The tests were performed by controlling the bending displacement amplitude Y_b of the conductor, which corresponds to the vertical displacement amplitude (peak-to-valley) of the conductor measured at 89 mm from the LPC. In (Fadel et al., 2012), the Y_b was kept constant during each test, and the tests were stopped after three wire breaks or at least 3×10^6 loading cycles without a wire break. On the other hand, the tests in (Murça, 2011) followed a block loading program with low-high and high-low sequences. In these tests, the initial level of bending displacement amplitude Y_{b1} was applied until a predetermined number of cycles was reached. The amplitude was then increased (low-high test) or reduced (high-low test) to a second level Y_{b2}, which was kept constant for the rest of the test. These tests were stopped after one wire break or at least 2×10^6 loading cycles without a wire break.

Table 5.2 summarizes the loading conditions applied in the CAL tests and the number of cycles to the rupture of the first, second, and third wires. The test program consisted in a total of 16 tests under five different levels of bending displacement amplitude Y_b, with at least two replicate tests for each level. The bending displacement amplitude vs. fatigue life data points are shown in Fig. 5.2. Note that the slopes of the Y_b vs. N_f curves for the first three wire breaks

are approximately identical, which indicates that these wire breaks are equally affected by the bending displacement amplitude applied in the test.

Table 5.2: Loading conditions and lives of the tests on ACSR Ibis conductors under constant amplitude loading.

Test ID	Y_{b} (mm)	$N_{\mathrm{f1st}} \times 10^6$ (cycle)	$N_{\mathrm{f2nd}} \times 10^6$ (cycle)	$N_{\mathrm{f3rd}} \times 10^6$ (cycle)
C01	1.38	0.42	1.05	1.19
C02	1.38	0.65	0.73	1.05
C03	1.27	0.99	1.47	1.64
C04	1.27	1.01	1.42	2.31
C05	1.10	0.98	2.45	2.49
C06	1.10	1.77	2.46	3.15
C07	1.10	0.64	1.07	1.84
C08	1.00	3.10	>3.90	>3.90
C09	1.00	1.24	3.51	3.71
C10	1.00	3.57	5.81	7.30
C11	1.00	1.36	2.73	5.74
C12	1.00	3.10	4.30	7.10
C13	0.90	5.00	>5.00	>5.00
C14	0.90	2.98	6.34	>9.03
C15	0.90	3.00	3.42	4.50
C16	0.90	1.90	7.44	9.10

Y_{b} = bending displacement amplitude; $N_{\mathrm{f1st}}, N_{\mathrm{f2nd}}, N_{\mathrm{f3rd}}$ = number of cycles to 1st, 2nd, and 3rd wire breaks.

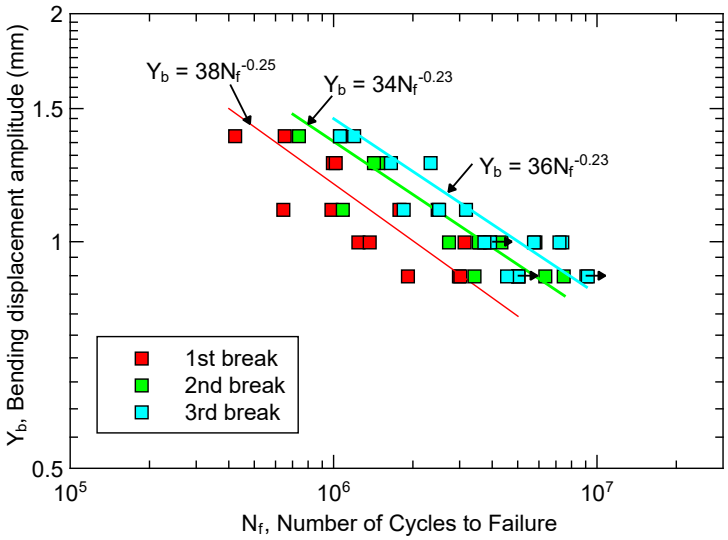

Figure 5.2: Bending displacement amplitude vs life data of the fatigue tests on ACSR Ibis conductor under constant amplitude loading.

Table 5.3 lists the loading conditions and the number of cycles to the first wire break of the VAL tests. A total of 14 tests were performed, with nine under a high-low sequence, and five under a low-high sequence. Note that several tests (for instance, tests V01 to V05) were performed under the same bending displacement amplitudes Y_{b1} and Y_{b2}, but with distinct numbers of cycles N_1 applied during the first loading block. The goal was to evaluate the effect of the damage produced during the first loading block on the failure of the conductor. It was observed that the lives of the tests are affected by the damage produced during the first block, and that this effect is more significant for the tests under high-low sequence. For instance, the life of the test V05 was more than five times longer than the life of the test V01.

Table 5.3: Loading conditions and lives of the tests on ACSR Ibis conductors under variable amplitude loading.

Test ID	Load sequence	Y_{b1} (mm)	Y_{b2} (mm)	$N_1 \times 10^6$ (cycle)	$N_{f1st} \times 10^6$ (cycle)
V01	High-low	1.39	0.90	0.37	0.77
V02	High-low	1.39	0.90	0.27	>4.27
V03	High-low	1.39	0.90	0.11	1.91
V04	High-low	1.39	0.90	0.11	>2.79
V05	High-low	1.39	0.90	0.11	>5.11
V06	High-low	1.27	1.00	0.70	2.15
V07	High-low	1.27	1.00	0.50	>2.05
V08	High-low	1.27	1.00	0.50	5.00
V09	High-low	1.27	1.00	0.20	3.30
V10	Low-high	0.90	1.39	2.20	2.35
V11	Low-high	0.90	1.39	1.50	1.52
V12	Low-high	0.90	1.39	0.85	0.99
V13	Low-high	1.00	1.27	1.55	1.57
V14	Low-high	1.00	1.27	0.62	0.93

Y_{b1}, Y_{b2} = bending displacement amplitudes of the 1s and 2nd blocks; N_1 = number of cycles applied in the 1st block, N_{f1st} = number of cycles to 1st wire break.

5.3 Methodology for life prediction of overhead conductors under variable amplitude loading

A methodology for life prediction of conductors subjected to constant amplitude loading (CAL) was proposed by Rocha et al. (2022). The methodology combines (i) a finite element (FE) three-dimensional model of the conductor-clamp system with (ii) two master fatigue curves defined using test data of wires under plain and fretting fatigue. The FE model is used to estimate the axial stresses along the conductor's wires for a given loading condition. The axial stresses are then used to calculate a fatigue parameter. Finally, the master curves are used to associate the fatigue parameter with the number of loading cycles that will cause the rupture of a specific number of wires (usually 10% of the conductor's wires). The methodology was evaluated in (Rocha et al., 2022, 2023) using fatigue test data of AAAC 900 MCM and ACSR Tern

conductors, showing that most of the predicted lives were within factors of 3 of the measured lives. These results have motivated us to extend the methodology proposed in (Rocha et al., 2022) to account for variable amplitude loading (VAL) conditions, as detailed in this section.

A schematic of the life prediction methodology is presented in Fig. 5.3. The input data for this approach consist of the loading conditions applied to the conductor-clamp system, and test data of wires under plain and fretting fatigue. These test data are used to define two master fatigue curves that relate a fatigue parameter with the number of loading cycles to wire rupture. A combination of the master curves with the rainflow method and Miner's rule is used to assess the fatigue damage fraction ΔD along the conductor's wires. A wire rupture is predicted to occur when the damage fraction in a wire reaches a critical value D_{c}. Details about this approach are described as follows.

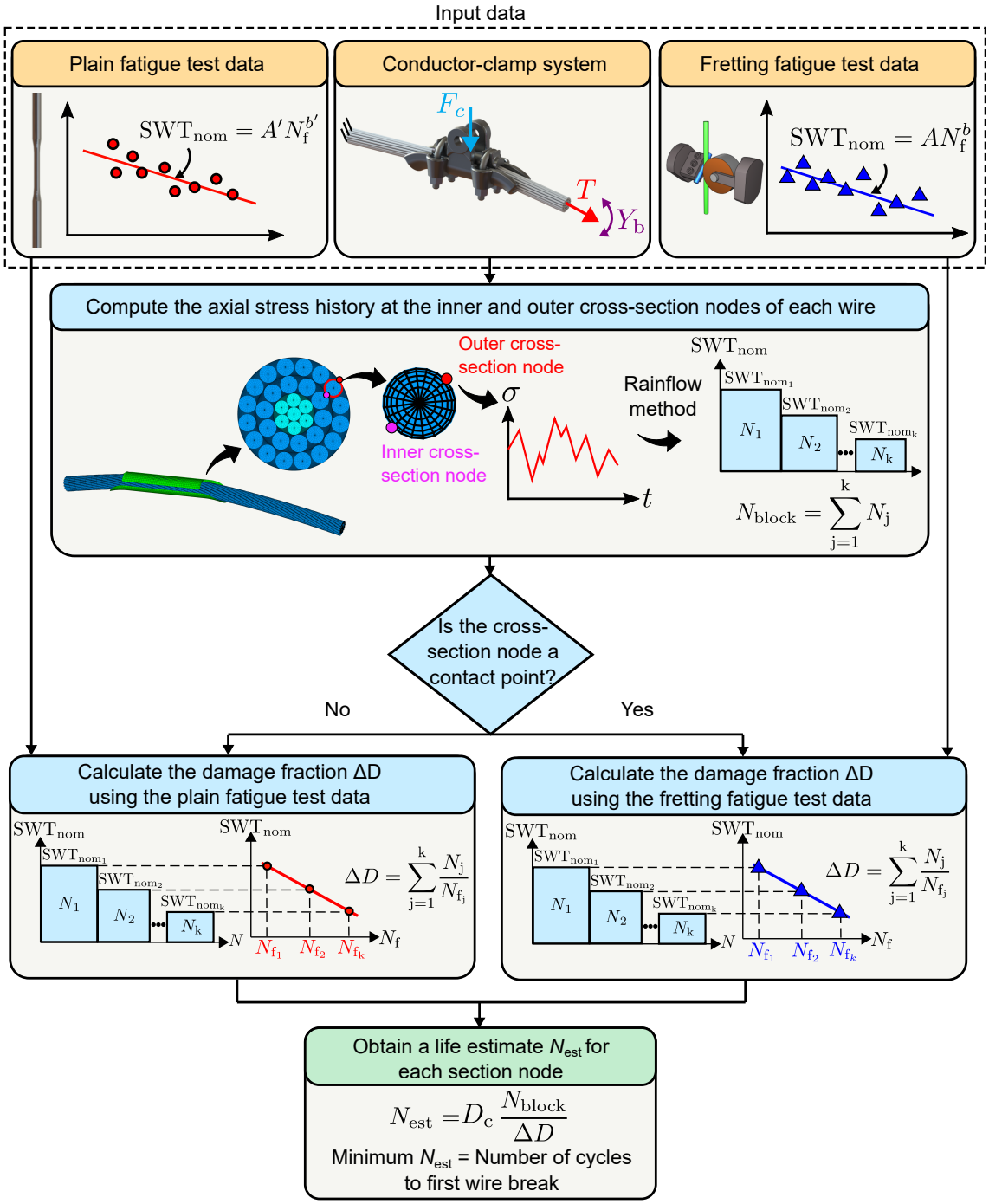

Figure 5.3: Schematic of the life prediction methodology for conductors under variable amplitude loading.

The FE model of the conductor-clamp system is shown in Fig. 5.4a. The model was proposed by Lalonde et al. (2017a, 2017b, 2018), and is adapted in this work to represent the ACSR Ibis conductor and the clamp used in the fatigue tests described in Section 5.2. A conductor's length of 1600 mm was considered and each wire was modeled using quadratic beam elements with three nodes and an element size of 10 mm. For the keeper and the clamp body, quadratic

rigid surface elements with an element size of 2.5 mm were used. The penalty formulation was employed to describe the contact interactions between wires of the same or of adjacent layers, and between wires of the external layer with the clamp. A friction coefficient of 0.3 was chosen for the steel-steel and steel-aluminum contact interactions, while a coefficient of 0.9 was adopted for the aluminum-aluminum interaction. Note that several studies (Baumann and Novak, 2017; Lalonde et al., 2017a, 2017b, 2018; Said et al., 2020; Rocha et al., 2022, 2023) have used the same or similar friction coefficient values to describe the contact interactions in FE simulations of overhead conductors.

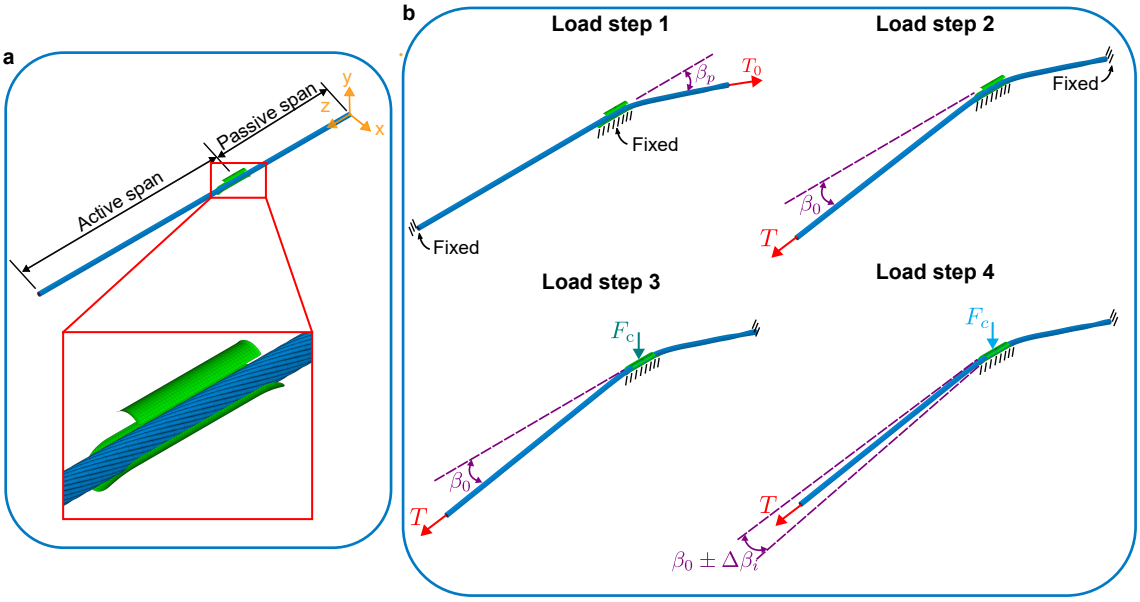

Figure 5.4: (a) Finite element model of the conductor-clamp system and (b) boundary conditions.

The linear elastic behavior of the steel and AA1350-H19 wires was defined using the mechanical properties listed in Table 5.1. In addition, an elastic-perfectly plastic behavior was defined for the AA1350-H19 wires using a yield stress of $\sigma_y = 165$ MPa. This value is typically found in the literature for this material (Aluminum Association, 1989; Anderson et al., 2019) and is the same value that was previously adopted in (Rocha et al., 2023) for their FE-based stress analyses of the ACSR Tern conductor. Thus, the use of this value facilitates a comparison between the results obtained in (Rocha et al., 2023) and those of the current research.

The conductor static loading is applied within three load steps in the FE simulations, as illustrated in Fig. 5.4b. In load step 1, the clamp body and the active end of the conductor are

fixed in place. Then a tension force $T_0 = 3.6$ kN is applied to the passive end of the conductor at an angle $\beta_{\text{p}} = 18°$. In load step 2, the passive end of the conductor is fixed in place and a tension force $T = 14.5$ kN is applied to the active end of the conductor at an angle $\beta_0 = 10°$. In load step 3, the keeper is moved in the negative direction of the y-axis until it comes into contact with the conductor. A clamping force $F_{\text{c}} = 59$ kN is then applied to the center of the keeper. Finally, the cyclic loading is applied in load step 4 by varying the angle β_0 at which the tension force T is applied by $\pm\Delta\beta$. Based on preliminary simulations, an association is made between the angle variation $\Delta\beta$ and the bending displacement amplitude Y_{b} of the conductor. Note that in the simulations of the CAL tests, a single $\Delta\beta$ value is used and two loading cycles are simulated. On the other hand, the simulations for the VAL test are performed by using two $\Delta\beta$ values and by simulating two loading cycles for each amplitude.

The FE simulations were used to determine the axial stress history along the AA1350-H19 wires of the ACSR Ibis conductor. After an FE simulation, the loading history is extracted from the inner and outer cross-section nodes (refer to Fig. 5.3) of each beam element that is used to model the AA1350 wires. The inner and outer cross-section nodes are identified as the nodes that are as close as possible to the contact points between wires of adjacent layers or between wires of the outermost layer with the clamp. Note that in the fatigue tests performed in (Murça, 2011; Fadel et al., 2012), all wire breaks occurred due to the initiation and propagation of cracks from the fretting marks of the AA1350 wires. Thus, the fatigue damage analyses in the present study are carried out considering only the layers composed of AA1350 wires.

For conductors subjected to variable amplitude loading, the axial stress history in the wires may be irregular, requiring the use of a cycle counting method to assess the fatigue damage. In this work, the rainflow method is considered to reduce the axial stress history into an equivalent loading block composed of k different stress levels of constant amplitude. Each level is associated with a stress pair $(\sigma_{\text{ax}}, \sigma_{\text{max}})$, where σ_{ax} is the axial stress amplitude, and σ_{max} is the maximum axial stress. The number of cycles in one loading block N_{block} is calculated as

$$N_{\text{block}} = \sum_{j=1}^{k} N_j \tag{5.1}$$

where N_j is the number of cycles counted for a given stress level $(\sigma_{\text{ax}}, \sigma_{\text{max}})$. The fatigue damage produced in each stress level is determined using a stress-based form of the Smith–Watson–Topper (SWT_{nom}) fatigue parameter, which can be expressed as

$$\text{SWT}_{\text{nom}} = \sqrt{\sigma_{\text{ax}} \langle \sigma_{\text{max}} \rangle} \tag{5.2}$$

Note that, by using the Macaulay brackets $\langle\rangle$, the SWT_{nom} parameter becomes zero for negative maximum stresses and thus, the criterion predicts no failure.

After counting the loading cycles using the rainflow method and associating the identified stress levels with the SWT_{nom} parameter, it is possible to estimate the fatigue damage fraction ΔD produced by one loading block using Miner's damage rule, which can be expressed by

$$\Delta D = \sum_{j=1}^{k} \frac{N_j}{N_{\text{f}_j}} \tag{5.3}$$

where N_{f_j} is the number of cycles to failure for a given stress level $(\sigma_{\text{ax}}, \sigma_{\text{max}})$. Two master fatigue curves are used to associate the SWT_{nom} parameter in each stress level with its corresponding number of cycles to failure N_{f}. One of the master curves is defined using test data of wires under fretting fatigue, which are fitted by the power law function $\text{SWT}_{\text{nom}} = AN_{\text{f}}^{b}$. This curve is used to evaluate the inner and outer cross-section nodes that represent contact points between a wire with the clamp or with another wire. The other master curve is defined in a similar manner, using test data of wires under plain fatigue and fitting the data by the power law function $\text{SWT}_{\text{nom}} = A' N_{\text{f}}^{b'}$. This curve is used to evaluate the outer cross-section nodes of the wires of the outermost layer that are not in contact with the clamp. Note that different fitting constants are assumed for each power law relation since aluminum alloy wires typically display higher resistance under plain fatigue than under fretting fatigue (Matos et al., 2022; Rocha et al., 2023).

After defining the fatigue damage fraction ΔD produced by the axial loading history, the estimated fatigue life N_{est} can be obtained using

$$N_{\text{est}} = D_{\text{c}} \frac{N_{\text{block}}}{\Delta D} \tag{5.4}$$

where D_{c} is the critical damage. Generally, the critical damage is assumed to be $D_{\text{c}} = 1$ or is determined from VAL tests carried out until the material rupture. The critical damage is defined from these tests as the fatigue damage fraction ΔD produced until the material's rupture, calculated using Eq. (5.3). Note that, by using Eqs. (5.1) to (5.4), a fatigue life estimate N_{est} will be obtained for each inner and outer cross-section node of the beam elements that are used to model the AA1350-H19 wires of the conductor. The shortest life estimate corresponds to the number of loading cycles that lead to the first wire rupture, the second shortest life to the number of cycles for the second wire rupture and so on.

5.4 Results and discussion

In this section, the life prediction methodology will be evaluated using the fatigue test data of ACSR Ibis conductors presented in Section 5.2. Firstly, the methodology will be validated by comparing the predicted and measured lives of the tests under constant amplitude loading. The approach will then be evaluated for its ability to predict the lives, the loading sequence effects, and the wire break locations for the tests under variable amplitude loading.

5.4.1 Life prediction under constant amplitude loading

The life prediction methodology described in Section 5.3 relies on the use of master fatigue curves to evaluate the axial stresses on the conductor's wires. The following analyses consider two fatigue curves, which were obtained in a previous study by part of the authors (Rocha et al., 2023) and are presented here for completeness. These curves were defined by correlating the lives of fatigue tests on AA1350-H19 wires with a nominal stress-based version of the Smith–Watson–Topper (SWT_{nom}) parameter. The data in Fig. 5.5a were obtained from fully reversed axial fatigue tests performed in (Rocha et al., 2019) using plain wire specimens, and were fitted by the power-law relation $\text{SWT}_{\text{nom}} = 221 N_{\text{f}}^{-0.07}$. This relation will be used to

estimate the fatigue damage at the outer cross-section nodes of wires of the external layer of the conductor which are not in contact with the clamp. Fig. 5.5b shows the data from fretting fatigue tests performed in (Rocha et al., 2019; Omrani et al., 2021) using wires under wire-wire and wire-clamp contact configurations. These data were fitted by the power-law relation $\mathrm{SWT}_{\mathrm{nom}} = 815N_{\mathrm{f}}^{-0.18}$, which will be used to evaluate the damage at outer and inner cross-section nodes of wires of the two outermost layers of the conductor that are in contact, either with another wire or with the clamp.

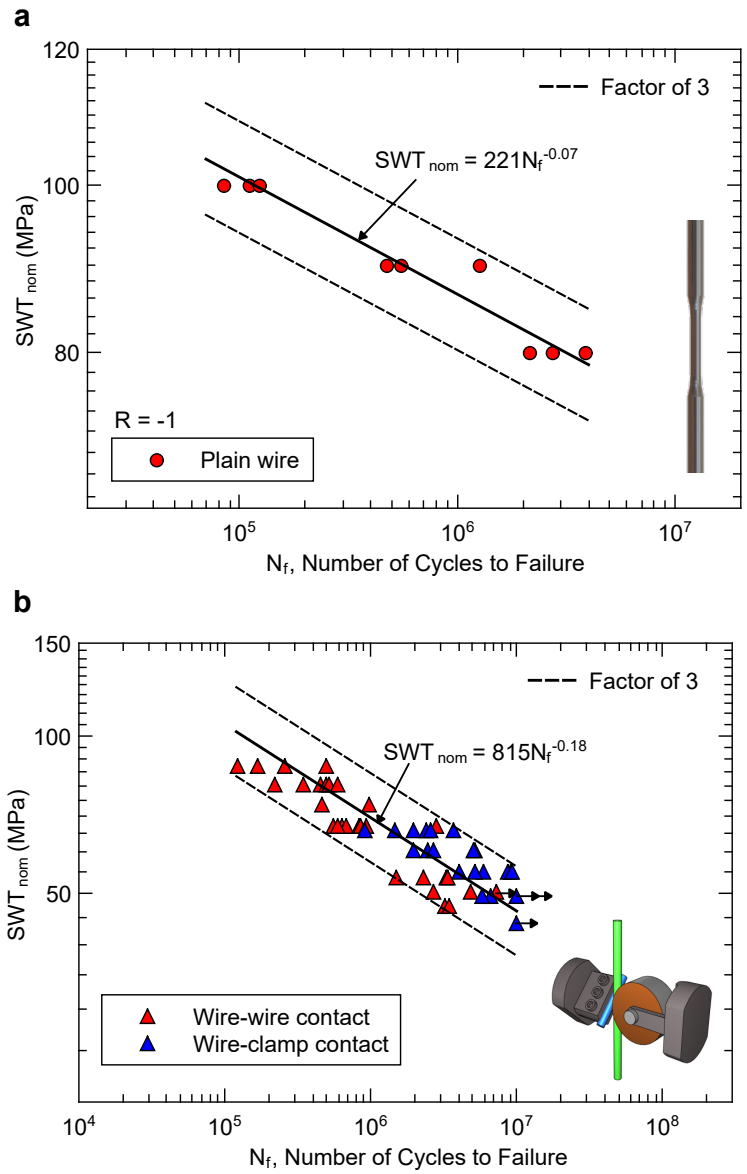

Figure 5.5: $\mathrm{SWT}_{\mathrm{nom}}$ parameter vs. fatigue life for AA1350-H19 wires under (a) plain fatigue and (b) fretting fatigue.

After defining the constants of the $\mathrm{SWT}_{\mathrm{nom}}$-$N_{\mathrm{f}}$ relations, the lives of the fatigue tests

on ACSR Ibis conductors under constant amplitude loading (CAL) were predicted using the methodology summarized in Fig. 5.3. For CAL conditions, the loading history of any inner or outer cross-section nodes of the wires is composed of a single stress level $\mathrm{SWT}_{\mathrm{nom}}$ applied during $N_{\mathrm{block}} = 1$ cycle, and the critical damage is $D_{\mathrm{c}} = 1$. Thus, the estimated life of a node is $N_{\mathrm{est}} = N_{\mathrm{f}}$, where N_{f} is the number of cycles to failure for a given stress level $\mathrm{SWT}_{\mathrm{nom}}$ obtained from one of the $\mathrm{SWT}_{\mathrm{nom}}$-$N_{\mathrm{f}}$ relations. The three shortest life estimates N_{est} correspond to the number of cycles to the rupture of the first three wires.

Fig. 5.6 shows a comparison between the predicted and measured lives of the CAL fatigue tests on the ACSR Ibis conductor. It can be seen that the methodology was able to predict the number of cycles for the first three wire breaks of the conductor in good agreement with the experimental data, with most predictions being within factors of 3 of the observed lives. Note that the data points are scattered along the line of perfect correlation (solid diagonal line), which indicates that the methodology can accurately take into account the effect of the bending displacement amplitude applied to the conductor on its fatigue life. The lives predicted in this work had an accuracy similar to that obtained in previous studies (Rocha et al., 2022, 2023), in which the methodology was applied to CAL fatigue test data of an ACSR Tern and an AAAC 900 MCM conductors. Like the ACSR Ibis, the ACSR Tern is also composed of AA1350 wires, but the conductor has a different geometry. Meanwhile, the wires of the AAAC 900 MCM conductor are manufactured using a different material, the AA6201. The results obtained for these three conductors show that the methodology can provide accurate life predictions for different conductor geometries and wire materials.

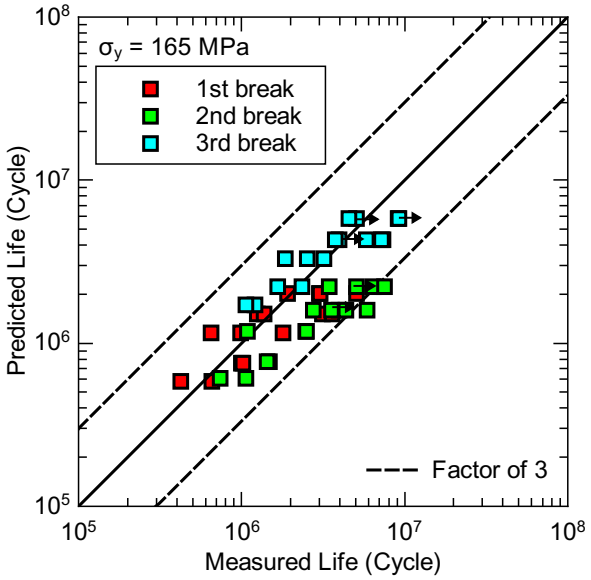

Figure 5.6: Predicted vs. measured lives for the fatigue tests on ACSR Ibis conductors under constant amplitude loading, considering a yield stress of 165 MPa.

5.4.2 Life prediction under variable amplitude loading

The use of the life prediction methodology for VAL conditions relies on the definition of the master fatigue curves SWT_{nom}-N_{f}, and the critical damage D_{c}. For the former, the same curves previously adopted in Section 5.4.1 for the CAL fatigue analyses will be employed here. As for the critical damage, a value of $D_{\text{c}} = 1$ is used in this study, following the guidelines provided by CIGRÉ (1979). These guidelines were proposed by a study committee organized by CIGRÉ (1979), who performed a series of VAL fatigue tests on AlMgSi conductors and evaluated the applicability of Miner's rule to fatigue damage analyses of conductors. The committee concluded that the critical damage should be lower than 1.5, and recommended the use of $D_{\text{c}} = 1$. Additionally, Matos et al. (2023) have shown that it is possible to obtain satisfactory life estimates for AA6201-T81 wires under fretting fatigue and VAL by employing Miner's rule with a critical damage $D_{\text{c}} = 1$, which motivates the use of the same value in the present study.

After defining the master fatigue curves and the critical damage, the lives of the tests on ACSR Ibis conductors under VAL were predicted, considering failure as the first wire break. A comparison between the predicted and measured lives is shown in Fig. 5.7. Most predictions were within factors of 3 of the measured lives for both high-low and low-high loading sequen-

ces, which is a similar accuracy to that obtained in Section 5.4.1 for the CAL tests. These results suggest that the methodology can be extended to VAL conditions and still provide life predictions with sufficient accuracy for engineering calculations.

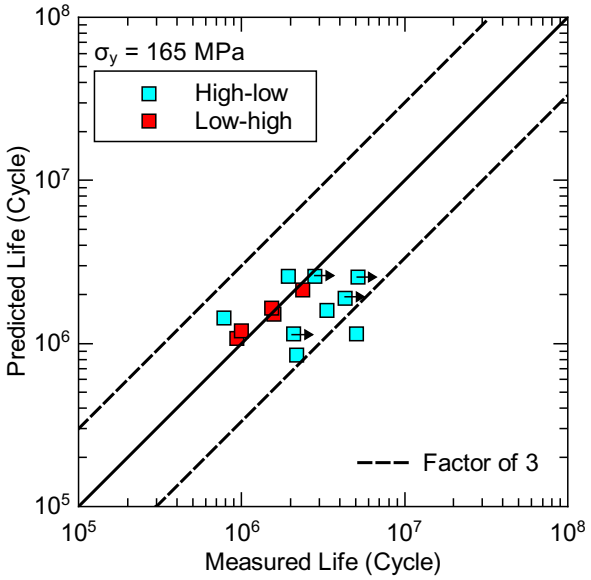

Figure 5.7: Predicted vs. measured lives for the fatigue tests on ACSR Ibis conductors under variable amplitude loading, considering a yield stress of 165 MPa.

5.4.3 Material yield stress and loading sequence effects

An important factor to consider in VAL tests is the effect of the loading sequence on fatigue failure. For the VAL tests performed in (Murça, 2011), the lives of the tests under high-low sequence were about two times longer than those under low-high sequence. In this regard, the methodology used in this study was able to take this effect into account, providing longer life estimates for the tests with high-low sequence than for the tests with low-high sequence. However, the difference between the predicted lives for the high-low and low-high tests was approximately 13%, significantly less than observed experimentally. In an attempt to improve the prediction of the loading sequence effect on the conductor's failure, new FE simulations were performed considering a yield stress of 141 MPa for the AA1350-H19 wires. This yield stress was defined from the stress-strain curve shown in Fig. 5.8, which was obtained from a tension test performed by (Wang et al., 2008) using a smooth wire specimen with a diameter of 4.57 mm in the gauge section. It is noted that the yield stress obtained by (Wang et al., 2008) is

slightly lower than the values of 160–165 MPa generally reported for this material (Aluminum Association, 1989; Anderson et al., 2019).

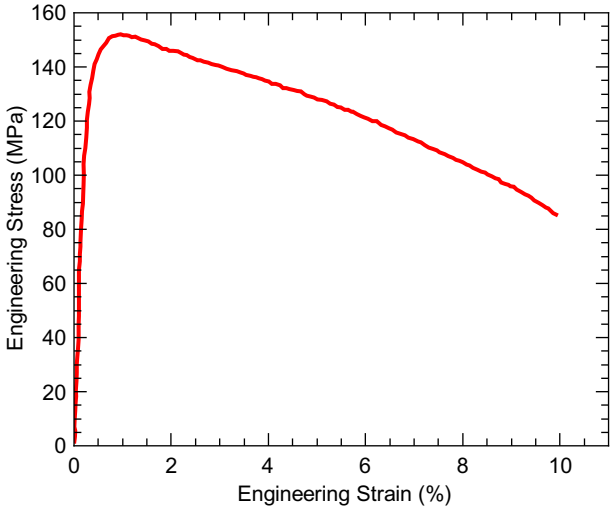

Figure 5.8: Monotonic tension curve of the AA1350-H19. Adapted from (Wang et al., 2008).

As a first step in evaluating the effect of the yield stress on the fatigue failure of the conductor, new life predictions were obtained for the CAL tests using the yield stress of 141 MPa as an input into the FE simulations. A comparison between the predicted and measured lives is shown in Fig. 5.9. Most of the predicted lives were within factors of 3 of the measured lives, which is an accuracy similar to that obtained for a yield stress of 165 MPa (refer to Fig. 5.6). These results indicate that either yield stress value can be used for the fatigue damage analysis of ACSR Ibis conductors under CAL conditions. It should be mentioned that the lives predicted using a yield stress of $\sigma_y = 141$ MPa were about 60% longer than those predicted by the model with $\sigma_y = 165$ MPa. Note that in the fatigue critical region, the wires undergo plastic deformation and, since an elastic-perfectly plastic material model was used, the maximum axial stresses in the wires were equal to the yield stress. Therefore, the maximum axial stresses in the wires were lower for the FE simulations performed with $\sigma_y = 141$ MPa than for those with $\sigma_y = 165$ MPa. As a result, the SWT_{nom} fatigue parameters were also lower, resulting in longer life predictions.

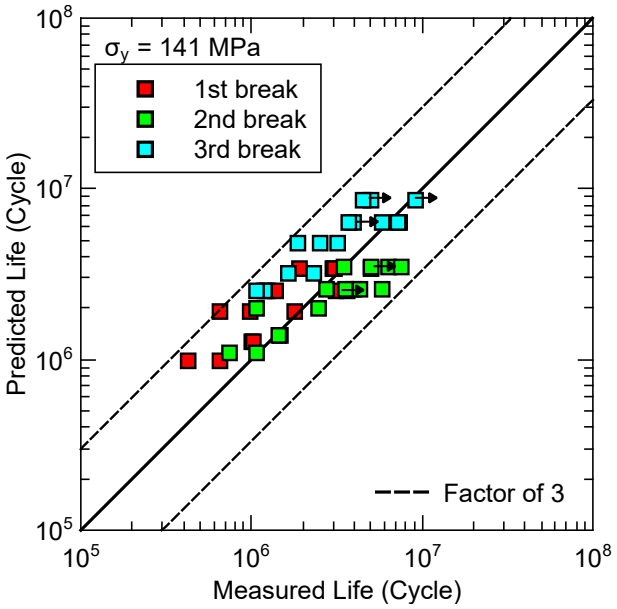

Figure 5.9: Predicted vs. measured lives for the fatigue tests on ACSR Ibis conductors under constant amplitude loading, considering a yield stress of 141 MPa.

The results shown in Figs. 5.6 and 5.9 indicate that the life predictions for the CAL tests are affected by the yield stress that is used as an input to the FE simulations. This motivates a further evaluation of the yield stress effect for the VAL tests. To this end, new FE simulations of the VAL tests were performed using a yield stress of $\sigma_y = 141$ MPa for the AA1350 wires. Fig. 10 shows a comparison between the predicted and measured lives. It can be seen that most of the predicted lives are within factors of 3 of the measured lives, which is similar to the accuracy obtained when a yield stress of $\sigma_y = 165$ MPa was used (refer to Fig. 5.7). It is also noted that the FE simulations with $\sigma_y = 141$ MPa provided longer life predictions and a more accurate representation of the loading sequence effect on the fatigue failure of the conductor. In general, the predicted lives for the high-low sequence tests were approximately 70% longer than for the low-high tests, which is in better agreement with the test data than the predictions obtained with $\sigma_y = 165$ MPa. For this reason, the following analyses will be performed considering only the simulations with a yield stress of 141 MPa.

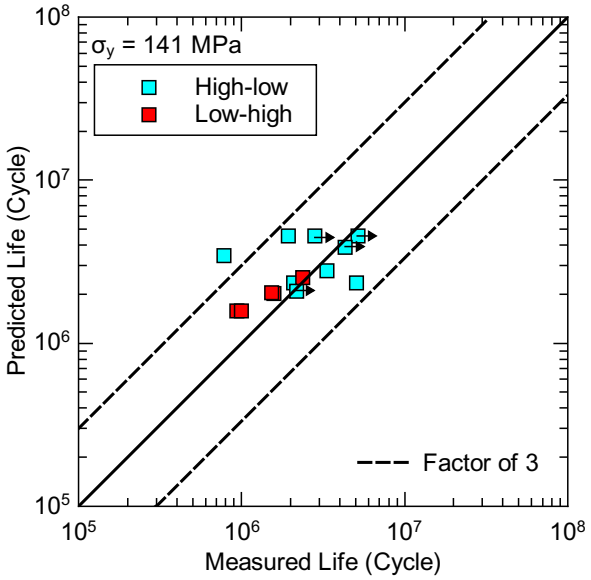

Figure 5.10: Predicted vs. measured lives for the fatigue tests on ACSR Ibis conductors under variable amplitude loading, considering a yield stress of 141 MPa.

The life prediction methodology used in this study is based on Miner's rule, which does not directly take into account the effect of the loading sequence on fatigue damage. Despite that, longer life predictions were obtained for the tests with a high-low sequence, as seen in Fig. 5.10. This indicates that the loading sequence affects the axial stresses in the conductor's wires that are obtained from the FE simulations. To further investigate how the axial stresses are affected by the loading sequence, a mapping of the $\mathrm{SWT}_{\mathrm{nom}}$ parameter on the AA1350 wires of the conductor was carried out. To facilitate the evaluation of the loading sequence effect, the VAL test conditions presenting the greatest difference between the high and low blocks were considered. Thus, the SWT distribution mappings for the low-high test with $Y_{\mathrm{b1}} = 0.90$ mm and $Y_{\mathrm{b2}} = 1.39$ mm, and for the high-low test with $Y_{\mathrm{b1}} = 1.39$ mm and $Y_{\mathrm{b2}} = 0.90$ mm were investigated.

Fig. 5.11 shows a comparison of the mapping of the $\mathrm{SWT}_{\mathrm{nom}}$ parameter during the low amplitude block for both test conditions. In these damage maps, each colored circle represents an inner or outer cross-section node of an AA1350-H19 wire of the ACSR Ibis conductor. The x-axis indicates the distance of the node from the clamp center, while the y-axis indicates its angular position. The color of each circle represents the value of the $\mathrm{SWT}_{\mathrm{nom}}$ parameter in the node, according to the scales shown. Note that in test condition 1, the low amplitude block

is applied first, while in test condition 2, it is preceded by a high amplitude block. Thus, the comparison between these damage maps allows us to evaluate how the high amplitude block affects the distribution and values of the SWT_{nom} parameters of the low amplitude block in the high-low test. In this regard, it can be seen that the distribution of the SWT_{nom} parameter was very similar for both test conditions. The values of the SWT_{nom} parameter were generally lower for the nodes located between the clamp center and the keeper edge (KE) and higher for the nodes located ahead of the KE. Furthermore, the nodes with the highest SWT_{nom} parameters in each layer were located near the top or bottom parts of the conductor, and near the last point of contact (LPC) between conductor and clamp. It is also noted that the maximum values of the SWT_{nom} parameter in each layer were slightly higher in test condition 1 than in test condition 2. Therefore, it can be concluded that, in a high-low sequence test, the high amplitude block causes the axial stresses in the wires to decrease during the low amplitude block without significantly changing the stress distribution.

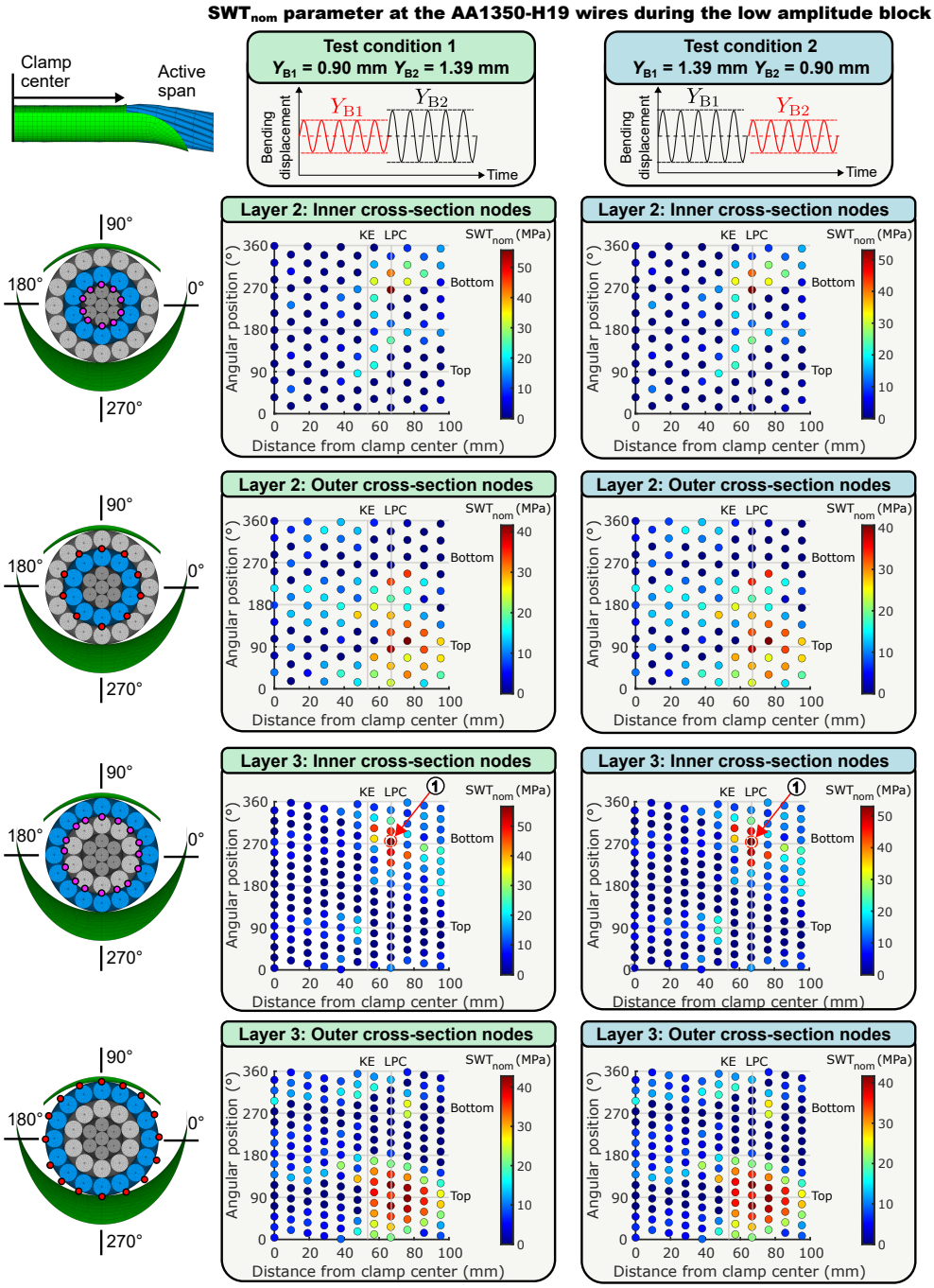

Figure 5.11: Mapping of the SWT_{nom} parameter at the AA1350-H19 wires during the low amplitude block for the tests under: low-high sequence with $Y_{b1} = 0.90$ mm and $Y_{b2} = 1.39$ mm, and high-low sequence with $Y_{b1} = 1.39$ mm and $Y_{b2} = 0.90$ mm.

Fig. 5.12 shows a similar comparison of the mapping of the SWT_{nom} parameter between the two selected test conditions, with emphasis on the high amplitude block. In test condition 1, the high block is preceded by a lower amplitude block, while in test condition 2 it is applied first. Therefore, comparing these maps allows us to assess the effects that the low block has

on the high block for the low-high sequence test. It can be seen that both the distribution and the values of the SWT_{nom} parameter along the wires are very similar for both test conditions. It can therefore be concluded that, in the low-high sequence test, the initial block does not have a significant effect on the axial stresses in the wires during the second block.

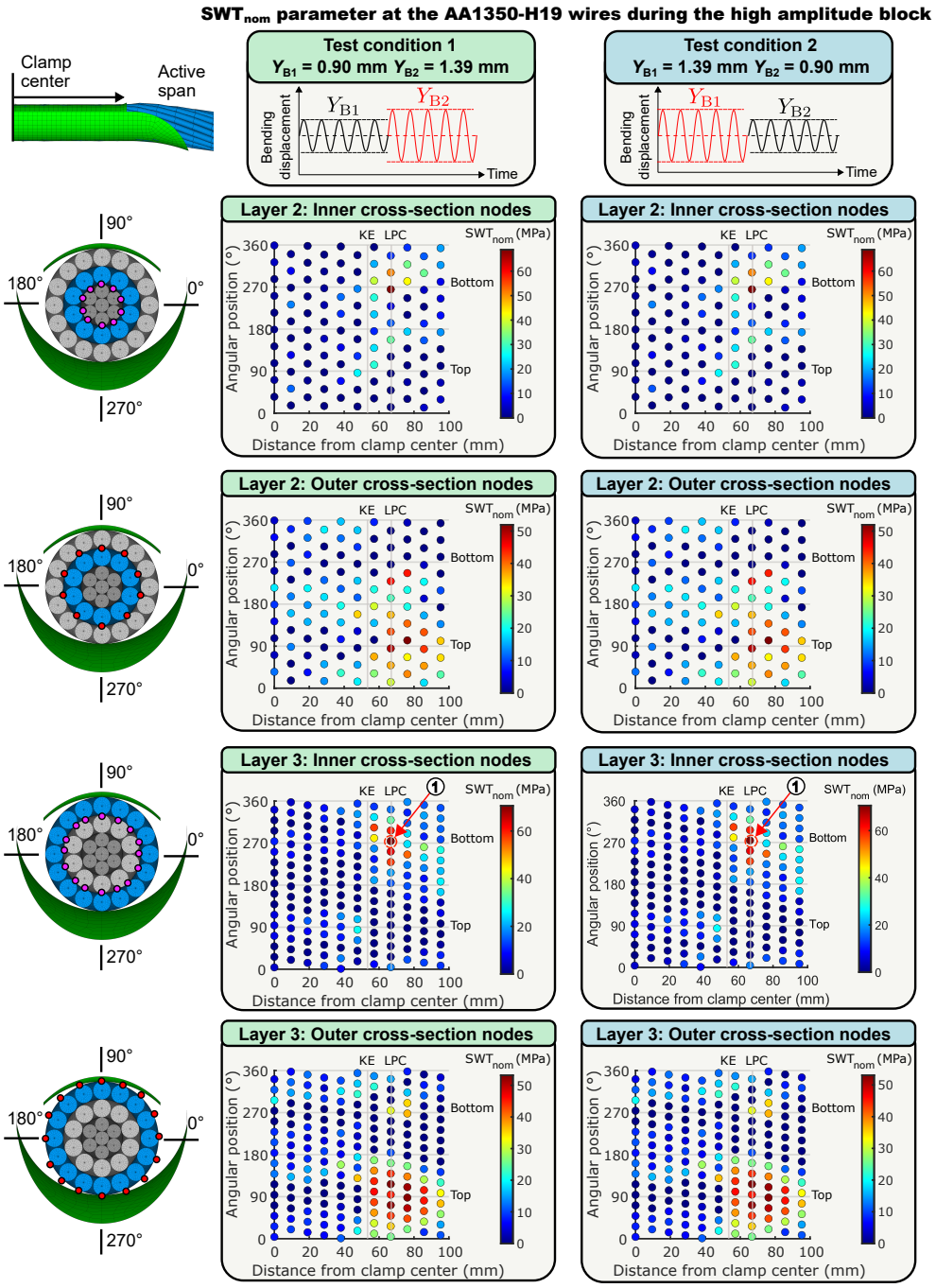

Figure 5.12: Mapping of the SWT_{nom} parameter at the AA1350-H19 wires during the high amplitude block for the tests under: low-high sequence with $Y_{b1} = 0.90$ mm and $Y_{b2} = 1.39$ mm, and high-low sequence with $Y_{b1} = 1.39$ mm and $Y_{b2} = 0.90$ mm.

Figs. 5.11 and 5.12 show that the loading sequence can affect the axial stresses in the conductor wires estimated by the FE simulations. This includes the stresses in the critical node, i.e. the node with the highest value of the SWT_{nom} parameter. In all test conditions simulated, the critical node corresponded to an inner node of an outer layer wire, located at a distance of 67 mm from the clamp center (indicated by the number 1 in Figs. 5.11 and 5.12). To further evaluate how the loading sequence affects the axial stress in the critical node and, consequently, the fatigue failure of the conductor, the axial stress history of the critical node was extracted from the simulations for each of the four loading conditions applied in the VAL tests.

Fig. 5.13 presents the extracted axial stress histories, as well as the values of the stress amplitude σ_{ax}, maximum stress σ_{max}, and SWT_{nom} parameter for each loading block. Comparing test conditions 1 and 2, it can be seen that the stress amplitude of the low block is the same, while the maximum stress is higher for test condition 1. This result suggests that, in a high-low test, the first loading block causes a slight reduction of the mean axial stress in critical node during the second block. On the other hand, the amplitude and maximum value of the axial stress are the same for the high amplitude block, which shows that, in a low-high test, the first block has no effect on the stresses of the second block. These results explain why longer life predictions were obtained for the tests under high-low sequence. The same conclusions can be obtained when comparing test conditions 3 and 4.

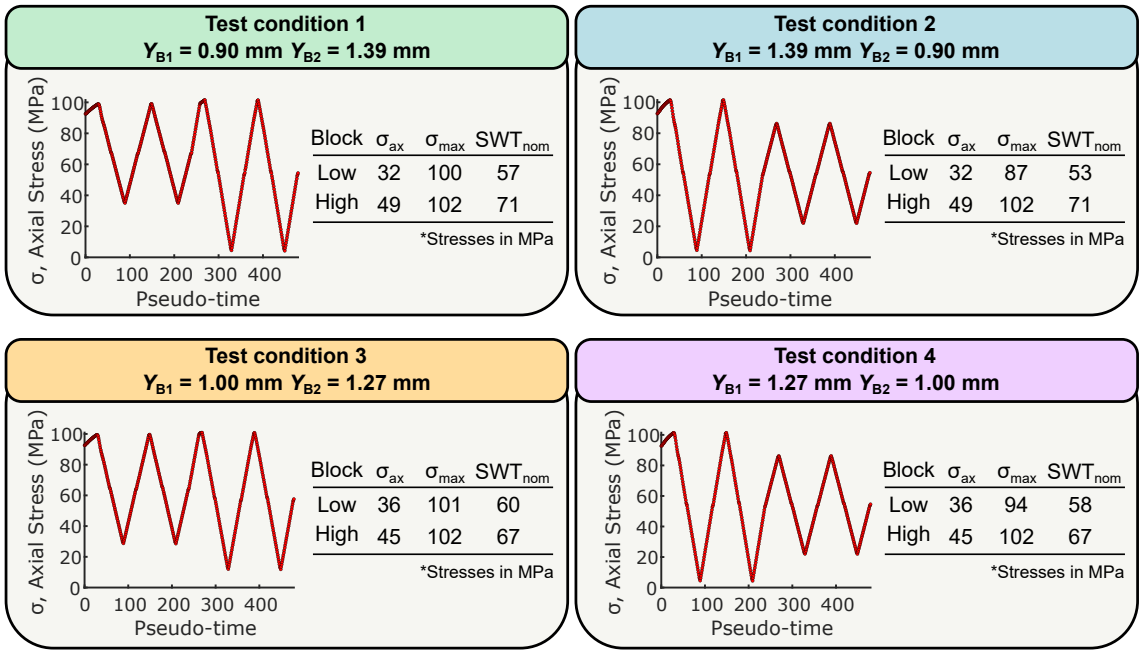

Figure 5.13: Axial stress history at the critical node for the tests on ACSR Ibis conductors under variable amplitude loading.

5.4.4 Failure analysis

The life prediction methodology was also evaluated regarding its capability to predict the regions of wire breakage for the VAL tests. For this failure analysis, the locations of the wire breaks reported in (Murça, 2011) were compared to those predicted by the methodology, with the results being summarized in Fig. 5.14. Each broken wire was identified by its axial position and its placement within the cross section of the conductor. The axial position was defined as the longitudinal distance between the position where the wire broke and the center of the suspension clamp. Regarding the placement within the cross section, wire breaks were classified as external or internal, depending on the layer in which they occurred, and as top or bottom, depending on which half of the cross section they took place.

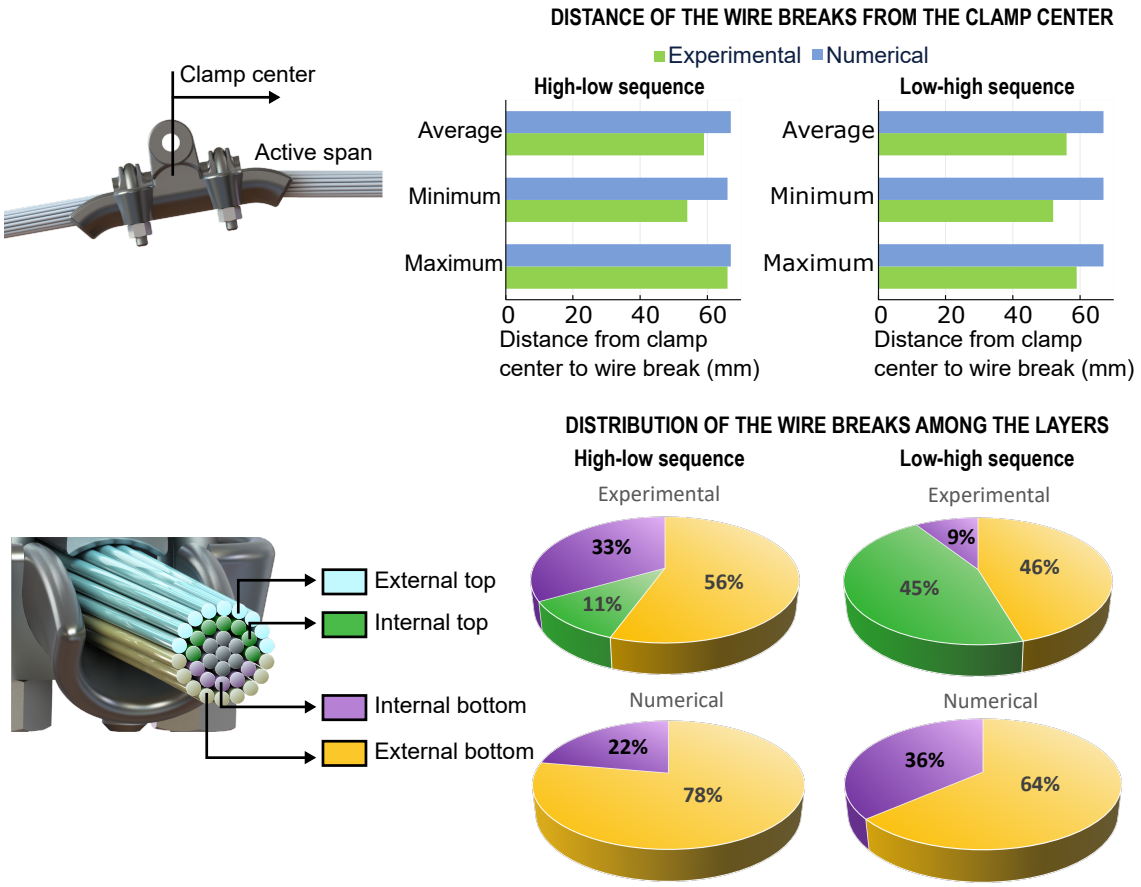

Figure 5.14: Comparisons between the locations of the wire breaks observed experimentally and those predicted by the methodology.

As shown in Fig. 5.14, the wire breaks in the VAL tests occurred at distances of 52 to 66 mm from the clamp center, which corresponds to the region located between the keeper edge and the last point of contact between conductor and clamp. The average distance between the wire break and the clamp center was similar for the tests under high-low and low-high sequences, indicating that the loading sequence does not have a significant effect on the axial position of the wire breaks. The numerical methodology also indicates that the wire breaks take place inside the suspension clamp, at a distance of about 67 mm from the clamp center. Note that that there is practically no dispersion in the numerical results, with nearly identical values being obtained for the maximum and minimum distances between the wire breaks and the clamp center. These results are expected, since the beam elements used to model the wires have a length of 10 mm, which limits the resolution in the prediction of the failure location. Despite these limitations, it is worth mentioning that the axial positions of the wire breaks predicted using the methodology

are within 10 mm of the average distances observed experimentally.

Regarding the distribution of wire breaks among the conductor layers, Fig. 5.14 shows that none of the simulations predicted the occurrence of wire breaks in the "external top"region, which is in agreement with the experimental results. The proportion of wires that broke in the external layer was higher for the tests under high-low sequence than for those under low-high sequence. The methodology accounted for this effect, but overestimated the number of wires that broke in the outer layer. In the fatigue tests, a significant percentage of the wire ruptures occurred in the upper half of the internal layer of the conductor, while the methodology did not predict wire ruptures in this region. The discrepancies between experimental and numerical results may be related to the simplifications assumed for the fatigue damage analysis of the conductor-clamp system. Note that the SWT_{nom} parameter used to determine the wire breaks was calculated using the axial stresses in the wires, while the contact forces were not taken into account. Additionally, it was assumed that no fatigue damage is produced when the maximum axial stress in the wire is compressive, which might not correspond to the experimental results. Despite these simplifications, it is noteworthy that the model was able to predict that the region of the conductor in contact with the clamp body is more critical to failure than the region in contact with the keeper, and that the loading sequence affects the distribution of wire breaks among the conductor layers.

5.5 Conclusions

In this paper, a life prediction methodology for overhead conductors was extended to variable amplitude loading conditions. The methodology relies on a finite element 3D model of the conductor-clamp system and two master fatigue curves, obtained from test data of wires under plain and fretting fatigue. The methodology was evaluated using fatigue test data of ACSR Ibis 397.5 MCM conductors under constant and variable amplitude loading. The main findings are summarized as follows:

(1) For the fatigue tests under constant amplitude loading (CAL), most of the life estimates were within a factor of 3 of the measured lives. This level of accuracy was similar to those

obtained in previous studies, in which the methodology was applied to fatigue test data of AAAC 900 MCM and ACSR Tern conductors. These results show that the methodology can be applied to different types of conductors and loading conditions.

(2) For the fatigue tests under variable amplitude loading (VAL), most of the predicted lives were within factors of 3 of the measured lives, regardless of the loading sequence applied. The accuracy of the life predictions was similar to that obtained for the tests under CAL, which shows that the methodology can be successfully extended to VAL conditions.

(3) The predicted lives of the tests under high-low loading sequence were longer than those of the tests under low-high sequence. These results are in accordance with the experimental data, indicating that the methodology can take into account the loading sequence effect on fatigue life.

(4) The methodology predicted the location of the fatigue critical region in good agreement with the experimental results. For the VAL tests, the methodology correctly predicted that all wire breaks would take place inside the suspension clamp, that the region of the conductor in contact with the clamp body is critical for fatigue failure, and that the loading sequence can affect the distribution of wire breaks within the conductor layers.

6 Conclusions

6.1 Summary of the main contributions

This thesis focused on the development of new fatigue life prediction methodologies for overhead conductors and their wires by means of experimental and numerical investigations. The main findings from the thesis were organized as three research papers. The first two (Chapters 3 and 4) were focused on the life prediction of wires under fretting fatigue, while the third paper (Chapter 5) was concerned with the durability of the conductor-clamp system. The main contributions from each part of the study are summarized as follows:

In Chapter 3:

- Production of new test data of 1120 aluminum alloy (AA) wires under fretting fatigue, plain fatigue, and monotonic tension.
- Evaluation of the crack initiation and propagation behaviors of V-notched and fretting wire specimens of AA1120 by examination of their fracture surfaces.
- Comparison of test data of AA1120 and AA1350 wires, showing that the former has a higher ultimate tensile strength, and is more resistant to plain and fretting fatigue.
- Comparison of test data of AA1120 and AA6201 wires, showing that the latter has a higher ultimate tensile strength and is more resistant to plain fatigue. However, both materials display approximately the same fretting fatigue strength.
- Evaluation of the capability of a nonlocal fatigue criterion to predict the lives of the fretting fatigue tests on AA1120 wires, showing that most predictions are within factors of 3 of the measured lives.

In Chapter 4:

- Production of new test data of AA6201 wires under fretting fatigue and variable amplitude loading (VAL).
- Proposal of a three-block loading history that can be used in fretting fatigue tests to represent the amplitude variation of the aeolian vibrations.
- Use of vibration data from an operating transmission line to define the parameters of the fretting fatigue tests.
- Discussion on the hypothesis that low bending displacement amplitude levels may have a more significant effect on the conductor's fatigue damage than higher levels, as the low amplitudes occur over a considerably higher number of loading cycles than the high amplitudes.
- Extension of two fatigue criteria to VAL conditions: one based on the Theory of Critical Distances and the other on a master fatigue curve.
- Evaluation of the fatigue criteria using the fretting fatigue test data, showing that both approaches can provide life predictions within factors of 4 of the measured lives.
- Demonstration that methodologies for life prediction of wires under fretting fatigue can be extended to VAL conditions and remain accurate.

In Chapter 5:

- Extension of a finite element-based methodology for life prediction of conductor-clamp systems to include VAL conditions.
- Evaluation of the methodology considering fatigue test data of ACSR Ibis conductors under constant amplitude loading (CAL) and a two-block loading history.
- Demonstration that the methodology can provide life predictions for the tests under CAL within factors of 3 of the measured lives, which is an accuracy similar to that obtained for the ACSR Tern and the AAAC 900 MCM conductors.

- Demonstration that the methodology can provide life predictions for the tests under high-low and low-high loading sequences with an accuracy similar to that obtained for the tests under CAL.
- Evaluation of the effect of the yield stress on the life prediction of the conductor-clamp system.
- Evaluation of the effect of loading sequence on the fatigue failure of the conductor.
- Comparison between the locations of the wire breaks predicted by the methodology with those observed in the VAL fatigue tests.

6.2 Suggestions for future work

Based on the results of the fretting fatigue tests and finite element (FE) simulations performed in this thesis, the following analyses are suggested for future studies:

- A comparative analysis could be performed between the tangential forces measured in the fretting fatigue tests with those estimated from the FE simulations of wires in contact.
- Regarding the fretting fatigue tests, an investigation could be made on the effect of the stress gradient caused by the contact between the wire specimen and the bearing on the fatigue life of the wire. This could be achieved by following the same FE-based methodology described in Chapter 3. However, instead of modeling the wire specimen as a half-cylinder, it would be modeled as a complete cylinder in contact with the pad and the bearing.
- In Chapter 3, it was observed that the AA1120 wires have lower resistance to axial fatigue than the AA6201 wires. However, both materials have approximately the same fretting fatigue strength. These results suggest that the resistance of an aluminum alloy wire to fretting fatigue could be affected by the material stiffness. Future studies could further evaluate this behavior by performing a series of fretting fatigue tests on two different wire materials subjected to the same loading conditions and investigating the contact and

fracture surfaces of the wire specimens. Additionally, studies could take this effect into consideration by adding a stiffness factor into the FE-based stress analysis.

- In this thesis, an elastic-perfectly plastic material model was considered for the aluminum alloy wires of the conductors. For simplicity, the plasticity was defined using mechanical properties of wires under monotonic tension. Future studies could focus on improving the FE model by obtaining cyclic stress-strain curves for the aluminum alloy wires, which could then be used as input for the FE-based stress analyses.

- In Chapters 3 and 4 of this thesis and in previous investigations (Rocha et al., 2019; Araújo et al., 2020; Matos et al., 2020), considerable efforts have been made to evaluate the nonlocal fatigue criterion in terms of its accuracy for different wire materials and loading conditions. Future studies could focus on investigating other parameters that may also affect the life of wires under fretting fatigue. For example, new studies could evaluate whether the criterion remains accurate when considering different wire geometries (such as trapezoidal wires) or higher temperatures, which are closer to the usual operating conditions of transmission lines.

- Chapters 4 and 5 considered fatigue test data of conductors and wires subjected to variable amplitude loading conditions. In these studies, block loading histories were used as a simplified representation of the amplitude variations of the aeolian vibrations. It could be worthwhile to perform new fatigue tests and finite element simulations on conductors and wires under fretting fatigue considering more realistic loading conditions, such as those found in (Ferreira et al., 2023).

- The fatigue tests on conductors and wires evaluated in this thesis were performed under lives of 10^5 to 10^7 cycles. However, the endurance limit typically used by power utilities for conductors is 5×10^8 cycles. Thus, future studies could prioritize performing tests under longer lives to evaluate if the methodologies proposed in this study remain accurate under ultra-high cycle fatigue.

References

Achiriloaiei D, Nes C, Dumitru I, Cernescu A. On the influence of the contact force and the angle between the wires on ACSR conductors' mechanical properties and durability. Key Eng. Mater. 2016;665:33–6.

Adriano VSR., Martínez JMG., Ferreira JLA, Araújo JA, da Silva CRM. The influence of the fatigue process zone size on fatigue life estimations performed on aluminum wires containing geometric discontinuities using the Theory of Critical Distances. Theor. Appl. Fract. Mec. 2018;97:265–78.

Aggarwal RK, Johns AT, Jayasinghe JASB, Su W. An overview of the condition monitoring of overhead lines. Electr. Power Syst. Res. 2000;53:15–22.

Akhtar A. Localized intrinsic strengthening approach (LISA): A practical method for determining the tensile strength of multistrand cables. J. Test. Eval. 1988;16:124–33.

Al Aqil MA, Kopsidas M. Modeling multi-layer OHL conductors undergoing wind-induced motion. IEEE Access 2020;8:104579–89.

Aluminum Association. Aluminum Electrical Conductor Handbook. Washington: The Aluminum Association; 1989.

Aluminum Association. International alloy designations and chemical composition limits for wrought aluminum and wrought aluminum alloys. Arlington: The Aluminum Association; 2015.

Alshwawreh N, Alhamarneh B, Altwarah Q, Quandour S, Barghout S, Ayasrah O. Electrical resistivity and tensile strength relationship in heat-treated all aluminum alloy wire conductors. Materials 2021;14:5738.

Anderson K, Weritz J, Kaufman G. ASM Handbook vol 2b - properties and selection of aluminum alloys. ASM International; 2019.

Araújo JA, Susmel L, Taylor D, Ferro J, Mamiya E. On the use of the Theory of Critical Distances and the Modified Wöhler Curve Method to estimate fretting fatigue strength of cylindrical contacts. Int. J. Fatigue 2007;29:95–107.

Araújo JA, Castro FC, Matos IM, Cardoso RA. Life prediction in multiaxial high cycle fretting fatigue. Int. J. Fatigue 2020;134:105504.

Araújo JA, Susmel L, Pires MST, Castro FC. A multiaxial stress-based critical distance methodology to estimate fretting fatigue life. Tribol. Int. 2017;108:2–6.

Araújo JA, Ferreira JLA, Kalombo RB, Matos IM, Castro FC. Overhead conductors. In: Liskiewicz T, Dini D, editors. Fretting Wear and Fretting Fatigue - Fundamental Principles and Applications. Cambridge: Elsevier; 2022. p. 565–97.

Araújo JA, Nowell D, Castro FC. Fretting fatigue. In: Aliabadi MHF, Soboyejo WO, editors. Comprehensive Structural Integrity. Elsevier; 2023, p. 249–82.

Arnaud P, Maruel V, Fouvry S, Said J, Yang C, Hafid F. Fretting tests for cyclic plastic law identification: Application to a 1XXX aluminium crossed wire contact. Tribol. Int. 2023;177:107958.

Australian Standard AS 3607-1989. Conductors - Bare overhead, aluminium and aluminium alloy-steel reinforced. Standards Australia 1989.

Azevedo CRF, Cescon T. Failure analysis of aluminum cable steel reinforced (ACSR) conductor of the transmission line crossing the Paraná River. Eng. Fail. Anal. 2002;9:645–64.

Azevedo CRF, Henriques AMD, Pulino Filho AR, Ferreira JLA, Araújo JA. Fretting fatigue in overhead conductors: Rig design and failure analysis of a Grosbeak aluminium cable steel reinforced conductor. Eng. Fail. Anal. 2009;16:136–51.

Barber KW, Callaghan KJ. Improved overhead line conductors using aluminium alloy 1120.

IEEE Trans. Power Deliv. 1995;10:403–9.

Barrett JS, Motlis Y. Allowable tension levels for overhead-line conductors. IEE Proc. Gener. Trans. Distrib. 2001;148:54–9.

Baumann R., Novak P. Efficient computation and experimental validation of ACSR overhead line conductors under tension and bending. CIGRE Sci. Eng. 2017;9:5–16.

Bhatti NA, Pereira K, Abdel Wahab M. A continuum damage mechanics approach for fretting fatigue under out of phase loading. Tribol. Int. 2018;117:39–51.

Boniardi M, Cincera S, D'Errico F, Tagliabue C. Fretting fatigue phenomena on an all aluminium alloy conductor. Key Eng. Mater. 2007;348–9:5–8.

Brunair RM, Ramey GE, Duncan III RR. An experimental evaluation of S-N curves and validity of Miner's cumulative damage hypothesis for an ACSR conductor, IEEE Trans. Power Deliv. 1988;3:1131–40.

Cardou A, Cloutier L, Lanteigne J, M'boup P. Fatigue strength characterization of ACSR electrical conductors at suspension clamps. Electr. Power Syst. Res. 1990;19:61–71.

Cardou A, Cloutier L, St-Louis M, Leblond A. ACSR electrical conductor fretting fatigue at spacer clamps. Standardization of Fretting Fatigue Test Methods and Equipment, ASTM STP 1159 1992:231–42.

Castro FC, Araújo JA, Zouain N. On the application of multiaxial high-cycle fatigue criteria using the theory of critical distances. Eng Fract Mech 2009;76:512–24.

Chen G, Wang X, Wang J, Liu J, Zhang T, Tang W. Damage investigation of the aged aluminium cable steel reinforced (ACSR) conductors in a high-voltage transmission line. Eng. Fail. Anal. 2012;19:13–21.

CIGRÉ TF 22.11.2. Guide to vibration measurements on overhead lines. Electra 1995;162:125–37.

CIGRÉ TF B2.11.04. Overhead conductor safe design tension with respect to aeolian vibrati-

ons. CIGRÉ 2005.

CIGRÉ WG 04 SC 22. Recommendations for the evaluation of the lifetime of transmission line conductors. Electra 1979.

CIGRÉ WG B2.30. Engineering guidelines relating to fatigue endurance capability of conductor/clamp systems. Electra; 2010.

Cosmai U, Van Dyke P, Mazzola L Lillien J. Conductor motions. In: Papailiou KO, editors. Overhead Lines. CIGRE Green books. Cham: Springer; 2017, p. 559–711.

Costa ER, Araújo JA, Veloso LACM, da Silva CRM, Ferreira JLA. Development of controlled heating for fatigue test in overhead conductors at high temperature. J. Braz. Soc. Mech. Sci. 2020;42:385.

Dawall PW, Gupta MM, Ukrainetz PR. Mathematical analysis of transmission line vibration data. Electr. Power Syst. Res. 1978;1:269–82.

Davies G. Aluminium alloy (6201, 6101A) conductors. International Conference on Overhead Line Design and Construction: Theory and Practice 1989:93–8.

Dowling NE, Calhoun CA, Arcari A. Mean stress effects in stress-life fatigue and the Walker equation. Fatigue Fract. Eng. Mater. Struct. 2009;32:163–79.

Dowling NE, Thangjitham S. An overview and discussion of basic methodology for Fatigue. Fatigue Fract. Mech. 2000;31:3–36.

Edwards AT, Boyd JM. Ontario Hydro live-line vibration recorder for transmission conductors. IEEE Trans. Power Appar. Syst. 1963;82:269–73.

EPRI. Transmission line reference book: Wind-induced conductor motion. Palo Alto: Electric Power Research Institute; 2006.

Fadel AA, Rosa D, Murça LB, Ferreira JLA, Araújo JA. Effect of high mean tensile stress on the fretting fatigue life of an Ibis steel reinforced aluminium conductor. Int. J. Fatigue 2012;42:24–34.

Ferreira JLA, Kalombo RB, Araújo JA, da Silva CRM. Fatigue behavior analysis and life prediction of overhead conductors subjected to narrowband vibration. IEEE Trans. Power Deliv. 2023;38:1120–8.

Frémond M, Nedjar B. Damage, gradient of damage and principal of virtual power. Int. J. Solids Struct. 1996;33:1083–103.

Fricke WG, Rawlins CB. Importance of fretting in vibration failures of overhead conductors. IEEE Trans. Power Appar. Syst. 1968;PAS-87:1381–4.

Frigerio M, Buehlmann PB, Bucheim J, Holdsworth SR, Dinser S, Franck Ch.M, Papailiou K, Mazza E. Analysis of the tensile response of a stranded conductor using a 3D finite element model. Int. J. Mech. Sci. 2016;106:176–83.

Fuchs RD. Transmissão de energia elétrica: Linhas aéreas. Rio de Janeiro, Escola Federal de Engenharia de Itajubá 1977.

Garcia MA, Veloso LACM, Castro FC, Araújo JA, Ferreira JLA, da Silva CRM. Experimental device for fretting fatigue tests in 6201 aluminum alloy wires from overhead conductors. Wear 2020;460–1:203448.

Gandiolle C, Fouvry S, Charkaluk E. Lifetime prediction methodology for variable fretting fatigue loading: Plasticity effect. Int. J. Fatigue 2016;92:531–47.

Ghoreishi SR, Messager T, Catraud P, Davies P. Validity and limitations of linear analytical models for steel wire strands under axial loading, using a 3D FE model. Int. J. Mech. Sci. 2007;49:1251–61.

Gonzales-Pociño A, Alvarez-Antolin JF, Asensio-Lozano J. In-service microstructural modifications caused by fatigue phenomena leading to the failure of a high-voltage cable. Pract. Mettalogr. 2019;56:288–302.

Goudreau S, Lévesque F, Cardou A. Analysis of variable amplitude loading fatigue tests on overhead conductor using Palmgren-Miner rule. Sixth International Symposium on Cable Dy-

namics; 2005.

Hardy C, Brunelle J. Principles of measurement and analysis with the new PAVICA conductor vibration recorder. Toronto: Canadian Electrical Association Centennial Conference; 1991.

Hoffmann JN, Mölhoff FR, Jolandek MA, Hoffmann A. Condutores de alumínio liga 1120 e alternativas de feixes para 500 kV. Seminário Nacional de Produção e Transmissão de Energia Elétrica - XXIII SNPTEE; 2015.

Houle S, Hardy C, Lapointe A, St-Louis M. Experimental assessment of spacer-damper system performance with regard to control of wind-induced vibrations of high-voltage transmission lines. IEEE/CSEE Joint Conference on High Voltage Transmission Systems; 1987.

IEC 62568. Overhead lines – Method for fatigue testing of conductors. International Standard; 2015.

IEEE. An introductory discussion on aeolian vibration of single conductors. Transmission & Distribution Comitee, Technical Report PES-TR17 2015.

IEEE. Guide for aeolian vibration field measurements of overhead conductors. IEEE Power Engineering Society; 2006.

IEEE. Standardization of conductor vibration measurements. IEEE Trans. Power Appar. Syst. 1966;PAS-85:10–22.

ISO 6507-1. Metallic materials - Vickers hardness test - part 1: Test method. International Standard; 2018.

Judge R, Yang Z, Jones SW, Beattie G. Full 3D finite element modelling of spiral strand cables. Constr. Build. Mater. 2012;35:452–9.

Kalombo RB, Araújo JA, Ferreira JLA, da Silva CRM, Alencar R, Capra AR. Assessment of the fatigue failure of an All Aluminium Alloy Cable (AAAC) for a 230 kV transmission line in the Center-West of Brazil. Eng. Fail. Anal. 2015;61:77–87.

Kalombo RB, Reinke G, Miranda TB, Ferreira JLA, da Silva CRM, Araújo JA. Experimental

study of the fatigue performance of overhead pure aluminium cables. Procedia Struct. Integr. 2019;19:688–97.

Kalombo RB, Miranda TB, Rocha PHC, Ferreira JLA, da Silva CRM, Araújo JA. Fatigue performance of overhead conductors tested under the same value of H/w parameter. Procedia Eng. 2018a;213:346–58.

Kalombo RB, Miranda TB, Rocha PHC, Ferreira JLA, da Silva CRM, Araújo JA. The effect of mean stress on the fatigue behaviour of overhead conductor function of the H/w parameter. MATEC Web Conf. 2018b;165:11001.

Kalombo RB, Pestana MS, Ferreira JLA, da Silva CRM, Araújo JA. Influence of the catenary parameter (H/w) on the fatigue life of overhead conductors. Tribol. Int. 2017;108:141–9.

Kanálik M, Margitová A, Beňa L. Temperature calculation of overhead power line conductors based on CIGRE Technical Brochure 601 in Slovakia. Electr. Eng. 2019;101:921–33.

Karabay S. Modification of AA-6201 alloy for manufacturing of high conductivity and extra high conductivity wires with property of high tensile stress after artificial aging heat treatment for all-aluminium alloy conductors. Mater. Des. 2006;27:821–32.

Kiessling F, Nefzger P, Nolasco JF, Kaintzyk U. Overhead power lines: planning, design, construction. Berlin Heidelberg: Springer Science & Business Media; 2003. p. 195–242.

Kouanga CT, Jones JD, Revill I, Wormald A, Nowell D, Dwyer-Joyce RS, Araújo JA, Susmel L. On the estimation of finite lifetime under fretting fatigue loading. Int. J. Fatigue 2018;112:138–52.

Kouanga CT, Jones JD, Revill I, Wormald A, Nowell D, Dwyer-Joyce RS, Susmel L. A variable amplitude fretting fatigue life estimation technique: Formulation and experimental validation. Tribol Int 2023;178:108055.

Kubelwa YD, Loubser RC, Moodley P. Experimental investigations of bending stresses of ACSR conductors due to aeolian vibrations. CIGRE Sci. Eng. 2017;9:17–26.

Lalonde S, Guilbault R, Langlois S. Numerical analysis of ACSR conductor–clamp systems undergoing wind-induced cyclic loads. IEEE Trans. Power Deliv. 2018;33:1518–26.

Lalonde S, Guilbault R, Légeron F. Modeling multilayered wire strands, a strategy based on 3D finite element beam-to-beam contacts - Part I: Model formulation and validation. Int. J. Mech. Sci. 2017a;126:281–96.

Lalonde S, Guilbault R, Langlois S. Modeling multilayered wire strands, a strategy based on 3D finite element beam-to-beam contacts - Part II: Application to wind-induced vibration and fatigue analysis of overhead conductors. Int. J. Mech. Sci. 2017b;126:297–307.

Lévesque F, Goudreau S, Cardou A, Cloutier L. Strain measurements on ACSR conductors during fatigue tests I - Experimental method and data. IEEE Trans. Power Deliv. 2010;25:2825–34.

Lequien F, Auzoux Q, Moine G, Rousseau M, Pasquier-Tilliette S, Holande A, Ammi S, Heurtault S, Prieur P. Characterization of an aluminum conductor steel reinforced (ACSR) after 60 years of operation. Eng. Fail. Anal. 2021;120:105039.

Martínez JMG, Adriano VSR, Araújo JA, Ferreira JLA, da Silva CRM. Numerical fatigue life estimation of aluminium 6201-T81 wires containing geometric discontinuities. MATEC Web Conf. 2018;165:10015.

Matos IM, Rocha PHC, Kalombo RB, Veloso LACM, Araújo JA, Castro FC. Fretting fatigue of 6201 aluminum alloy wires of overhead conductors. Int. J. Fatigue 2020;141:105884.

Matos IM, Araújo JA, Castro FC. Fretting fatigue performance and life prediction of 1120 aluminum alloy wires of overhead conductors. Theor. Appl. Fract. Mech. 2022;121:103521.

Matos IM, Araújo JA, Castro FC. Life prediction of 6201-T81 aluminum alloy wires under fretting fatigue and variable amplitude loading. Tribol. Int. 2023;183:108407.

McColl IR, Waterhouse RB, Harris SJ, Tsujikawa M. Lubricated fretting wear of a high-strength eutectoid steel rope wire. Wear 1995;185:203–12.

McGill PB, Ramey GE. Effect of suspension clamp geometry on transmission line fatigue. J. Energy Eng. 1986;112:168–84.

Miranda TB, Kalombo RB, Araújo JA, da Silva CRM, Ferreira JLA. Fatigue evaluation of All Aluminium Alloy Conductors fitted with elastomeric and metallic suspension clamps. IEEE Trans. Power Deliv. 2022;37:539–46.

Murça LB. Estudo experimental do efeito da sequência de carregamento sobre a resistência à fadiga de cabos condutores. M.S. thesis, Department of Mechanical Engineering, University of Brasilia; 2011.

Nawrocki A, Labrosse M. A finite element model for simple straight wire rope strands. Comput. Struct. 2000;77:345–59.

Neuber H. Theory of notch stresses: Principles for exact calculation of strength with reference to structural form and material, first ed., Berlin: Springer; 2017.

Nishioka K, Hirakawa K. Fundamental investigations of fretting fatigue. Bull. JSME 1972;15:135–44.

Noiseux DU, Hardy C, Houle S. Statistical methods applied to aeolian vibrations of overhead conductors. J. Sound Vib. 1987;113:245–55.

Omrani A, Dieng L, Langlois S, Van Dyke P. Friction properties at the contact interfaces of overhead line aluminium conductors. IEEE Trans. Power Deliv. 2022;37:442–8.

Omrani A, Langlois S, Van Dyke P, Lalonde S, Karganroudi SS, Dieng L. Fretting fatigue life assessment of overhead conductors using a clamp/conductor numerical model and biaxial fretting fatigue tests on individual wires. Fatigue Fract Eng. Mater. Struct. 2021;44:1498–514.

Ouaki B, Goudreau S, Cardou A, Fiset M. Fretting fatigue analysis of aluminium conductor wires near the suspension clamp: Metallurgical and fracture mechanics analysis. J. Strain Anal. Eng. Des. 2003;38:133–47.

Pereira RL, Díaz JIM, Ferreira JLA, da Silva CRM, Araújo JA. Numerical and experimental

analysis of fretting fatigue performance of the 1350-H19 aluminum alloy. J. Braz. Soc. Mech. Sci. 2020;42:419.

Peterson RE. Notch sensitivity. In: Sines G, Waisman JL, editors. Metal fatigue. New York: McGraw Hill; 1959, pp. 293–306.

Pinto AL, Cardoso RA, Talemi R, Araújo JA. Fretting fatigue under variable amplitude loading considering partial and gross slip regimes: Numerical analysis. Tribol. Int. 2020;146:106199.

Pinto AL, Talemi R, Araújo JA. Fretting fatigue total life assessment including wear and varying critical distance. Int. J. Fatigue 2022;156:106589.

Poffenberger JC, Swart RL. Differential displacement and dynamic conductor strain. IEEE Trans. Power Appar. Syst. 1965;84:281–9.

Ramey GE, Silva JM. An experimental evaluation of conductor aeolian fatigue damage mitigation by amplitude reduction. IEEE IEEE Trans. Power Appar. Syst. 1981;PAS-100:1935–40.

Rawlins CB, Harvey JR. Improved systems for recording conductor vibration. Trans. AIEE. Part III: Power Appar. Syst. 1959;78:1494–500.

Rocha PHC. Studies on fatigue of two contacting wires of overhead conductors: Experiments and modeling. M.S. thesis, Department of Mechanical Engineering, University of Brasilia; 2019.

Rocha PHC., Díaz JIM, da Silva CRM, Araújo JA, Castro FC. Fatigue of two contacting wires of the ACSR Ibis 397.5 MCM conductor: Experiments and life prediction. Int. J. Fatigue 2019;127:25–35.

Rocha PHC, Langlois S, Lalonde S, Araújo JA, Castro FC. A general life estimation method for overhead conductors based on fretting fatigue behavior of wires. Theor. Appl. Fract. Mech. 2022;121:103443.

Rocha PHC, Langlois S, Lalonde S, Araújo JA, Castro FC. Influence of 1350 and 6201 aluminum alloys on the fatigue life of conductors - a finite element analysis. Tribol. Int.

2023;186:108661.

Ruhlman JR, Poffenberger JC, Grosshandler S. A mobile vibration laboratory unit for monitoring dynamic characteristics of overhead transmission lines (Dynalab). Trans. AIEE. Part III: Power Appar. Syst. 1959;78:624–37.

Said J, Garcin S, Fouvry S, Cailetaud G, Yang C, Hafid F. A multi-scale strategy to predict fretting-fatigue endurance of overhead conductors. Tribol. Int. 2020a;143:106053.

Said J, Fouvry S, Cailetaud G, Yang C, Hafid F. Shear driven crack arrest investigation under compressive state: Prediction of fretting fatigue failure of aluminium strands. Int. J. Fatigue 2020b;136:105589.

Said J, Fouvry S, Cailletaud G, Basseville S, Coulangeon M, Brocard J, Yang C, Hafid F. A global-local approach to predict the fretting-fatigue failure of clamped aluminum powerline conductors: From mono-contact crossed wires to full conductor vibrational tests. Eng Fail Anal 2023;146:107073.

Sanders R, Staley J. A history of wrought aluminum alloys and applications, properties and selection of aluminum alloys. In: Anderson K, Weritz J, Kaufman JG, editors. Properties and selection of aluminum alloys, vol 2B. ASM International; 2019,

Sandoval CFB, Malcher L, Canut FA, Araújo LM, Doca TCR, Araújo JA. Micromechanical Gurson-based continuum damage under the context of fretting fatigue: Influence of the plastic strain field. Int. J. Plast. 2020;125:235–64.

Sarhan AAD, Zalnezhad E, Hamdi M. The influence of higher surface hardness on fretting fatigue life of hard anodized aerospace AL7075-T6 alloy. Mater. Sci. Eng. A 2013;560:377–87.

Shen F, Ke L, Zhou K. A debris layer evolution-based model for predicting both fretting wear and fretting fatigue lifetime. Int. J. Fatigue 2021;142:105982.

Sonsino CM. Fatigue testing under variable amplitude loading. Int J Fatigue 2007;29:1080–9.

Sproule JE, Edwards AT. Progress towards optimum damping of transmission conductors. Trans.AIEE. Part III: Power Appar. Syst. 1959;8:844–7.

Steidel RF. Factors affecting vibratory stresses in cables near the point of support. Trans. AIEE. Part III: Power Appar. Syst. 1959;78:1207–12.

Steier VF, Doca T, Araújo JA. Fretting wear investigation of 1350-H19 aluminum wires tested against treated surfaces. Wear 2018;415–415:1–8.

Sun Z, Xu C, Peng Y, Shi Y, Zhang Y. Fretting tribological behaviors of steel wires under lubricating grease with compound additives of graphene and graphite. Wear 2020;454–5:203333.

Susmel L. Multiaxial Notch Fatigue: From nominal to local stress/strain quantities. Cambridge: Woodhead; 2009.

Susmel L, Taylor D. A novel formulation of the theory of critical distances to estimate lifetime of notched components in the medium-cycle fatigue regime. Fatigue Fract. Eng. Mater. Struct. 2007;30:567–81.

Susmel L, Taylor D. A critical distance/plane method to estimate finite life of notched components under variable amplitude uniaxial/multiaxial fatigue loading. Int. J. Fatigue 2012;38:7–24.

Taylor D. Geometrical effects in fatigue: A unifying theoretical model. Int. J. Fatigue 1999;21:413–20.

Tebo GB. Measurement and control of conductor vibration. AIEE summer convention, Toronto, Ontario 1941:1188–93.

Varney T. Notes on the vibration of transmission-line conductors. Trans. AIEE. 1926;XLV:791–5.

Vieira ER. Análise comparativa do efeito da fadiga por fretting nos fios de cabos condutores formados pelas ligas de alumínio 1120 e AA 6201. M.S. thesis, Department of Mechanical Engineering, University of Brasilia; 2020.

Wang JJ, Wang JJ, Lara-Curzio E, King Jr. TJ. The integrity of ACSR full tension single-stage splice connector at higher operation temperature. IEEE Trans. Power Deliv. 2008;23:1158-1165

Watanabe L. Análise da vida à fadiga de cabos condutores de energia submetidos a carregamentos aleatórios. PhD thesis, Department of Mechanical Engineering, University of Brasilia; 2014.

Wright EM, Mini Jr. J. Field tests on conductor vibration. Electr. Eng. 1934;53:1123–7.

Xu C, Peng Y, Zhu Z, Tang W, Huang K. Fretting behavior evolution of steel wires with helical structure after adding ore particles in lubricating grease. Eng. Fail. Anal. 2021;124:105332.

Zhang T, Zheng W, Xie Y, Yuan J, Xu T, Wang P, Liu G, Guo D, Zhng G, Liang Y. A case study of rupture in 110 kV overhead conductor repaired by full-tension splice. Eng. Fail. Anal. 2020;108:104349.

Zhou ZR, Cardou A, Fiset M, Goudreau S. Fretting fatigue in electrical transmission lines. Wear 1994a;173:179–88.

Zhou ZR, Cardou A, Goudreau S, Fiset M. Fretting patterns in a conductor-clamp contact zone. Fatigue Fract. Eng. Mater. Struct. 1994b;17:661–9.

Zhou ZR, Cardou A, Goudreau S, Fiset M. Fundamental investigations of electrical conductor fretting fatigue. Tribol. int. 1996;29:221–32.

Zhou ZR, Fiset M, Cardou A, Cloutier L, Goudreau S. Effect of lubricant in electrical conductor fretting fatigue. Wear 1995;189:51–7.

Zhou ZR, Vincent L. Lubrication in fretting - a review. Wear 1999;225–9:962–7.